

Olivacine plus Coadjuvants in the Treatment of Murine Leukaemia

Marilda Meirelles de Oliveira*

Department of Organic Chemistry, Instituto Butantan, Av. Vital Brasil 1500, São Paulo, SP, Brazil

Rufino Antunes de Alencar Filho

Department of Clinical Pathology, Instituto Biológico, São Paulo, SP, Brazil

Administration of olivacine, 1,5-dimethyl-6H-pyrido[4,3-b] carbazole to mice inoculated with 10^5 , 10^3 and 10^2 leukaemic cells (L_{1210}) produced significant survival in all treated groups which was not altered by association with the naturally occurring nucleoside deoxycytidine. Treatment with olivacine plus heterologous serum caused leucocytosis due to neutrophilia, lymphocytosis and monocytosis, as opposed to treatment with olivacine alone, which produced leucopenia due to neutropenia and lymphocytopenia.

Keywords: olivacine; pyrido-carbazole; L_{1210} leukaemia; deoxycytidine; heterologous serum; leucopenia.

INTRODUCTION

Spontaneous regression of cancer is rare and may happen with a frequency of less than 1 in 100 000 cases (Emerson and Cole, 1966). Skipper *et al.* (1964) in exhaustive research with L_{1210} leukaemia showed that one residual cancer cell may lead to the death of the animal when multiplication reaches the lethal number of 1.5×10^9 cells. Better response to chemotherapy, radiotherapy or surgery is attained when the immunological reaction is improved by activation of T cells, macrophages, NK cells and even SRE stimulation has been widely used. Also treatment, the mechanism of which is not yet clear, such as with BCG currently tested in nude mice inoculated with human cancer (Machado *et al.*, 1988) or in human clinical experiments (Garvin *et al.*, 1990; Benson *et al.*, 1989) has been used. Therefore immune stimulants and chemotherapy must be tested to improve therapeutic efficacy.

Olivacine and ellipticine, pyridocarbazole alkaloids represent a group of anticancer substances which still attract the attention of several investigators. New syntheses have been attempted (Karmakar *et al.*, 1991) and several derivatives have been prepared in order to obtain better antineoplastic compounds (Gribble *et al.*, 1992; Modi *et al.*, 1991) or to be tested as a new anti-AIDS drug (Li *et al.*, 1992).

Olivacine, a natural product, has been extracted in Brazil and elsewhere (Gilbert, 1965). It is found in *Aspidosperma nigricans* in sufficient amounts for more advanced studies than just primary screening, when this means working with small animals or cell culture.

The objective of this paper is to observe the action of olivacine on L_{1210} leukaemic mice inoculated with different numbers of cells:

- when associated with deoxycytidine looking for a possible potentiation of antitumoural effect;
- when associated with a hyperimmune heterologous

* Author to whom correspondence should be addressed.

serum, looking for haematological changes that might improve the therapeutic response.

The association with deoxycytidine was made in view of the results obtained by investigators (Sylven, 1969) who showed that cancerous cells release toxins which are harmful to the host organism. *In vitro* experiments with fibroblasts, under optimal experimental and culture conditions, showed that fibroblast growth can be stopped when small amounts of sterilized interstitial liquid from mouse mammary tumour or Walker tumour are added (Holmberg, 1968). When deoxyribonucleosides are added, the cells grow normally. Holmberg (1968) postulated that it may be a matter of interference with the process of deoxyribonucleic acid synthesis; therefore the need for increased availability of deoxyribonucleosides.

On the basis of the results obtained by these investigators and several experimental studies with deoxycytidine (its phosphorylated metabolite competes for DNA polymerase and for incorporation into DNA) (Bhalla *et al.*, 1987) and the fact that the substance itself is being used as modulator against high dose ARA-C toxicity (Bhalla *et al.*, 1990), we tried to determine if deoxycytidine could potentiate olivacine antitumour activity.

MATERIAL AND METHODS

Olivacine. This was obtained from the root bark of *Aspidosperma nigricans* or *Aspidosperma olivaceum*, extracted with ethanol and purified in the usual way for pyridocarbazole alkaloids (Gilbert, 1965).

Deoxycytidine. A dose of 50 mg/kg of 2-deoxycytidinium chloride (Merck, Darmstadt, FRG) was injected intraperitoneally on a daily regimen.

Coadjuvant. Heterologous hyperimmune serum (horse), supplied by Dr P. Bueno (Instituto Biológico, São Paulo), was used; 0.2 mL ampules were applied subcutaneously at 5-day intervals.

Animals. BDF₁ (C57BL/6 × DBA/2) mice were utilized, originating from pure A.D. Little strains (USA) and raised at the Instituto Biológico. Their weight varied between 18 and 21 g for males, and 17–20 g for females.

L₁₂₁₀ tumours. The tumours were kept in liquid nitrogen and then transplanted into BDF₁ and DBA/2 mice, alternately, on a weekly basis.

Biological test. Briefly the bioassay follows the procedure established by the National Cancer Institute (Geran *et al.*, 1972): BDF₁ mice, duly identified and weighed, were inoculated intraperitoneally with a predetermined number of viable cells (trypan blue-counting) on day 0, and treated 24 h later on alternate days, intraperitoneally. The animals were observed daily at the same time of day, and any death or anomaly was recorded. On day 5 the animals were weighed again. The mean survival time of treated and control animals was calculated and the result given as the percentage of inhibition in relation to the controls or increase in life span.

Haematological determinations. Blood was collected, by puncturing the mouse retro-orbital plexus with a Pasteur pipette, in a sufficient volume for several determinations, on day 7, day 30 (end of treatment) and also on day 75 and 120. Cell counts were done electronically (Coulter Counter, model D, Hylealez, Florida, USA). Haemoglobin was measured by photocolorimetry (Hemoglobinometer Atago, Tokyo, Japan) as cyano-metahaemoglobin. Cell volume was determined with a

Table 1. Therapeutic effect of 25 mg/kg and 50 mg/kg olivacine doses on alternate days in mice with L₁₂₁₀ leukaemia, as related to the number of leukaemic cells

Number of cells	Mean of survival (days) in controls	Mean of survival (days) in treated ^b
10 ⁶ ^a	8.4 ± 0.5 ^d	17.8 ± 2.3 ^c
10 ⁵	9.0 ± 0.39	15.8 ± 5.2 ^c
10 ³	10.4 ± 0.27	25.3 ± 5.6 ^c
10 ²	12.3 ± 1.4	22.7 ± 8.4 ^c

^a 50 mg on alternate days.

^b Day 30 was the evaluation day.

^c Significant by t-test.

^d mean ± standard deviation.

Universal microhaematocrit. Blood smears for leucocyte formula were stained by the method of May-Grünwald-Giemsa.

RESULTS

Olivacine (25 mg/kg body weight) administered on alternate days to BDF₁ mice showed activity at all levels of cells used in the experiments, as can be seen in Table 1, with a significant increase in survival compared with the controls. Figure 1 correlates the percentage of live animals with days of survival in a series of experiments. While no animal survived the treatment when inoculated with 1 × 10⁵ leukaemic cells, this is not the case with animals receiving 10²–10³ cells. The percent-

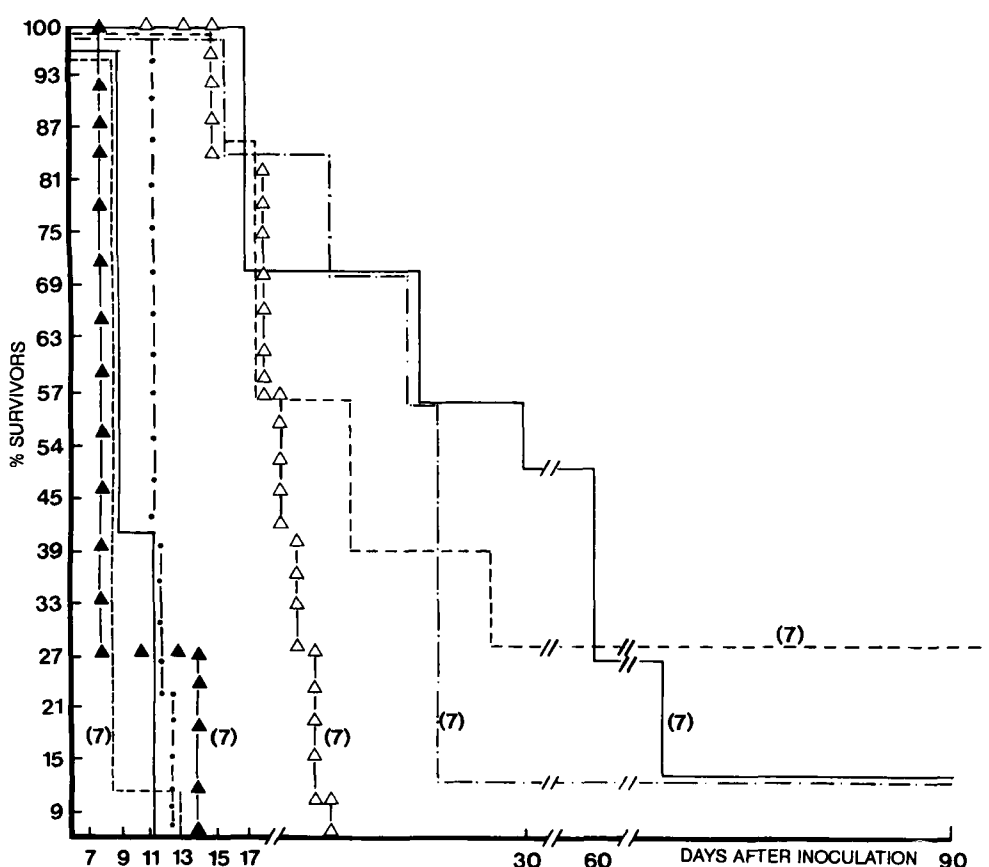


Figure 1. Survival curves after administration of olivacine (25 mg/kg), on alternate days, to mice inoculated with ▲, 10⁵; ●, 10⁴; —, 10³; —, 10² leukaemic cells, respectively. Each symbol indicates an experiment; the filled symbols indicate the respective control. The number in parentheses indicates the number of animals used.

Table 2. Percentage of killed cells in animals inoculated with 10^2 or 10^3 L₁₂₁₀ leukaemia cells after treatment with 25 mg/kg olivacine on alternate days

Experiment	Number of inoculated cells	Approximate percentage of the leukaemia population killed by treatment	Experiment	Number of inoculated cells	Approximate percentage of the leukaemia population killed by treatment			
			I	VI	VII	VIII	IX	X
II	1000	99.9999		100	99.9999			
III	1000	99.9628		100	99.9999			
IV	1000	99.9573		100	99.9999			
V	1000	99.5830		100	99.9999			

Table 3. Survival of mice with L₁₂₁₀ leukaemia elicited by olivacine and the combination of olivacine plus deoxycytidine, as a function of inoculated leukaemia cells

Number of inoculated cells	Olivacine % increase in survival as related to controls	Olivacine and deoxycytidine % increase in survival as related to controls
10 ⁵	94	123
10 ⁵	123	114
10 ⁵	66	90
10 ⁵	88	74
10 ⁵	40	34
10 ²	44	81
10 ²	86	112
10 ²	105	92
10 ²	115	105
10 ²	121	86
10 ²	101	100
10 ²	130	112

The two treatments do not differ by Snedecor's F-test.

age of the population of leukaemic cells destroyed by the treatment in these multiple dose experiments (Table 2) was calculated according to Skipper *et al.* (1964) assuming that their therapeutic effect should be equivalent to that of a single dose X, that eliminates most leukaemic cells in the population of an animal group and produces the same number of survivors.

Based on the data of Skipper *et al.*, it was thought that a 15 × 9 mg/kg dose of 1,3-bis(2-chloro-ethyl)-nitrosourea should be equivalent to a single 66 mg/kg dose (both regimens produce 2/10 survivors in mice inoculated with 10⁵ L₁₂₁₀ leukaemic cells).

Association of deoxycytidine with olivacine (Table 3) did not change the results of the medication. Values were found favouring one group or the other, but they were not significant by Snedecor's F-test.

The use of heterologous serum as a coadjuvant for the olivacine treatment of animals which received 10²-viable cells, besides producing a 'cure' in several animals, alive 120 days later (Table 4), also induced haematological alterations which were different to those observed in animals treated with olivacine alone. Olivacine medication resulted in lymphopenia as shown in Table 5 which also gives normal leucogram values.

Association of olivacine with horse serum elicited an increase in survival compared with the controls (a fact also noted when olivacine alone is used), plus leucocytosis and lymphocytosis observed at the end of the treatment (day 30). These leukaemic symptoms, of course, were also found in untreated animals, whose blood was collected 5 days after implantation of leukaemic cells. We wish to point out that the 'cured' animals appeared to be clinically healthy up to 120 days after the beginning of the experiment.

Table 4. Mean survival time and survivors on days 30, 60 and 120 of mice implanted with 10² leukaemic cells and treated with olivacine (25 mg/kg i.p.), olivacine (25 mg/kg i.p.) plus heterologous serum (0.2 mL s.c. every 5 days). Controls mean survival time is also given

Experiment	Treatment	Change in mouse body weight between day 1 and 5		Mean survival time		Inhibition %	Day 30 ^a		Survivors Day 60		Day 120	
		Treated	Control	Treated	Control		T	C	T	C	T	C
I	Olivcine	-0.40	+1.20	23.00 ± 2.20 ^a	13.10 ± 0.78	175.57	2/10	2/9	0/10	2/9	0/10	2/9
	Olivacine + serum	0.00	+1.20	18.60 ± 1.50	13.10 ± 0.78	141.98	4/10	2/9	3/10	2/9	3/10	2/9
II	Olivacine	-0.75	+1.00	27.00 ± 2.80	11.30 ± 0.89	238.93	3/9	0/9	3/9	0/9	3/9	0/9
	Olivacine + serum	0.00	+1.00	26.30 ± 0.89	11.30 ± 0.89	232.15	9/9 ^c	1/9	7/9	1/9	7/9	1/9
III	Olivacine	-1.10	-0.90	26.50 ± 6.40	18.70 ± 4.70	141.71	6/9 ^b	0/9	6/9	0/9	6/9	0/9
	Olivacine + serum	-1.50	-0.90	30.00 ± 0.00	18.70 ± 4.70	160.42	9/9 ^c	0/9	9/9	0/9	9/9	0/9
IV	Olivacine	-1.90	-0.90	30.00 ± 0.00	15.80 ± 2.11	189.87	8/9 ^c	1/9	8/9	1/9	8/9	1/9
	Serum	-0.10	-0.90	22.70 ± 7.40	15.80 ± 2.11	143.03 ^f	4/9	1/9	4/9	1/9	4/9	1/9
V	Olivacine + serum	-1.90	-0.90	29.30 ± 2.00	15.80 ± 2.11	185.44	8/9 ^c	1/9	8/9	1/9	7/9	1/9
	Serum	0.00	+0.30	12.30 ± 2.20	13.00 ± 1.50	105.69	0/10	1/10	0/10	1/10	0/10	1/10
	Olivacine + serum	-1.00	+0.30	26.20 ± 4.80	13.00 ± 1.50	201.58	9/10 ^c	1/10	9/10	1/10	9/10	1/10

^a Mean ± SD

^{b, c} Significant by the exact Fischer test: ^b p = 0.024; ^c p = 0.004. Difference compared with control.

^d Inhibition ≥ 125% means activity.

^e Day 30, evaluation day to compute inhibition.

^f Results not reproducible in our experiments with L₁₂₁₀.

Table 5. Effects of treatment with olivacine and olivacine plus serum on leucogram of BDF₁ mice inoculated with 10² cells of L₁₂₁₀

	Normal	Increased	Decreased	Observations
I. Observation on global leucometry				
Normal value: range per mm ³	4000–7900			
Inoculated animals untreated	0	+	0	The increases varied between 11 000 and 23 000, especially for lymphocytopenia
Inoculated animals treated with olivacine	0	0	+	Decrease was between 2900 and 3100, especially for cytopenia
Inoculated animals treated with olivacine + serum	0	+	0	
II. Observation on neutrophils				
Normal values: range per mm ³	680–2535			
Inoculated animals untreated	0	+	0	The increases (absolute neutrophilia) varied between 2790 and 5280 mm ³
Inoculated animals treated with olivacine	0	0	+	Decrease (absolute neutropenia) was between 348 and 540/mm ³
Inoculated animals treated with olivacine + serum	0	+	0	
III. Observation on lymphocytes				
Normal values: range per mm ³	2880–6000			
Inoculated animals untreated	0	+	0	The increases (absolute lymphocytosis) varied between 7670 and 18367/mm ³
Inoculated animals treated with olivacine	0	0	+	Decrease (absolute lymphopenia) was between 1742 and 2378/mm ³
Inoculated animals treated with olivacine + serum	0	+	0	
IV. Observation on monocytes				
Normal values: range per mm ³	80–624			
Inoculated animals untreated	0	+	0	The observed increase varied between 684 and 1533/mm ³
Inoculated animals treated with olivacine	0	+	0	
Inoculated animals treated with olivacine + serum	0	+	0	
V. Cytological observations on lymphocytes				
Inoculated animals untreated	0	+ ^a	+ ^b	
Inoculated animals treated with olivacine	0	0 ^a	0 ^b	The cytological alteration concerns nuclear and/or cytoplasmatic polymorphism, Grumpecht's nuclear shadows, free nuclei etc.
Inoculated animals treated with olivacine + serum	0	± ^a	0 ^b	

^a Altered. ^b Greatly altered.

DISCUSSION

The greater efficiency of olivacine as the number of inoculated cells decreases corresponds to what one would expect according to the studies of Skipper *et al.*, who showed that the percentage of cell populations of different sizes destroyed by a given effective dose is reasonably constant. Thus, in spite of cell multiplication, the probability of obtaining cured animals increases as the number of inoculated cells decreases.

We believe that, possibly, the immunological reaction may eliminate the few residual cells. The number of residual cells after treatment was calculated for the animals that received 10³ and 10² cancerous cells (using a greater number of experiments). In this case of chronic dose therapy, the approximate percentage of destroyed cells for each experimental group which received 10² and 10³ cells, calculated as described in the results, still gives an idea of the almost constant percentage of cells killed by the treatment. We used chronic treatment, after years of experimental work

(Linardi *et al.*, 1975; De-Oliveira, 1988) in contrast to the work of Skipper, who points to a single high dose as being a more successful therapy than a fractional daily dose. It must be remembered that delayed therapy is seldom used in L₁₂₁₀ leukaemia and metastatic cancer is an important factor to be considered when looking for curability. Also, despite L₁₂₁₀ being a very good model, sensitive to most human anticancer drugs, it has the same limitation as Ehrlich ascitic tumour, as an *in vivo* experiment carried out (both drug and leukaemic cells injected i.p.) *in vitro* and a single dose on day 1 may eliminate a great number of leukaemic cells, acting perhaps as chemosurgery, but not resembling human metastatic leukaemia. For this reason and also because of the nonsynchronous multiplication of cancerous cells we believe chronic doses to be a quite efficient choice, and immunological stimulation (frequently drugs are immunosuppressants) could promote better results.

Olivacine in association with deoxycytidine did not potentiate the action of the drugs, however, association with the heterologous serum gave quite promising results.

The mice inoculated with leukaemic cells, but untreated, showed leucocytosis varying between 11 400/mm³ and 23 250/mm³, especially in terms of increased and cytologically altered lymphocytes. An increase in neutrophils was observed in untreated mice and in mice treated with olivacine plus heterologous serum (horse). The lymphocytes clearly increased in the untreated animals (leukaemic lymphocytes) and in those treated with olivacine plus heterologous serum, indicating, in the latter case, immunologically competent lymphocytes, since the animals were 'cured' after more than 120 days' survival (when the leucogram attained normal borderline values for neutrophils, monocytes and leucocytes). Treatment with olivacine alone caused leucopenia, mainly in terms of lymphocy-

topenia and neutropenia. Similar results for a decrease in white blood cells have been described (Cros *et al.*, 1975) for treated mice infected by L₁₂₁₀ leukaemia with another pyridocarbazole alkaloid, 9-hydroxy-ellipticine: a reduction in polynuclear neutrophils was observed after 19 injections, when the drug was administered once every 3 days. Leucopenia was also observed in dogs (Pham-Huu-Chanh *et al.*, 1974) when doses of 5 to 10 mg/kg ellipticine were applied over a period of 2 to 5 weeks. Possibly the presence of a methyl group in position 1 or 11, not suppressing the biological activity, does not alter the mechanism of action of the isomeric olivacine, i.e. the same intercalation in cellular DNA, causing chromosome aberrations, as those observed for the ellipticine derivative.

Cytological examination of the white cells, lymphocytes in particular, showed that of the two significant treatments, that combining olivacine and heterologous serum allowed better preservation of the cells. Cytology of the red cells showed no signs of anaemia. Thus, the associated use of two seemingly antagonistic factors, olivacine which produces lymphopenia in healthy animals, and serum, elicited a good response in the animals studied. This type of association seems potentially viable to us for tumour treatment, considering that a single L₁₂₁₀ cell can lead to the death of an animal. They may be particularly useful in avoiding relapses, since the conditions of our experiments—the use of a small number of tumoural cells—are close to those of patients who have just completed a treatment that has eliminated most of their cancerous cells.

Acknowledgements

We thank Joaquim Moraes de Oliveira for technical assistance and Fundação de Amparo à Pesquisa do Estado de São Paulo (FAPESP) for financial support.

REFERENCES

- Benson III, A. B., Rosen, S. I., Salwen, S. *et al.* (1989). A pilot study of active specific immunotherapy with autologous tumor cell BCG vaccine and 5-fluoro-uracil (5-FU) in metastatic colorectal carcinoma. *Eightieth Annual Meeting of Am. Cancer Res. Proc. Am. Assoc. Cancer Res.* **30**, 380.
- Bhalla, K., Kamar, M., Baker, M., and Grant, S. (1990). Deoxycytidine (IND 28108) protects against the infusion of high doses ARAC, without abrogating antileukemic effects. *Eightieth Annual Meeting of Am. Cancer Res.* **31**, 208.
- Bhalla, K., MacLaughlin, W., Cole, J., *et al.* (1987). Deoxycytidine preferentially protects normal versus leukemic myeloid progenitor cells from cytosine-arabinose-mediated cytotoxicity. *Blood* **70**, 568–571.
- Cros, S., Sorbara, R., Moisand, Ch., Dat-Xuong, N., Lecointe, R., and Paoletti, C. (1975). Toxicological and pharmacological studies on 9-hydroxy-ellipticine in mice. *Toxicol. Appl. Pharmacol.* **33**, 484–497.
- Darnell, R. B. and DeAngelis, L. M. (1993). *Lancet* **341**, 21–22.
- De-Oliveira, M. M. (1988). Synthesis of olivacine and their salts. Anticancer tests. *Brazilian and German Meeting on the Chemistry of Natural Compounds. October 3–6 Rio de Janeiro, Brazil. Abstracts by Federal University of Rio de Janeiro.*
- Emerson, T. C. and Cole, W. H. (1966). *Spontaneous Regression of Cancer*. Philadelphia W13, Saunders. Apud
- Garvin, T. J., Yuan, J. J. J., Rattliff, T., and Catalona, W. J. (1990). The effect of cigarette smoking on bladder cancer response to intravesical bacillus Calmette-Guérin (BCG). *Eighty-first Annual Meeting of Am. Ass. Cancer Res. Proc. Am. Cancer Res.* **31**, 187.
- Geran, R. J., Greenberg, M. H., Schumacher, M. M., and Abbott, B. J. (1972). Protocol for screening chemical agents and natural products against animal tumors and other biological systems. *Cancer Chemother. Rep.* **3**, 1–103.
- Gilbert, B. (1965). The alkaloids of *Aspidosperma*, *Diplorrhynchus*, *Kapsia*, *Ochrosia*, *Pleiocarpa* and related genera. In, *The Alkaloids*, Volume VIII, ed. by R. H. Manske, pp. 474–477 and references therein. Academic Press, New York.
- Gribble, G. W., Saulnier, M. G., Obazanutailis, J. A., and D. M. Ketcha, (1992). A versatile and efficient construction of the 6H-pyrido[4,3b] carbazole ring system of antitumor alkaloids ellipticine, 9-methoxy-ellipticine and olivacine and their analogues. *J. Org. Chem.* **57**, 5891–5899.
- Holmberg, B. (1968). Studies on a dialysable polypeptide from tumor fluid. *Eur. J. Cancer* **4**, 263–269.
- Karmakar, A. C., Kar, G. K., and Ray, J. K. (1991). Efficient synthesis of 5-demethyl-6-methylisoellipticine and utilization of the methodology to prepare angular and linear pyridocarbazoles. *J. Chem. Soc. Perkin Trans. 1*, 1997–2002.
- Li, D., Balzarini, J., Schols, D., Meunier, B., and Declercq, E. (1992). Anti human immunodeficiency virus effects of cationic metalloporphyrin-ellipticine complexes. *Biochem. Pharmacol.* **44**, 1675–1679.

- Linardi, M. C. F., De-Oliveira, M. M. and Sampaio, M. R. P. (1975). A lapachol derivative active against mouse lymphocytic leukemia P-388. *J. Med. Chem.* **18**, 1159–1161.
- Machado, L. D., Machado, J. C., Ogata, T. R. P. et al. (1988). BCG action in immunotherapy of new-born nude mice heterotransplanted with human tumors cell line (KB). *Acta Oncol. Bras.* **8**, 90–94.
- Modi, P. S., Michael, M. A., and Archer, S. (1991). An efficient synthesis of C-11 substituted 6H-pyrido[4,3b] carbazoles. *Tetrahedron* **47**, 6539–6548.
- Pham-Huu-Chanh, Sorbara, R., Dat-Xuong, N., Le Pecq, J. B., and Poletti, C. (1974). Actions cardiovasculaires et toxicites de l'hydroxy-9-ellipticine chez le chien. *C R Acad. Sci. (Serie D)* **270**, 1039–1041.
- Skipper, H. E., Schabel, F. M. Jr, and Wilcox, W. S. (1964). Experimental evaluation of potential anticancer agents XIII. On the criteria and kinetics associated with curability of experimental leukemia. *Cancer Chemother. Rep.* **35**, 1–111.
- Sylven, B. (1969). Factors produced by tumoral cells which contribute to the death of cancer patients. Lecture delivered at the Carlo Erba Foundation, Milan, Italy. February 26.

***In vitro* cytotoxicity of S16020-2, a new olivacine derivative**

Stéphane Léonce, Valérie Perez, Marie-Rose Casabianca-Pignede, Monique Anstett, Emile Bisagni¹, Alain Pierré and Ghanem Atassi

Division de Cancérologie Expérimentale, Institut de Recherches Servier, 92150 Suresnes, France; ¹Institut Curie, Recherche, UMR 176 CNRS, Centre Universitaire, 91045 Orsay, France

Key words: S16020-2, adriamycin, multidrug resistance, P-glycoprotein, flow cytometry, topoisomerase

Summary

S16020-2 is a new olivacine derivative which has recently shown a marked antitumor activity in various experimental models. This study was undertaken in order to measure the inhibition of the proliferation of various sensitive and resistant tumor cell lines, by S16020-2, and to obtain information concerning its mechanism of action.

For a continuous exposure, S16020-2 was as cytotoxic as adriamycin (ADR) (mean IC₅₀ of about 28 nM) and on average, 46 fold more potent than elliptinium acetate (ELP), against a panel of 20 non-multidrug resistant cell lines. With a short exposure (1 hour) followed by a post-incubation of 95 hours in drug-free medium, S16020-2 was 5 and 6 fold more cytotoxic than ADR for human lung A549 and murine melanoma B16 cells, respectively. Furthermore, S16020-2 inhibited more actively the formation of colonies issued from proliferating cells, compared to colonies issued from quiescent A549 cells. Because quiescent cells demonstrated a 3 fold lower level of topoisomerase IIα (topo II) than proliferating cells, these results suggest that this enzyme could be a potential target for S16020-2. In addition, as demonstrated by flow cytometric studies, S16020-2 intercalated into DNA and induced a cell cycle arrest in G2.

Cell lines displaying the multidrug resistance (MDR) phenotype, P388/ADR-1, P388/ADR, P388/VCR-20, KB-A1, DC-3F/AD, S1/tMDR, and Colo320DM, were more sensitive to S16020-2 than to ADR or ELP, as shown by the mean resistance factors, 8, 201, and 23 respectively. In addition, the two cell lines displaying the pure classical MDR phenotype, linked exclusively to the P-glycoprotein (P-gp) overexpression (P388/VCR-20 and S1/tMDR), were as sensitive to S16020-2 as their sensitive parental counterparts, although they were resistant to ADR.

S16020-2 is thus one of the most potent olivacine and ellipticine derivative yet characterized. The good cytotoxicity of S16020-2 against cells displaying a P-gp-mediated multidrug resistance, and its antitumor activity *in vivo* delineate an important chemotherapeutic potential for this drug.

Introduction

S16020-2 is a new pyridocarbazole derivative characterized by a basic N-dialkyl aminoalkyl-carboxamido group grafted onto an olivacine chromophore (Figure 1). S16020-2 has been recently selected from a series of derivatives, on the basis of its high cytotoxicity for L1210 cells and strong antitumor activity against murine P388 leukemia and Colon 38 adenocarcinoma [1]. More recent studies have shown a marked antitumor ac-

tivity of S16020-2 in various experimental models, particularly the s.c. or i.v. Lewis lung carcinoma in which this compound was curative [2]. It is thus important to further characterize the *in vitro* pharmacology of this compound, particularly against a panel of human cell lines including resistant lines.

Considering the polycyclic structure of S16020-2, and the fact that this compound was shown to intercalate into DNA and to interact with the topo II enzymes in a cell-free system [3], one or both of two mechanisms of resistance can be envisaged: i)

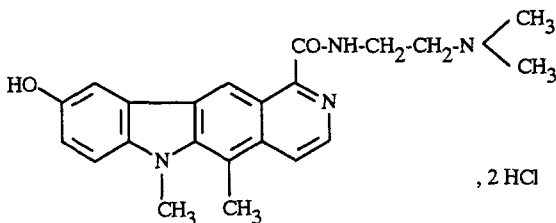


Figure 1. Chemical structure of S16020-2.

the classical MDR linked to the overexpression of the membrane-associated P-gp which reduces the intracellular drug accumulation [4], and ii) the atypical MDR due to qualitative and/or quantitative modification of the target enzymes, the topo II [5, 6].

The present study was undertaken in order to measure the cytotoxicity of S16020-2 on murine and human cell lines of various histological types, both sensitive and resistant, and to further characterize its mechanism of action at the cellular level. In this aim, we have measured the inhibition of the proliferation of 27 rodent and human cell lines, some of them displaying the MDR phenotype, by S16020-2, and, as reference molecules, ADR and ELP, an ellipticine analogue previously shown to have a modest, but definite activity in the clinic in the treatment of advanced breast cancer [7].

Three approaches were used to study the mechanism of action of S16020-2: i) the inhibition of ethidium bromide (EtBr) intercalation into DNA of intact nuclei, ii) the perturbation of the cell cycle, and iii) the comparison of the sensitivity of exponentially growing cells with that of plateau phase cells, in which topo II content is reduced. This latter study was carried out on a human lung cancer cell line, A549, and its sensitivity was measured by a colony forming assay after a brief exposure of the cells to the drug. These experimental conditions are probably more relevant of the clinical situation than a continuous exposure of proliferating cells to the drugs.

Materials and methods

Compounds

ADR was purchased from Farmitalia, ELP from Pasteur (France), and Amsacrine (m-AMSA) from

Subtantia, (France). S16020-2 was synthesized in our institute as previously described [1]. All the compounds were solubilized at 10⁻² M in distilled water, aliquoted and stored at -20°C. The solutions were thawed only once, just before the experiments.

Cell lines

The origin and the characteristics of the cell lines used are listed in Table 1. All the cells were maintained in RPMI1640 medium (except the KB-3-1 and KB-A1 cells cultivated in DMEM medium) supplemented with 10% decomplemented fetal calf serum (FCS), 2 mM L-glutamine, 100 U/ml penicillin, 100 µg/ml streptomycin and 10 mM Hepes, pH 7.4. Cells were grown in this complete culture medium at 37°C in 5% CO₂/95% air. All media and supplements were from Gibco.

The P-gp expression was quantified as previously described [4]. Briefly, sensitive and resistant cells were fixed with methanol, washed twice in phosphate-buffered saline (PBS) and reacted for 1 hour with 5 µg/ml of a fluorescein isothiocyanate-conjugated anti P-gp antibody (C219-FITC, Centocor Inc., Malvern, PA, USA) in PBS containing 0.5% bovine serum albumin, 0.3% Tween-20. After 1 hour of incubation at 4°C, samples were washed twice, resuspended in PBS, and analyzed on an ATC3000 flow cytometer (Bruker, France). Results are expressed as relative P-gp overexpression: mean of C219-FITC fluorescence of resistant cells/mean of C219-FITC fluorescence of corresponding sensitive cells. For each cell line, controls done with an FITC-conjugated isotypic antibody showed no P-gp-related fluorescence.

Standard proliferation assay

The principle of this assay and its application to anticancer drug screening has been the subject of numerous publications [8]. Briefly, adherent cells were trypsinized and seeded in 96 well-microplates at the indicated densities, previously determined to maintain control cells in exponential phase of growth for the duration of the experiment and to obtain a linear relationship between the opti-

Table 1. Cell line characteristics

Cell lines	Origin	Histological type	DT ^a
Murine			
L1210	ATCC	Lymphocytic leukemia	9
P388	NCI	Lymphocytic leukemia	11
P388/ADR	NCI	Lymphocytic leukemia	12
P388/ADR-1	b	Lymphocytic leukemia	13
P388/VCR-20	c	Lymphocytic leukemia	16
M5076	NCI	Reticulosarcoma	28
C38	NCI	Colon adenocarcinoma	24
B16	ATCC	Melanotic melanoma	20
LLC	NCI	Lewis lung carcinoma	27
Hamster			
DC-3F	d	Immortalized normal lung	18
DC-3F/AD	d	Immortalized normal lung	19
Human			
<i>Lung</i>			
NCI-H146	ATCC	Small cell carcinoma	144
NCI-H125	NCI	Adenocarcinoma	27
A-427	ATCC	Carcinoma	44
A-549	ATCC	Carcinoma	20
Calu-6	ATCC	Anaplastic carcinoma	35
NCI-H460	ATCC	Carcinoma	21
S1	e	Epidermoid carcinoma	19
S1/tMDR	e	Epidermoid carcinoma	24
SK-MES-1	ATCC	Epidermoid carcinoma	44
<i>Colon</i>			
Colo320DM	ATCC	Adenocarcinoma	26
<i>Leukemia</i>			
HL60	ATCC	Promyelocytic	36
<i>Breast</i>			
MCF7	ATCC	Adenocarcinoma	70
MDA-MB-231	ATCC	Adenocarcinoma	25
BT20	ATCC	Carcinoma	120
<i>Miscellaneous</i>			
KB-3-1	f	Epidermoid carcinoma	19
KB-A1	f	Epidermoid carcinoma	26

^a Abbreviations used: DT, doubling time (hours).^b Dr S. Cros (L.P.T.F., CNRS Toulouse, France).^c Institut de Recherches Servier, Suresnes, France.^d Dr A. Jacquemin-Sablon (IGR, Villejuif, France).^e Dr F. Bass (The Netherlands Cancer Institute, Amsterdam, The Netherlands).^f Dr M. Gottesman (NCI, Bethesda, USA).

bated for 4 hours at 37°C. The medium was aspirated and the formazan solubilized by 100 µl of Dimethylsulfoxide. The optical density (O.D.) was read at 540 nm with a plate reader (Multiskan MCC, Labsystem) connected to a computer. The percentage of growth was calculated for each well: % growth = (O.D. treated cells/O.D. control cells) × 100. The percentages of growth of the tri- or hexuplicate were then averaged and plotted as a function of the log of the concentration. The IC₅₀ (concentration reducing by 50% the O.D.) was calculated by a linear regression performed on the linear zone of the curve. For a given compound and a given line, the mean IC₅₀ ± s.e.m. was calculated.

For a brief exposure, a similar protocol as described above was used, except that B16 and A549 cells were exposed to the drugs for only 1 hour, washed twice with drug-free culture medium and incubated for 95 hours.

Colony forming assay

A549 cells were seeded (10⁵ cells/flask per tested concentration) as monolayer cultures for 24 hours in complete culture medium (proliferating cells), or for 3 days in complete culture medium followed by 3 days in medium without FCS (plateau cells). Cells were then exposed for 1 hour to various concentrations of S16020-2 or ADR, trypsinized and seeded at 5000 cells/dish (3 dishes/concentration) in complete medium containing 0.3% agarose type VII (Sigma). Cells were incubated at 37°C for 14 days for colony formation, stained with MTT, and colonies were counted on an image analyzer AMS 40-10 (Systèmes analytiques, France). The plating efficiency was, for untreated cells, about 20% and was not affected by cell density. Results are expressed as percentages of colonies with respect to untreated cells normalized at 100%.

Identification of proliferating cells

Proliferating and quiescent A549 cells were quantified by flow cytometry after fixation and double-staining by 10 µg/ml of the FITC-conjugated monoclonal antibody Ki-67 (Dako, France), and 25 µg/ml of propidium iodide (PI, Sigma) in the pres-

cal density and the number of viable cells [9]. The plates were incubated with the tested compounds for 4 doubling times, the maximum duration being 7 days. At the end of this period, 15 µl of 5 mg/ml 3-(4,5-dimethylthiazol-2-yl)-2,5-diphenyltetrazolium bromide (MTT, Sigma Chemical, Co., St. Louis, MO) were added to each well and the plates incu-

ence of 100 µg/ml RNase (Type III A, Sigma). This staining procedure has been documented in numerous studies [10, 11]. Results are expressed as percentages of resting cells (Ki-negative cells).

Topoisomerase IIα level

To measure the relative cellular content of topo IIα, proliferating and quiescent A549 cells were fixed, washed twice in PBS, and reacted for 30 min, as described [12], with 50 µl of the 6G2 monoclonal antibody, specific for the 170 kD isoform of the DNA topo II [13]. Cells were washed twice in PBS containing 1% bovine serum albumin, 0.2% Tween-20, and incubated for 30 min with 10 µl of FITC conjugated goat anti-mouse antibody (Becton-Dickinson, France). Cells were

then washed twice, resuspended in PBS containing 100 µg/ml RNase, 10 µg/ml PI. The mean FITC fluorescence intensity was measured by flow cytometry.

Cell cycle analysis

L1210 cells (2.5×10^5 /ml) were incubated for 21 hours (approximately two doubling times) with various concentrations (2.5 to 800 nM) of cytotoxic drugs. Cells were then fixed by 70% ethanol, washed twice with PBS and incubated for 30 min in PBS containing 100 µg/ml RNase, 25 µg/ml PI. For each sample, 10,000 cells were analyzed by flow cytometry. Results are expressed as the percentage of cells accumulated in the G2+M phase of the cell cycle.

Table 2. Inhibition of the proliferation of 20 cell lines

Cell line	IC ₅₀ (nM) ± s.e.m.			
	TE ^a	ADR	ELP	S16020-2
<i>Animal</i>				
L1210	48	24.4 ± 2.3	39.4 ± 3.2	6.0 ± 0.4
P388	48	16.0 ± 2.4	33.4	5.5 ± 1.8
M5076	96	26.2 ± 1.3	112.0 ± 2.0	4.9 ± 1.7
LLC	96	7.3 ± 1.9	228.4 ± 51.9	3.2 ± 0.8
DC-3F	72	22.9 ± 10.2	238.0 ± 25.1	11.8 ± 6.4
C38	96	11.3 ± 1.7	37.8 ± 7.8	7.7 ± 1.2
B16	96	6.0 ± 0.7	109.3 ± 17.2	4.8 ± 0.4
<i>Human</i>				
<i>Lung</i>				
NCI-H146	168	9.3	137.9	4.1
S1	96	36.0 ± 8.6	8379.8 ± 2114.1	48.6 ± 16.9
Calu-6	144	10.6 ± 2.5	> 5000	15.7 ± 2.3
A-549	96	42.2 ± 7.8	138.8	29.2 ± 7.3
NCI-H125	120	27.7 ± 7.1	1240.0 ± 863.7	39.8 ± 3.8
NCI-H460	72	42.6 ± 15.3	299.3	43.0 ± 14.2
A-427	168	3.8 ± 0.7	54.7 ± 5.4	6.0 ± 1.3
SK MES-1	168	7.4 ± 1.0	663.5 ± 109.5	19.9 ± 2.8
<i>Leukemia</i>				
HL-60	144	7.1 ± 0.8	927.4 ± 278.3	10.0 ± 0.5
<i>Breast</i>				
MCF7	168	14.0 ± 1.2	390.0 ± 56.7	40.1 ± 9.9
MDA-MB-231	96	209.6 ± 56.8	12175.0 ± 3581.3	231.6 ± 27.1
BT-20	168	14.7 ± 4.6	47.8 ± 13.1	34.7 ± 3.1
<i>Miscellaneous</i>				
KB-3-1	96	10.7 ± 1.9	251.2 ± 48.9	16.6 ± 1.9
Mean IC ₅₀		27.5	1342.3	29.2

^aAbbreviation used: TE, time of exposure (hours).

Inhibition of EtBr intercalation into DNA

L1210 nuclei were isolated by incubating the cells ($10^6/\text{ml}$) for 6 minutes in PBS containing 0.3% nonidet P40. Nuclei were then washed in PBS, incubated for 30 min at 37°C in PBS containing 50 μM EtBr (Sigma), 100 $\mu\text{g/ml}$ RNase in the presence of various concentrations of ADR, S16020-2, or m-AMSA (a well-known intercalating drug), and directly analyzed by flow cytometry. Results are expressed as the mean fluorescence intensity of the G1 phase of the cell cycle. Previous experiments have shown that the best resolution (in terms of coefficient of variation) of the G1 peak was obtained at a concentration of 50 μM EtBr.

Results

Inhibition of cellular proliferation

Sensitive cells

Table 2 shows the mean of the IC_{50} 's obtained on the 7 rodent and 13 human cell lines after a continuous exposure (4 doubling time) of the cells to the drugs. S16020-2 is a potent cytotoxic compound, globally as potent as ADR (mean IC_{50} of about 28 nM) and on average, 46 fold more potent than ELP.

Out of the 20 non-MDR cell lines tested, the HL-60 leukemia and three human pulmonary lines (NCI-H146, A-427 and Calu-6) appeared to be the more sensitive to the action of S16020-2, based on the lower individual IC_{50} values compared to the mean IC_{50} value. No direct relation exists between the rate of proliferation (i.e. the doubling time of the cells) and the sensitivity to S16020-2, or ADR.

The dependence of the cytotoxic effect on the duration of exposure to the drug was then studied on two cell lines, B16 and A549. These cell lines, also used for *in vivo* experiments, were almost as sensitive to ADR as to S16020-2 when treated for 4 doubling times (Figure 2). In contrast, when the same cells were exposed to the drugs for only 1 hour, then washed and incubated for 95 hours in drug-free medium, S16020-2 was significantly more cytotoxic than ADR, with IC_{50} values of 29 and 166 nM (B16 cells), or 206 and 1009 nM (A549 cells), respectively.

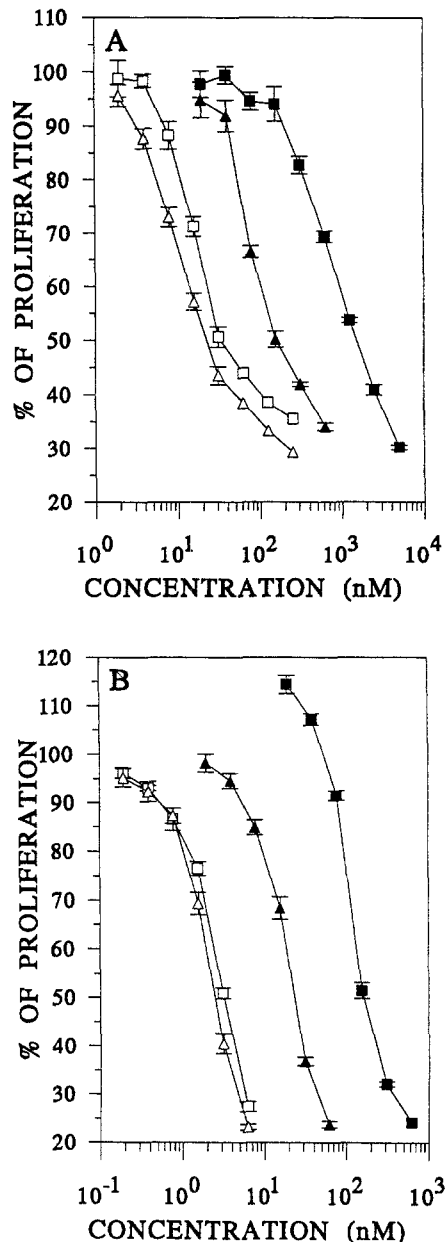


Figure 2. Inhibition of A549 (A) and B16 (B) proliferation by ADR and S16020-2. Cells were incubated with ADR (■, □), or S16020-2 (▲, Δ), for 1 hour (closed symbols), then washed and incubated in drug-free medium for 95 hours. Continuous exposure was for 96 hours (open symbols). The cytotoxicity was determined by the MTT assay. Bars: s.e.m. obtained in 3 independent experiments.

These results, obtained by the MTT colorimetric assay, were confirmed by the colony forming assay performed on the same cell line. S16020-2 was about 5 fold more potent than ADR at reducing by

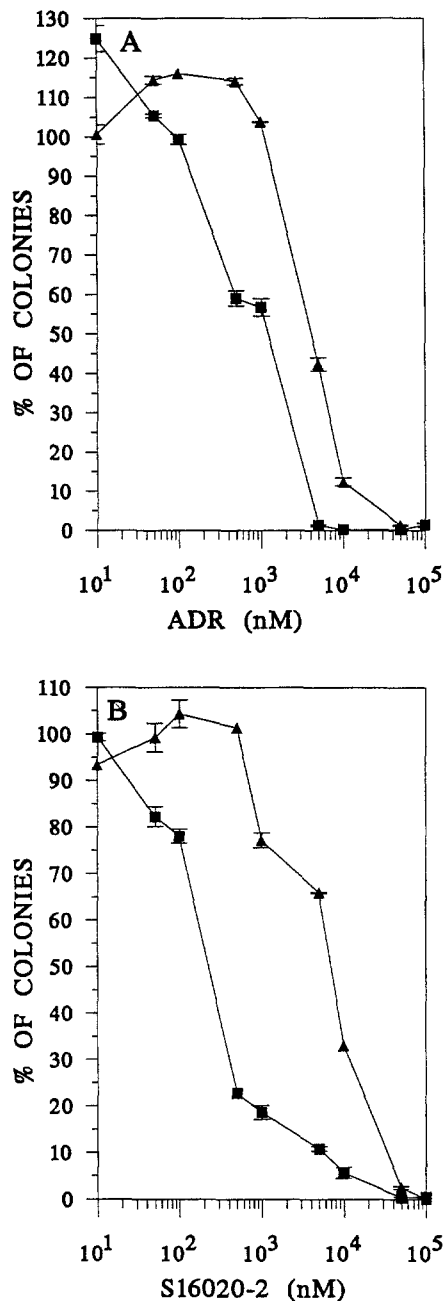


Figure 3. Growth inhibitory effect of ADR (A) and S16020-2 (B) in A549 cells. Proliferating (■) and confluent (▲) cells were treated for 1 hour with ADR or S16020-2, washed and plated for 14 days in agar for colony formation. Results are expressed as percentages of colonies with respect to untreated cells (mean \pm s.e.m. of 3 wells).

50% the formation of the colonies issued from proliferating A549 cells treated for 1 hour (Figure 3).

To study the effect of the drugs on quiescent, non proliferating cells, A549 cells were maintained

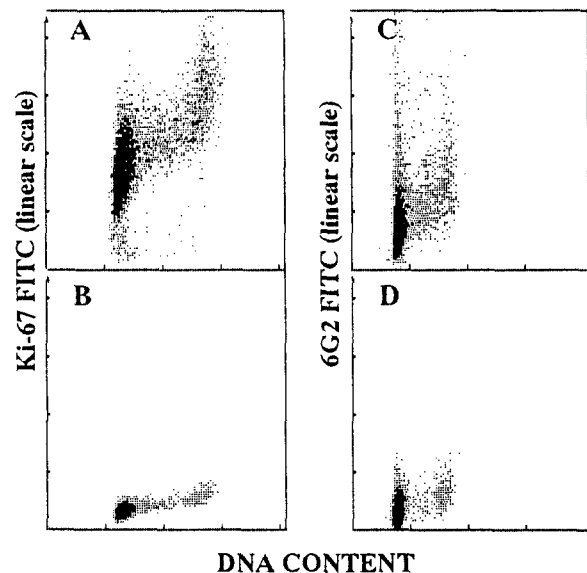


Figure 4. Flow cytometric determination of the proliferation state and topo II α level in A549 cells. Proliferating (A, C) and confluent (B, D) cells were reacted with the antibody Ki-67 (A, B) for proliferation, or the antibody 6G2 (C, D) for topo II α expression. Cells were double-stained with PI for DNA content.

at the plateau phase by serum starvation of high density cultures. In these conditions, 90% of the cells were detected as quiescent by Ki-67 staining (Figure 4B), as compared to proliferating cells (Figure 4A), these cells being viable as demonstrated by their plating efficiency equivalent to that of proliferating cells. S16020-2 was 25 fold less potent on these plateau phase cells than on exponentially growing cells, the difference being less marked in the case of ADR.

Since topo II is the probable target of these compounds, we measured by flow cytometry the relative cellular content of the α isoform in the two different culture conditions. The cellular content of topo II α was shown to be 3 fold lower in quiescent (Figure 4D) than in proliferating cells (Figure 4C).

Resistant cells

The expression of P-gp was measured in 7 resistant cell lines, and compared to that of their corresponding sensitive counterparts. Figure 5 shows the values of P-gp overexpression measured in the MDR cell lines. Compared to the sensitive cells, the resistant cells (P388/ADR-1, P388/ADR, KB-A1, P388/VCR-20, S1/tMDR, and DC-3F/AD),

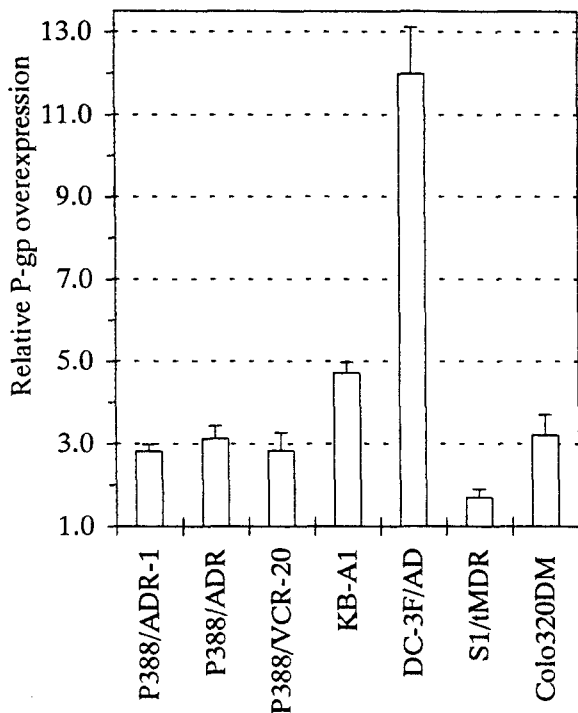


Figure 5. P-gp overexpression in MDR cells. The P-gp expression was determined by flow cytometry after labeling of the cells by the FITC conjugated C219 antibody. Results are expressed as relative P-gp overexpression: mean of C219-FITC fluorescence of resistant cells/mean of C219-FITC fluorescence of corresponding sensitive cells, except for Colo320 DM cells which were compared to the negative control. Bars: s.e.m. obtained in at least 3 independent experiments.

overexpressed the P-gp, DC-3F/AD being the cell line for which the overexpression was the highest. Colo320 DM cells also expressed the P-gp when compared to the control done with the isotypic antibody.

The sensitivity of these cells to the drugs was then measured by the MTT assay performed in standard conditions. Table 3 shows the resistance factors, defined as the ratio IC_{50} resistant cells/ IC_{50} sensitive cells. Overall, the resistant cell lines were less sensitive to ADR and ELP than to S16020-2 (mean factor of resistance 201, 23, and 8, respectively). All the cell lines whose resistance was induced by ADR (the P388/ADR, P388/ADR-1 and KB-A1 lines) were also resistant to S16020-2, but much less so than to ADR. More interestingly, the 2 cell lines displaying the pure classical MDR phenotype, P388/VCR-20 and S1/tMDR, were as sen-

sitive to S16020-2 as their sensitive parental counterparts, although they were resistant to ADR. ELP was also equally cytotoxic against resistant and sensitive S1 cells, but nevertheless 172 and 92 fold less potent than S16020-2 on S1 and S1/tMDR cells, respectively.

Perturbation of the L1210 cell cycle

Figure 6A shows a typical flow cytometric analysis of the cycle of control L1210 cells with an identification of cells in the G0-G1 phase (33%), S phase (48%) and G2+M phase (19%). After treatment with 50 nM S16020-2, a massive accumulation of L1210 cells was observed in the G2+M phase of the cell cycle (Figure 6B). The same type of perturbation was observed with ADR or ELP, but at higher concentrations. The percentage of cells accumulated in the G2+M phase, after treatment for 21 hours was measured for each tested concentration and is outlined in Figure 6C. A dose-dependent effect can be observed with the 3 tested compounds. S16020-2 appears to be the most potent with more than 80% of L1210 cells accumulated in G2+M, at 50 nM. A similar perturbation of the cell cycle was observed with 100 nM ADR and 400 nM ELP. In our experimental conditions, neither abundant debris (lysed cells), mitotic cells, nor polyploid cells (up to 8N DNA) were detected.

Inhibition of EtBr binding to DNA

To investigate the binding of S16020-2 to DNA of intact nuclei, a competition assay was performed using the intercalating dye EtBr whose fluorescence is strongly enhanced when intercalated into DNA [14]. Figure 7A shows an example of flow cytometric histograms obtained after labeling of nuclei by EtBr in the presence of various concentrations of ADR. A decrease in EtBr fluorescence intensity can be observed in the presence of increasing concentration of ADR. Mean fluorescence of the G1 phase was measured for each tested concentration of ADR, S16020-2, or m-AMSA, and reported (expressed as % of control), in Figure 7B. S16020-2 clearly induced a dose-dependent reduction of EtBr fluorescence, and thus,

Table 3. Inhibition of the proliferation of MDR cell lines

Cell line	TE	IC_{50} (nM) \pm s.e.m. and corresponding resistance factor		
		ADR	ELP	S16020-2
P388	48	16.0 \pm 2.4	33.4	5.5 \pm 1.8
P388/ADR	48	3513.0 \pm 1045.8	467.6 \pm 78.9	65.8 \pm 12.4
RF ^a		219.4	14.0	12.1
P388/ADR-1	48	4231.0 \pm 601.5	738.4 \pm 328.6	53.3 \pm 6.1
RF		264.3	22.1	9.8
P388/VCR-20	48	266.3 \pm 24.5	111.2 \pm 11.1	6.7 \pm 1.4
RF		16.6	3.3	1.2
DC-3F	72	22.9 \pm 10.2	238.0 \pm 25.1	11.8 \pm 6.4
DC-3F/AD	96	4559.6 \pm 886.6	1146.0 \pm 212.3	178.3 \pm 45.3
RF		199.5	4.8	15.1
KB-3-1	96	10.7 \pm 1.9	251.2 \pm 48.9	16.6 \pm 1.9
KB-A1	96	5403.0 \pm 712.9	24106.8 \pm 5090.5	124.2 \pm 27.3
RF		505.0	96.0	7.5
S1	96	36.0 \pm 8.6	8379.8 \pm 2114.1	48.6 \pm 16.9
S1/tMDR	96	107.5 \pm 41.1	2327.5 \pm 483.7	25.3 \pm 2.6
RF		3.0	0.3	0.5
COLO320DM	96	162.4 \pm 30.0	4698.8 \pm 805.4	31.4 \pm 7.8
Mean RF		201.3	23.4	7.7

^aAbbreviation used: RF, resistance factor = IC_{50} resistant cells/ IC_{50} sensitive cells.

of its binding to DNA. The ratios (G2+M)/G1, as well as the percentages of cells in the three phases of the cell cycle were constant, indicating that the binding of these drugs was not dependent on the cell cycle phase. The inhibitory effect of S16020-2 was weaker than that of ADR but stronger than that of m-AMSA, suggesting that the affinity of S16020-2 to DNA, in these conditions, is intermediate between those of m-AMSA and ADR.

Discussion

S16020-2 is a new pyridocarbazole derivative characterized by a basic N-dialkyl aminoalkylcarboxamido group grafted onto an olivacine chromophore [1]. The present study was undertaken in order to measure the cytotoxicity of S16020-2 on murine and human cell lines and to obtain information concerning its mechanism of action at the cellular level.

For a continuous exposure of the cells, S16020-2

was a potent cytotoxic compound, globally as cytotoxic as ADR (mean IC_{50} on non-MDR cells of about 28 nM), and 46 fold more than ELP. These results identify S16020-2 as one of the most potent olivacine and ellipticine derivatives yet characterized. Considering the limited number of human cell lines tested per tissue, it is difficult to draw any definitive conclusions on the specificity of S16020-2 for a given histological type. However, 3 lung cell lines and the HL60 leukemia line appeared particularly more sensitive than the other cell lines tested.

After a 1 hour exposure to the drugs, B16 and A549 cells appeared 5 to 6 fold more sensitive to S16020-2 than to ADR, even though both compounds were equitoxic for a continuous exposure suggesting a higher cellular accumulation of S16020-2 than ADR, and/or a facilitated ability to reach its target.

Using a colony forming assay we have shown that S16020-2 and ADR inhibited the formation of colonies issued from proliferating A549 cells

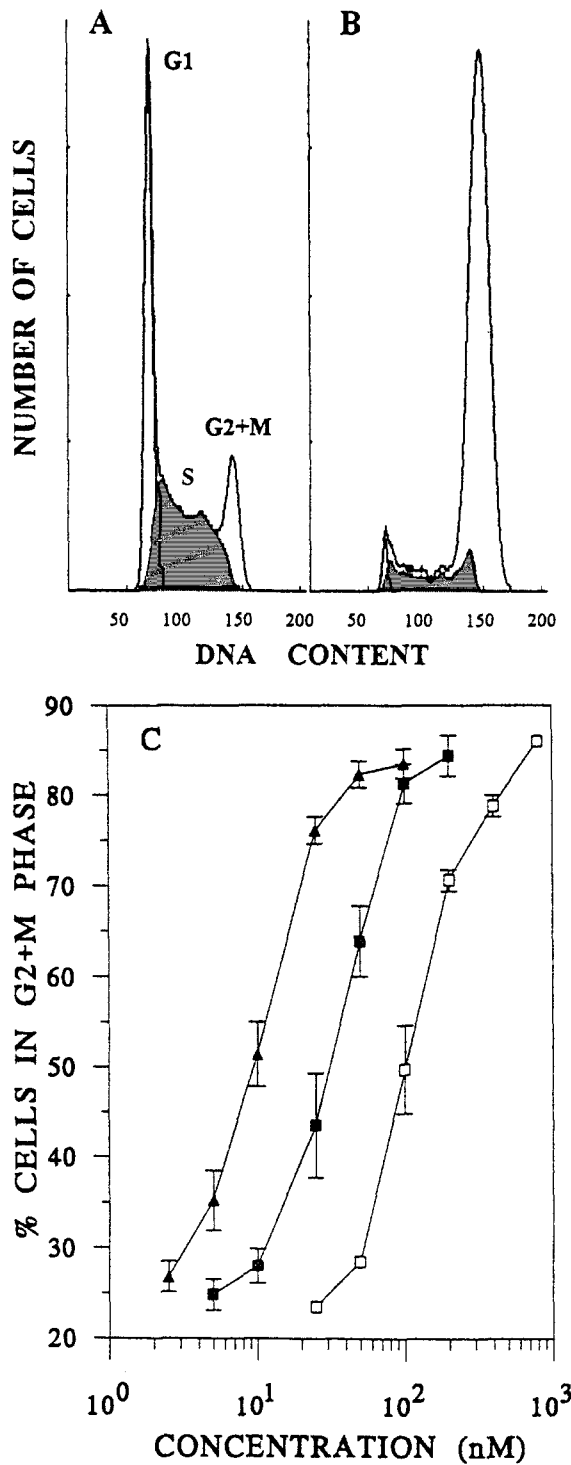


Figure 6. Effect of ADR, ELP, and S16020-2 on the cell cycle of L1210 cells. A: typical flow cytometric histogram of untreated L1210 cells stained with PI; B: effect of 50 nM S16020-2 on L1210 cells treated for 21 hours. C: dose-effect of ADR (■), ELP (□), and S16020-2 (▲) on the percentage of cells accumulated in the G2+M phase of the cell cycle. Bars: s.e.m. obtained in at least 3 independent experiments.

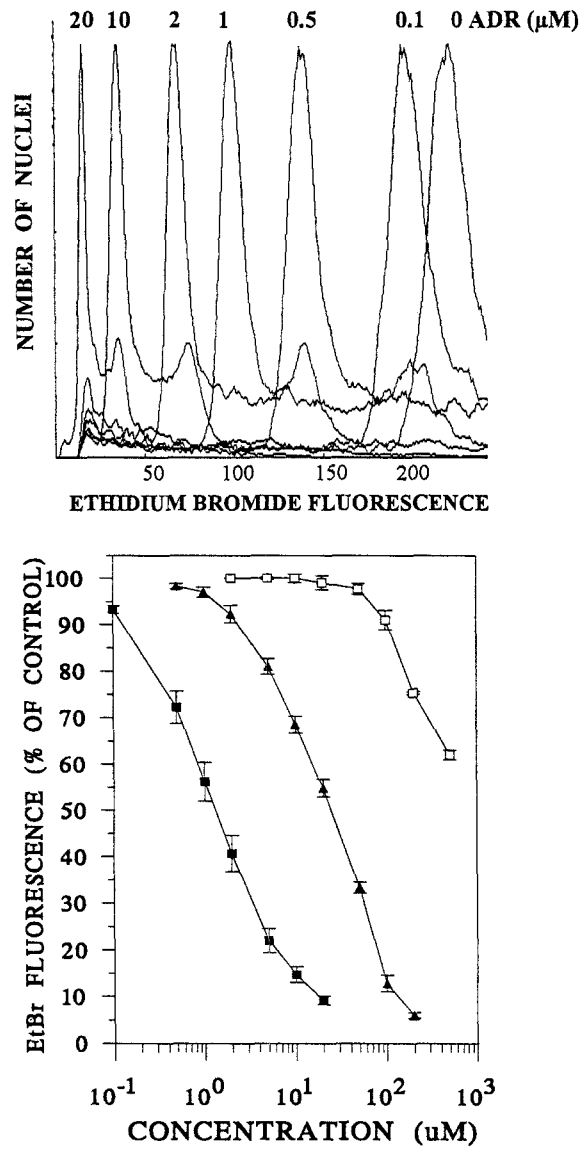


Figure 7. Inhibition of EtBr binding to DNA. A: typical histograms of EtBr fluorescence obtained after labeling of L1210 nuclei by 50 μ M EtBr in the presence of various concentrations of ADR. B: Dose-effect of ADR (■), m-AMSA (□), and S16020-2 (▲) on the decrease in EtBr fluorescence intensity. Results are expressed as the mean fluorescence of the G1 phase, with respect to control cells. Bars: s.e.m. obtained in 3 independent experiments.

ELP (□), and S16020-2 (▲) on the percentage of cells accumulated in the G2+M phase of the cell cycle. Bars: s.e.m. obtained in at least 3 independent experiments.

treated for 1 hour. This result demonstrates that S16020-2, as well as ADR-induced irreversible lesions in cells, and confirmed the higher potency of S16020-2 over ADR for short exposure times.

The clonogenic assay was also carried out with plateau phase A549 cells, which were 90% Ki-67 negative. Both ADR and S16020-2 were more active on proliferating than on confluent cells, but this trend was more pronounced for S16020-2 which was 25 fold more active at reducing by 50% the formation of colonies issued from proliferating rather than from confluent A549 cells. This confluence-dependent resistance has been demonstrated for anthracyclines in several *in vitro* studies [15, 16] and explained, in part, by a decrease of drug accumulation in confluent cells related to modifications of the membrane fluidity. However, at similar intracellular concentrations, certain anthracyclines still killed more dividing than plateau-phase cells [17]. On the other hand, plateau-phase cells are principally quiescent (resting cells) and the 170 kD-isoform of the DNA topo II has been shown to be markedly reduced in quiescent cells [18, 19]. Furthermore, a good relationship has been established between the level of topo II and sensitivity to ADR [20]. The fact that the confluent A549 cells used in this study: i) were 90% quiescent cells, ii) expressed a relatively low level of the topo II α enzyme (3 fold lower than in proliferating cells), and iii) were less sensitive to S16020-2 than proliferating cells, suggests that the topo II α could be a potential target for S16020-2, as is the case for ADR [21] and ELP [22].

We have tested S16020-2 cytotoxicity in parental sensitive versus resistant cell lines, the latter overexpressing the P-gp. Globally, the resistant cells were more sensitive to S16020-2 than to ADR, the mean factor of resistance being 8 and 201, respectively. The 2 cell lines displaying the pure classical MDR phenotype, P388/VCR-20 and S1/tMDR (transfected by the human *mdr1* gene), were as sensitive to S16020-2 as their sensitive parental counterparts, although they were resistant to ADR. In contrast, cells whose resistance was induced by ADR (P388/ADR-1, P388/ADR, and KB-A1), although markedly more sensitive to S16020-2 than to ADR, were still significantly cross-resistant to S16020-2. These cells are known to have different mechanisms of resistance, the two

main ones being the over-expression of the P-gp and qualitative and/or quantitative modification of the target enzymes, such as the topo II [23]. These results could be interpreted in the sense that S16020-2 can overcome the pure classical MDR phenotype, only linked to the P-gp overexpression, but is not able to circumvent other types of resistance as, for example, those due to alterations of topo II. This is consistent with the reduced sensitivity of quiescent A549 cells, expressing a low level of topo II α , to S16020-2.

ADR, S16020-2, and ELP induced a similar dose-dependent accumulation of L1210 cells in the G2+M phase of the cell cycle, but S16020-2 was 2 fold more potent than ADR and 8 fold more than ELP, on this particular cell line. The good relationship between the inhibition of the proliferation and the accumulation of L1210 cells in the G2+M phase suggests that the cell death induced by these 3 drugs is the consequence of this blockage of the cell cycle. Moreover, the similar profile of the cell cycle obtained after treatment with these three compounds suggests that they share, at least at the cellular level, the same mechanism of action. Furthermore, the G2+M block induced by these drugs was not associated with an increase in the number of polyploid cells or of the mitotic index as in the case of tubulin inhibitors [24, 25].

Preliminary experiments, performed in cell-free systems with purified components have demonstrated the intercalation of S16020-2 into DNA and the stabilization of the cleavable complex formed between topo II and DNA [3]. In intact nuclei, S16020-2, ADR and m-AMSA inhibited in a dose-dependent manner the intercalation of EtBr into DNA. The inhibitory effect of m-AMSA was weaker than that of ADR, as previously described in an acellular system, using purified DNA [26], the apparent affinity of S16020-2 was intermediate between those of ADR and m-AMSA.

Together, these results suggest that the potent cytotoxic activity of S16020-2 is probably the consequence of an interaction with the topo II α enzyme following its intercalation into DNA. Moreover, its high potency *in vitro* against sensitive and P-gp mediated MDR cell lines and the recent promising activity obtained *in vivo* against experimental human solid tumors [2], identify S16020-2 as an interesting candidate for clinical evaluations.

Acknowledgements

We thank Dr. B. Lockhart for critical reading of the manuscript. The 6G2 antibody was kindly provided by Dr. G. Astraldi Ricotti (C.N.R., I.G.B.E., Pavia, Italia).

References

- Jasztold-Howorko R, Landras C, Pierre A, Atassi G, Guilbaud N, Kraus-Berthier L, Leonce S, Rolland Y, Prost JF, Bisagni E: Synthesis and evaluation of 9-hydroxy-5-methyl-(5,6-dimethyl)-6H-pyrido[4,3b] carbazole-1-N([dialkylamino)alkyl] carboxamides, a new promising series of antitumor olivacine derivatives. *J Med Chem* 37:2445–2452, 1994
- Kraus-Berthier L, Guilbaud N, Leonce S, Saint-Dizier D, Rouillon MH, Jan M, Burbridge M, Pierre A, Atassi G: Antitumor effect of S16020-2 against experimental lung carcinoma. *Proc Am Assoc Cancer Res* 36:386, 1995
- Le Mee S, Markovits J, Pierre A, Atassi G, Bisagni E, Jacquemin-Sablon A, Saucier JM: *In vitro* studies of S16020-2, a new antitumour pyridocarbazole derivative. The fifth conference on DNA topoisomerases in therapy. New York, 1994
- Leonce S, Pierre A, Anstett M, Perez V, Genton A, Bizzari JP, Atassi G: Effects of a new triazinoaminopiperidine derivative on adriamycin accumulation and retention in cells displaying P-glycoprotein-mediated multidrug resistance. *Biochem Pharmacol* 44:1707–1715, 1992
- Charcosset JY, Saucier JM, Jacquemin-Sablon A: Reduced DNA topoisomerase II activity and drug-stimulated DNA cleavage in 9-hydroxyellipticine resistant cells. *Biochem Pharmacol* 37:2145–2149, 1988
- Danks MK, Schmidt CA, Cirtain MC, Suttle DP, Beck WT: Altered catalytic activity of and DNA topoisomerase II from human leukemic cells selected for resistance to VM-26. *Biochemistry* 27:8861–8869, 1988
- Rouësse J, Spielmann M, Turpin F, Le Chevalier T, Azab M, Mondesir JM: Phase II study of elliptinium acetate salvage treatment of advanced breast cancer. *Eur J Cancer* 29A:856–859, 1993
- Alley MC, Scudiero DA, Monks A, Hursey ML, Czerwinski MJ, Fine DL, Abbott BJ, Mayo JG, Shoemaker RH, Boyd MR: Feasibility of drug screening with panels of human tumor cell lines using a microculture tetrazolium assay. *Cancer Res* 48:589–601, 1988
- Pierre A, Kraus-Berthier L, Atassi G, Cros S, Poupon MF, Lavielle G, Berlion M, Bizzari JP: Preclinical antitumor activity of a new vinca alkaloid derivative, S12363. *Cancer Res* 51:2312–2318, 1991
- Gerdes J, Lemke H, Baisch H, Wacker HH, Schwab U, Stein H: Cell cycle analysis of a cell proliferation-associated human nuclear antigen defined by the monoclonal antibody Ki-67. *J Immunol* 133:1710–1715, 1984
- Baisch H, Gerdes J: Simultaneous staining of exponentially growing versus plateau phase cells with the proliferation-associated antibody Ki-67 and propidium iodide: analysis by flow cytometry. *Cell Tissue Kinet* 20:387–391, 1987
- Prosperi E, Sala E, Negri C, Oliani C, Supino R, Astraldi Ricotti GBC, Bottiroli G: Topoisomerase II α and β in human tumor cells grown *in vitro* and *in vivo*. *Anticancer Res* 12:2093–2100, 1992
- Negri C, Chiesa R, Cerino A, Bestano M, Sala C, Zini N, Maraldi M, Astraldi Ricotti GBC: Monoclonal antibodies to human-DNA topoisomerase I and the two isoforms of DNA topoisomerase II: 170- and 180-kDa isozymes. *Exp Cell Rec* 200:452–459, 1992
- Le Pecq JB, Paoletti C: A fluorescent complex between ethidium bromide and nucleic acids. Physical-chemical characterization. *J Mol Biol* 27:87–106, 1967
- Pelletier H, Millot JM, Chauffert B, Manfait M, Genne P, Martin F: Mechanisms of resistance of confluent human and rat colon cancer cells to anthracyclines: alteration of drug passive diffusion. *Cancer Res* 50:6626–6631, 1990
- Dimanche-Boitrel MT, Pelletier H, Genne P, Petit JM, Le Grimmellec C, Canal P, Ardiel C, Bastian G, Chauffert B: Confluence-dependent resistance in human colon cancer cells: role of reduced drug accumulation and low intrinsic chemosensitivity of resting cells. *Int J Cancer* 50:677–682, 1992
- Bhuyan BK, McGovren JP, Crampton SL: Intracellular uptake of 7-con-O-methylnogarol and adriamycin by cells in culture and its relationship to cell survival. *Cancer Res* 41:882–887, 1981
- Hsiang YH, Wu HY, Liu LF: Proliferation-dependent regulation of DNA topoisomerase II in cultured human cells. *Cancer Res* 48:3230–3235, 1988
- Woessner RD, Mattern MR, Mirabelli CK, Johnson RK, Drake FH: Proliferation- and cell cycle-dependent differences in expression of the 170 kilodalton and 180 kilodalton forms of topoisomerase II in NIH-3T3 cells. *Cell growth Diff* 2:209–214, 1991
- Davies SM, Robson CN, Davies SL, Hickson ID: Nuclear topoisomerase II levels correlate with the sensitivity of mammalian cells to intercalating agents and epipodophyllotoxins. *J Biol Chem* 263:17724–17729, 1988
- Zunino F, Capranico G: DNA topoisomerase II as the primary target of anti-tumor anthracyclines. *Anti-Cancer Drug Design* 5:307–317, 1990
- Fosse P, Rene B, Charra M, Paoletti C, Saucier JM: Stimulation of topoisomerase II-mediated DNA cleavage by ellipticine derivatives: structure-activity relationship. *Mol Pharmacol* 42:590–595, 1992
- De Isabella P, Capranico G, Binaschi M, Tinelli S, Zunino F: Evidence of DNA-topoisomerase II-dependent mechanisms of multidrug resistance in P388 leukaemia cells. *Mol Pharmacol* 37:11–16, 1990
- Leonce S, Anstett M, Perez V, Pierre A: Flow cytometric

- evaluation of the cell cycle perturbations induced by S12363, a new vinca-alkaloid derivative. *Anti-cancer Drugs* 1:179–183, 1990
25. Solary E, Leteurtre F, Paul KD, Scudiero D, Hamel E, Pommier Y: Dual inhibition of topoisomerase II and tubulin polymerization by azatoxin, a novel cytotoxic agent. *Biochem Pharmacol* 45:2449–2456, 1993
26. Yoshinari T, Yamada A, Uemura D, Nomura K,

Arakawa H, Kojiri K, Yoshida E, Suda H, Okura A: Induction of topoisomerase I-mediated DNA cleavage by a new indolocarbazole, ED-110. *Cancer Res* 53:490–494, 1993

Address for offprints: Stéphane Léonce, Division de Cancérologie Expérimentale, Institut de Recherches Servier, 11 rue des Moulineaux, 92150 Suresnes, France. Fax: 1 41 18 24 40

In Vitro and *in Vivo* Pharmacological Characterizations of the Antitumor Properties of Two New Olivacine Derivatives, S16020-2 and S30972-1¹

Hugues Malonne, Sophie Farinelle,
Christine Decaestecker, Laurence Gordower,
Jeanine Fontaine, Françoise Chaminade,
Jean-Marie Saucier, Ghanem Atassi,
and Robert Kiss²

Laboratoire de Physiologie et de Pharmacologie Fondamentales, Institut de Pharmacie [H. M., J. F. G. A.], Laboratoire d'Histopathologie, Faculté de Médecine [S. F., C. D., R. K.], and Service de Médecine Interne, Hôpital Erasme [L. G.], Université Libre de Bruxelles, 1070 Brussels, Belgium; Unité Mixte de Recherche 8532, Centre National de la Recherche Scientifique, Institut Gustave Roussy, Villejuif, France [F. C., J.-M. S.]; and Division de Cancérologie Expérimentale, Institut de Recherches Servier, Suresnes, France [G. A.]

ABSTRACT

S16020-2, a new olivacine derivative and a topoisomerase II inhibitor, has recently entered clinical trials. New analogues and derivatives have been synthesized from the S16020-2 compound. Preliminary data indicate that S30972-1, one of these S16020-2 derivatives, may exhibit a comparatively higher level of antitumor potency associated with an improved therapeutic index than does S16020-2. The antitumor activities of S16020-2 and S30972-1 were therefore characterized both *in vitro* and *in vivo*, with Adriamycin and etoposide chosen as reference compounds. The *in vitro* data show that S30972-1 is a topoisomerase II inhibitor, mediating its activity through an ATP-dependent mechanism such as S16020-2. The two olivacine derivatives exhibited similar activities *in vitro* at the levels of the global growth of six human cancer cell lines, of the induction of apoptosis, and of the G₂ cell cycle phase arrest. The *in vivo* antitumor activity characterization included the use of two murine leukemia types (P388-LEU and L1210-LEU), two murine lymphoma-like models (P388-LYM and L1210-LYM), two mammary adenocarcinomas (MXT-HI and MXT-HS), and one melanoma (B16). The data show that S30972-1 is actually more

efficient *in vivo* than S16020-2, a feature that may relate to the fact that S30972-1 is less toxic than S16020-2. The S30972-1 compound exhibited *in vivo* a level of antitumor activity that was also actually higher than that exhibited by Adriamycin and similar to that exhibited by etoposide.

INTRODUCTION

As emphasized by Burden and Osheroff (1), topoisomerase II is a ubiquitous enzyme that is essential for the survival of all eukaryotic organisms and that plays critical roles in virtually every aspect of DNA metabolism. This enzyme unknots and untangles DNA by passing an intact helix through a transient double-stranded break that it generates in a separate helix (1, 2). Inhibitors of DNA topoisomerase II are therefore widely used as chemotherapeutic agents in cancer treatment (1–3). These inhibitors include DNA-intercalating anthracyclines, anthraquinones, ellipticines, acridines, and non-DNA-intercalating epipodophyllotoxin derivatives (1–3). These topoisomerase-interfering compounds can be divided into poisons and catalytic inhibitors, two general categories based on the mechanism of drug action (4). A peculiarity of DNA topoisomerase poisons is that their action is invariably DNA sequence specific (2, 4); this sequence specificity of the poisons targeting eukaryotic DNA topoisomerase II (including ADR,³ ellipticine, and VP-16) is detailed by Capranico *et al.* (4). DNA is thus the major target for topoisomerase II inhibitors, and the stabilization of cleavable topoisomerase II-DNA complexes rather than the inhibition of topoisomerase II catalytic activity is essential for drug cytotoxicity (3). Six antineoplastic drugs that target topoisomerase II (*i.e.*, doxorubicin, daunorubicin, idarubicin, mitoxantrone, VP-16, and teniposide) have been currently approved for clinical use in the United States (5). New investigational antitopoisomerase drugs are under analysis. Among them is the S16020-2 olivacine derivative.

S16020-2 (NSC 659687) is a pyridocarbazole derivative characterized by a basic N-dialkylaminoalkylcarboxamido group grafted onto an olivacine chromophore (see Fig. 1). It binds through intercalation between adjacent DNA bp, thus inducing an unwinding of the double helix by 10 degrees (6, 7). Although S16020-2 does not interfere with the catalytic cycle of DNA topoisomerase I, it does stimulate the DNA topoisomerase II-mediated DNA cleavage via a strictly ATP-dependent mechanism (7). Quiescent cells demonstrate a significantly lower sensitivity to S16020-2 than proliferating cells, a feature that

Received 2/18/00; revised 6/23/00; accepted 6/26/00.

The costs of publication of this article were defrayed in part by the payment of page charges. This article must therefore be hereby marked advertisement in accordance with 18 U.S.C. Section 1734 solely to indicate this fact.

¹ This work was supported by grants awarded by the Fonds de la Recherche Scientifique Médicale, Belgium. C. D. and R. K. are Research Associate and Senior Research Associate with the Fonds National de la Recherche Scientifique, Belgium, respectively.

² To whom requests for reprints should be addressed, at Laboratory of Histopathology, Faculty of Medicine, Université Libre de Bruxelles, CP620, 808 route de Lennik, 1070 Brussels, Belgium. Phone: 322 555 63 80; Fax: 322 555 62 85; E-mail: rkiss@med.ulb.ac.be.

³ The abbreviations used are: ADR, Adriamycin; VP-16, etoposide; ATCC, American Type Culture Collection; MTT, 3-(4,5-dimethylthiazol-2-yl)-2,5-diphenyltetrazolium bromide; MTD, maximum tolerated dose; T/C, treated/control; NOS, not otherwise specified.

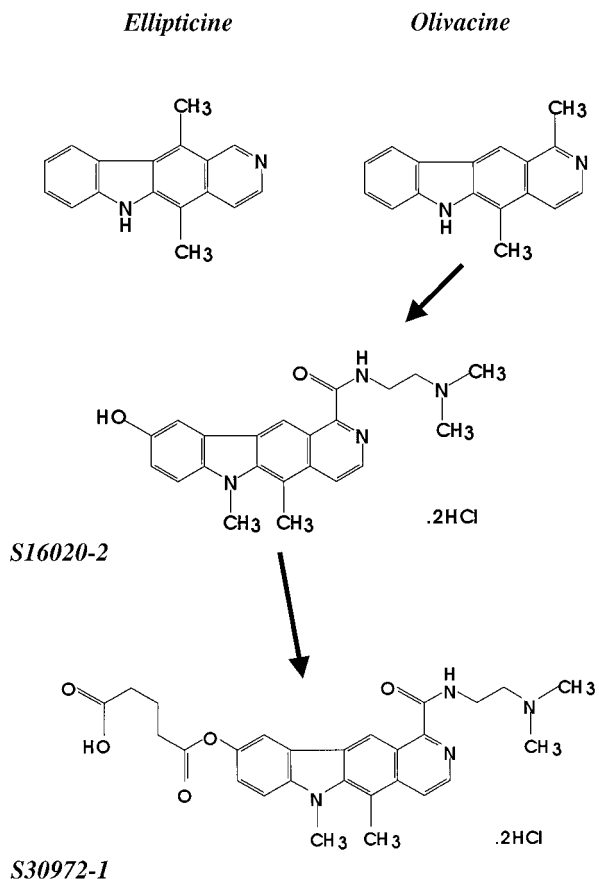


Fig. 1 Chemical structures of olivacine, the natural isomer of ellipticine, and of two synthetic derivatives of olivacine, *i.e.*, S16020-2 and S30972-1.

suggests that topoisomerase II α is the main potential target for S16020-2 (6). Koo *et al.* (3) have shown that among the inhibitors of topoisomerase II tested in the National Cancer Institute's *In Vitro* Antineoplastic Drug Screen, NSC 284682 (3'-hydroxydaunorubicin) and NSC 659687 (*i.e.*, S16020-2) are the only compounds that are more cytotoxic to tumor cells harboring an activated *ras* oncogene than to tumor cells bearing wild-type *ras* alleles. In fact, activated *ras* oncogenes appear to enhance the sensitivity of human tumor cells to topoisomerase II inhibitors by potentiating an apoptotic response (3).

S16020-2 was selected on the basis of its *in vitro* cytotoxicity and its *in vivo* antitumor activity against P388 leukemia and the colon 38 adenocarcinomas (8). S16020-2 was then shown on a large panel of murine and human tumors to be as active as, or more active than, several chemotherapeutic agents including cyclophosphamide (9) and ADR (10), which are routinely used in hospitals. Due to its antitumor activity in experimental models, its favorable pharmacokinetic characteristics, and its acceptable toxicity (9, 10), S16020-2 is currently being studied in clinical trials (11). New analogues and derivatives have been synthesized from the S16020-2 compound, with some of these new drugs exhibiting comparatively higher levels of antitumor potency with an improved therapeutic index (12).

Among these newly synthesized S16020-2 derivatives is the S30972-1 compound (the structure of which is illustrated in Fig. 1). The aim of the present work is therefore to provide an extensive pharmacological characterization of both the *in vitro* and the *in vivo* antitumor activities of S30972-1 in comparison with S16020-2, from which it derives. ADR and VP-16 have been chosen as reference compounds. The *in vitro* characterization of antitumor activity includes investigations conducted at the level of global growth, cell proliferation, apoptosis, and topoisomerase II targeting. The *in vivo* characterization includes the use of murine leukemias, lymphomas, mammary adenocarcinomas, and melanomas.

MATERIALS AND METHODS

In Vitro Determination of Global Growth. Six human tumor cell lines were obtained from the ATCC, Manassas, VA, and included two glioblastomas (U373 and U87) and two non-small cell lung (A549 and A427) and two colon (HCT-15 and LoVo) cancer models. The ATCC numbers of these cell lines are HTB 14 (U87), HTB 17 (U373), CCL 185 (A549), HBT 53 (A427), CCL 225 (HCT-15), and CCL 229 (LoVo). The cells were cultured at 37°C in sealed (airtight) Falcon plastic dishes (Nunc, Life Technologies, Inc., Merelbeke, Belgium) containing Eagle's minimal essential medium (MEM, Life Technologies, Inc.) supplemented with 10% FCS. All of the media were supplemented with a mixture of 0.6 mg/ml glutamine, 200 IU/ml penicillin, 200 IU/ml streptomycin, and 0.1 mg/ml gentamicin (all from Life Technologies, Inc.). The FCS was heat inactivated for 1 h at 56°C.

The six cell lines were incubated for 24 h in 96-microwell plates (at a concentration of 10,000 cells/ml culture medium) to ensure adequate plating before cell growth determination, which was carried out by means of the colorimetric MTT assay as detailed previously (13). This assessment of cell population growth is based on the capability of living cells to reduce the yellow product MTT (Sigma, St. Louis, MO) to a blue product, formazan, by a reduction reaction occurring in the mitochondria. The number of living cells is directly proportional to the intensity of the blue, which is quantitatively measured by spectrophotometry on a DIAS microplate reader (Dynatech Laboratories, Guyancourt, France) at a 570 nm wavelength (with a reference of 630 nm). Each experiment was conducted in sextuplicate. We validated the MTT-related data using two alternative techniques, namely the direct cell counting and the genomic incorporation of [³H]thymidine (data not shown).

Nine concentrations ranging from 10⁻⁵ to 10⁻⁹ M were assayed for each of the four drugs under study, *i.e.*, the two olivacine derivatives S16020-2 and S30972-1 (see Fig. 1) and the two antitopoisomerase II reference compounds ADR and VP-16.

In Vitro Determination of Cell Kinetics. The influence of S16020-2 and S30972-1 on the cell kinetics (the distribution of the cells into the various phases of the cell cycle) of two human tumor cell lines, *i.e.*, the fast-growing human U373 glioblastoma (cell cycle doubling time=20 ± 2 h) and the slow-growing human COLO 205 colon cancer (cell cycle doubling time=74 ± 3 h; ATCC CCL 222) models was assayed at two distinct concentrations (10 and 1000 nM). The experimental

schedule was identical with that previously described (14). Briefly, 40,000 cells/ml medium were taken in a logarithmic phase of growth for each of the 2 cell lines under study and plated in 35- × 10-mm Petri dishes (Becton Dickinson), each of which contained an 18- × 18-mm glass coverslip on its bottom and 3 ml of MEM (Life Technologies, Inc.). The two cell lines were incubated for 24 h before the addition of the drugs (or their nonaddition in the control condition) to ensure adequate plating. The experiments were stopped (by the fixation of the coverslips during 30 min in buffered formalin) 72 h after the addition of the drugs to the culture medium. The coverslips supporting the tumor cells were then submitted to the Feulgen reaction, as detailed elsewhere (15). The nuclear DNA content of each cell nuclei was quantitatively determined by means of computer-assisted microscopy (the SAMBA 2005 system; Samba Technologies Inc., Grenoble, France), thus enabling a DNA histogram to be drawn up for each experimental condition. The percentages of cells in the G₁, S, G₂, and M phases were then computed from each DNA histogram (16). Six hundred cell nuclei were analyzed for each experimental condition, and each experimental condition was performed in sextuplicate.

In Vitro Determination of Apoptosis Level. The levels of apoptosis were determined in the human U373 glioblastoma and COLO 205 colon cancer cell lines by means of a photometric enzyme immunoassay (Cell Death Detection ELISA^{PLUS}; Boehringer-Mannheim, Brussels, Belgium). This assay permitted the quantitative *in vitro* determination of the cytoplasmic histone-associated DNA fragments in the cell cultures exhibiting cell deaths occurring through apoptotic features (17). The experimental protocol was the same as described previously (18).

Topoisomerase II Targeting. Restriction endonucleases and DNA polymerase I (Klenow fragment) were purchased from New England BioLabs, Ltd. (Hitchin, United Kingdom) and proteinase K from Merck (Darmstadt, Germany). Human DNA topoisomerase IIα was provided by TopoGEN, Inc. (Columbus, OH). Closed circular pSP65 plasmid and yeast DNA topoisomerase II were prepared as described previously (7). Circular pSP65 DNA was cleaved with EcoRI restriction endonuclease and labeled at its 3'-end with [α -³²P]dATP (ICN Biomedical, Costa Mesa, CA) using DNA polymerase I, Klenow fragment (7). The labeled DNA was cleaved with restriction endonuclease *Hind*III into two fragments (2976 and 29 bp), each labeled at one end.

The cleavage reactions were conducted for 10 min at 30°C with yeast DNA topoisomerase II or at 37°C with human DNA topoisomerase IIα. The incubation mixture (15 μ l) contained labeled pSP65 DNA (8×10^4 dpm) and either 19 nm yeast DNA topoisomerase II or 2 units of human DNA topoisomerase IIα in the cleavage buffer [10 mM Tris-HCl (pH 7.5), 50 mM KCl, 10 mM MgCl₂, 0.1 mM EDTA] with or without 1 mM ATP. The reaction was stopped by the addition of SDS and proteinase K to the final concentrations of 0.8% and 63 μ g/ml, respectively, and the mixtures were incubated for an additional hour at 50°C. After the addition of 2 μ l of loading buffer (150 mM EDTA, 50% glycerol, 0.4% bromphenol blue, 0.4% xylene cyanol), the samples were heated at 65°C for 2 min and then analyzed by electrophoresis (2 V/cm) for 20 h in a 1.2% agarose gel con-

taining 0.1% SDS in 90 mM Tris-borate, 2.5 mM EDTA buffer. The gel was dried and autoradiographed.

In Vivo Determination of Antitumor Activity. The S16020-2- and S30971-1-mediated antitumor activities were characterized on seven different murine tumor models including the P388 and L1210 leukemia types, the P388 and L1210 lymphoma-like models, the MXT-HI and MXT-HS mammary carcinomas, and the B16 melanoma.

The P388 and L1210 leukemia types were developed at the beginning of the 1950s (19). In our present experiments, we used them for primary *in vivo* screening because we had observed that they exhibit distinct sensitivities to topoisomerase I (20) and II (21) inhibitors. The P388 (P388-LEU) and L1210 (L1210-LEU) leukemias are maintained in our laboratory by weekly transplantations of an inoculum of 10^6 cells i.p. into 6-week-old female DBA/2 mice (Iffa Credo, L'Arbresle, France) for the P388 model and into 6-week-old female C57BL × DBA/2f F₁ (B6D2F₁) mice (Iffa Credo) for the L1210 model. Without treatment, the animals die between 9 and 14 days after the injection. For the experiments under discussion, we used 6-week-old female CDF₁ mice (Iffa Credo).

As detailed in "Discussion," we developed two lymphoma-like models from these P388 and L1210 leukemia types. Briefly, we established solid s.c. tumors by inoculating 10^6 P388 or L1210 leukemic cells under the skin of the mice. These lymphoma-like models had been maintained for 2 years in our laboratory preceding the experiments under discussion. The transfer from one passage to the next was performed every 3 weeks for the L1210 lymphoma-like model (L1210-LYM) and every 2 weeks for the P388 lymphoma-like one (P388-LYM). At each transfer three L1210 or P388 tumors were minced into 10-mm pieces or larger, and these pieces were randomly s.c. inoculated into the right flanks of three "new bank" mice by means of a trochar (13-gauge). The same type of mouse was used for the lymphoma-like models as for the leukemia models.

The MXT-HS model described here is a hormone-sensitive form of the MXT model, whereas the MXT-HI model is a hormone-insensitive variant. The way in which we obtained these HS and HI variants from the original MXT tumor is detailed in "Discussion." The MXT-HI and MXT-HS tumors are maintained in our laboratory by monthly s.c. transplantations into 6-week-old female B6D2F₁ mice (Iffa Credo). The same procedure is used to maintain the B16 melanoma on B6D2F₁ mice (Iffa Credo).

We determined the MTD for the S16020-2 and S30972-1 compounds. This MTD determination was conducted by defining the maximum dose of the drug that can be administered acutely (*i.e.*, in one i.p. single dose) to healthy animals (B6D2F₁), *i.e.*, not grafted with tumors. The survival and weight of the animals were recorded for up to 14 days postinjection. Five different doses of each drug (10, 20, 40, 80, and 160 mg/kg) were used for the MTD index determination with each experimental group being composed of three mice for this purpose. All of the mice died that had received single 160-mg/kg i.p. injections of either S16020-2 or S30972-1, whereas all mice survived with a single i.p. injection of 80 mg/kg of each of these two compounds. The MTD for both olivacine derivatives was therefore defined as 80 mg/kg in the present study. In the case of each of the seven tumor models under study, three

doses were assayed [MTD/2 (40 mg/kg), MTD/4 (20 mg/kg) and MTD/8 (10 mg/kg)] in comparison with control. Each experimental group contained nine mice. The MTD values for ADR and VP-16 were 10 and 40 mg/kg, respectively.

The mice inoculated i.p. at day 0 with either 10^6 P388 or L1210 cells received one i.p. injection per day of either 0.2 ml of saline (control group) or the antitumor drug for 4 consecutive days, from day 1 to day 4.

The mice were grafted with the P388 lymphoma-like tumors at day 0 and treated 9 times (for the three following weeks) at days 5, 7, 9, 12, 14, 16, 19, 21, and 23 postgraft. A similar experimental protocol was adopted for the L1210 leukemia model, but the first drug administration started at day 7, with the following drug administrations performed at days 9, 11, 14, 16, 18, 21, 23, and 25 postgraft. The experimental schedule for the MXT-HI and MXT-HS mammary carcinomas and the B16 melanoma was identical with that for the L1210 model.

All of the animals were kept in plastic cages in a room with a controlled temperature ($22 \pm 1^\circ\text{C}$), light exposure (from 6 a.m. to 6 p.m.), and 40–70% relative humidity. Food (AO4; Usine Alimentaire Rationnelle, Villemoisson, France) and water were provided *ad libitum*. The present experiments were conducted with Animal Use Approval provided by the local Animal Ethic Committee of the Faculty of Medicine of the Université Libre de Bruxelles.

Solid tumor (the P388 and the L1210 lymphoma-like models, the MXT-HI and MXT-HS mammary carcinomas, and the B16 melanoma models) sizes were measured weekly by means of a caliper and expressed as an area (mm^2) by multiplying together the two largest perpendicular diameters.

The S16020-2 and S30972-1-induced influence on the survival periods of the tumor-bearing animals was evaluated by means of the T/C index [the ratio of the average survival time of the treated mice (the death of the fifth mouse in a given treated group of nine mice) to the average survival time of the control mice (the death of the 5th control mouse) multiplied by 100 (20, 21)]. On the basis of this evaluation, a compound is considered to be significantly active if it increases the T/C index by at least 30% ($T/C = 130\%$). If the T/C index is higher than 300%, the compound is considered as leading to the “long term survival” (if not the cure) of the animals. If the T/C index is <70%, the compound is considered to be toxic.

Statistical Analysis. Results are presented as the mean \pm SEM. The statistical comparisons of the data were conducted by means of the Fisher *F* (one-way ANOVA for more than two groups) or the Student *t* (for two groups) tests after a check of the equality of variance by means of the Levene test, and of the fit of the data to a normal distribution by means of the χ^2 test of goodness-of-fit. When these parametric conditions were not satisfied, the nonparametric Kruskall-Wallis (for more than two groups) or the Mann-Whitney (for two groups) tests were conducted. All of the statistical analyses were carried out with Statistica (Statsoft, Tulsa, OK).

RESULTS

In Vitro Determination of Global Growth. Table 1 shows that the two olivacine derivatives, S16020-2 and S30972-1 (see Fig. 1), exhibited significantly ($P < 0.05$ to $P <$

Table 1 Determination of the IC_{50} (in nm) associated with the S16020-2, S30972-1, ADR, and VP-16 drugs

The IC_{50} (*i.e.*, the drug concentration that inhibits the growth of the cell line under analysis by 50% as compared with the control value) were determined from nine concentrations ranging from 10^{-5} to 10^{-9} M. The influence of each drug concentration on each cell line was assayed in sextuplicate by means of the colorimetric MTT assay.

Cell lines	Drugs			
	ADR	VP-16	S16020-2	S30972-1
HCT-15	240 $P < 0.01$ 960 $P < 0.0001$		72 NS	79
LoVo	40 NS	260 $P < 0.001$	39 NS	42
U373	430 NS	740 $P < 0.01$	260 $P < 0.05$	310
U87	85 NS	270 $P < 0.01$	66 $P < 0.05$	110
A549	260 NS	440 $P < 0.05$	340 $P < 0.05$	337 NS
A427	84 NS	210 $P < 0.01$	67 NS	72

0.0001) higher cytotoxic activities than VP-16 on all six human cancer cell lines under study. The differences in cytotoxic activities between these two olivacine derivatives and ADR were less marked than what was observed with respect to VP-16 (Table 1).

In Vitro Determination of Cell Kinetics. We assessed the drug-induced influences at the level of cell kinetics by determining the percentage of cells in the G_2 phase of the cell cycle. We chose this cell kinetic marker because actual topoisomerase II inhibitors (see below) induce an increase in the G_2 phase length due to the fact that cells treated by such drugs try to repair their damaged DNA during this G_2 phase before undergoing mitosis. The level of DNA damage is therefore indirectly reflected by the length of the G_2 phase and, consequently, by the percentage of cells engaged in this specific phase of the cell cycle. Fig. 2 shows that both the S16020-2 and the S30972-1 compounds induced marked increases in the percentages of U373 cells arrested in the G_2 phase of their cell cycles. In slowly proliferating COLO 205 colon cancer cells, the S30972-1 compound induced significantly higher G_2 arrest features than the S16020-2 compound while at the same time exhibiting activities similar to those of the S16020-2 compound in highly proliferating U373 glioblastoma cells (Fig. 2). The kinetics of G_2 phase arrest induced by either S16020-2 or S30972-1 were not the same, a feature that should be compared with the fact that these two compounds did not display similar *in vivo* antitumor activities (see below).

In Vitro Determination of Apoptosis Level. Of the four topoisomerase II inhibitors under study, *i.e.*, the two olivacine derivatives (S16020-2 and S30972-1) and the two reference compounds (ADR and VP-16), the two olivacine derivatives induced the most marked apoptotic features in the highly proliferating U373 human glioblastoma cells (Table 2). In the

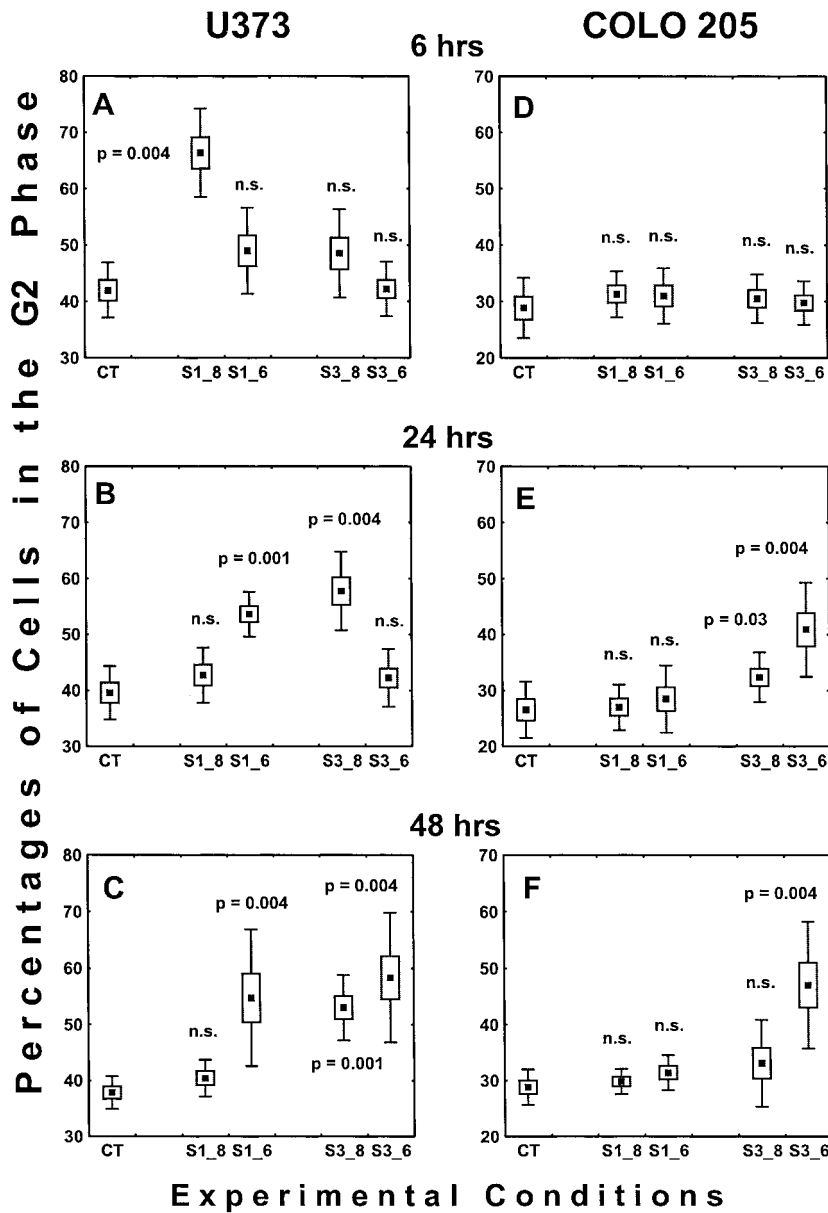


Fig. 2 Influence of S16020-2 at 10^{-8} (S1_8) and 10^{-6} (S1_6) and S30972-1 at 10^{-8} (S3_8) and 10^{-6} (S3_6) M on the percentages of tumor cells present in the G₂ phase of the cell cycle of the human U373 glioblastoma (A-C) and COLO 205 colon (D-F) tumor models. The G₂ cell percentages were determined by means of the computer-assisted microscope analyses of Feulgen-stained nuclei after 6 (A and D), 24 (B and E), and 48 (C and F) h of drug treatment. The results are presented as mean values (■) \pm their SE (□) \pm SD (bars). The Ps of statistical significance as compared with each control condition (CT) are indicated for each drug-treated condition [n.s., not significant ($P > 0.05$)].

slowly proliferating cells (the human COLO 205 colon cancer model), S30972-1 appeared to be more effective than S16020-2 (Table 2).

Topoisomerase II Targeting. Fig. 3 shows that both compounds (S16020-2 and S30972-1) induced the formation of cleavable complexes. In this experiment, the yeast enzyme was more efficient on DNA cut effects than the human DNA topoisomerase II. However, it was not possible to compare the two enzyme concentrations.

The data shown in Fig. 3 confirm a previous report showing that the cuts induced by topoisomerase II in presence of S16020-2 are ATP dependent (7). The same observation can be made for S30972-1 (Fig. 3). However, the S30972-1 effects induced on topoisomerase II cuts of DNA were lower than the

S16020-2 effects and considerably less efficient than the etoposide effects (Fig. 3). Lastly, the cut induction was biphasic with respect to the S30972-1 concentration, as it was with the S16020-2. However, the effects were maximum at $\sim 150 \mu\text{M}$ S30972-1, in contrast to the optimal S16020-2 concentration, which was 20 times lower (Fig. 3).

In Vivo Determination of Antitumor Activity. The 2 leukemia models appeared to be less selective than the five solid tumor models in discriminating between the antitumor activities of the four topoisomerase II inhibitors under study. Indeed, the four compounds cured a high number of leukemic mice in several different experimental protocols (Table 3). In contrast, the five solid tumor models enabled a clear-cut distinction to be drawn between the antitumor activity of these four anticancer

Table 2 S16020-2- and S30972-1-induced effects at apoptosis level

The data are expressed as mean percentages of cytoplasmic histone-associated-DNA fragments (as compared with the control value = 100%) \pm SE ($n = 4$).

Cell line	Drug	Concentration (nM)	Drug exposure (h)		
			6	24	48
U373	S16020-2	0.1	137 \pm 22	141 \pm 23	117 \pm 12
		10.0	131 \pm 18	129 \pm 17	235 \pm 15 ^a
		1000.0	129 \pm 19	250 \pm 42 ^b	650 \pm 37 ^b
	S30972-1	0.1	104 \pm 15	166 \pm 14 ^a	108 \pm 10
		10.0	114 \pm 12	189 \pm 17 ^a	115 \pm 12
		1000.0	134 \pm 15	270 \pm 25 ^a	940 \pm 56 ^b
ADR	S16020-2	0.1	140 \pm 15	115 \pm 16	124 \pm 15
		10.0	168 \pm 11 ^a	141 \pm 19	138 \pm 19
		1000.0	320 \pm 24 ^b	387 \pm 34 ^b	129 \pm 15
	VP-16	0.1	111 \pm 10	125 \pm 13	142 \pm 16
		10.0	125 \pm 11	137 \pm 12	128 \pm 16
		1000.0	141 \pm 17	135 \pm 15	215 \pm 19 ^a
COLO 205	S16020-2	0.1	115 \pm 10	91 \pm 8	89 \pm 8
		10.0	101 \pm 10	95 \pm 15	78 \pm 10 ^a
		1000.0	89 \pm 10	71 \pm 8	27 \pm 10 ^b
	S30972-1	0.1	101 \pm 10	168 \pm 11 ^a	121 \pm 12
		10.0	115 \pm 11	257 \pm 17 ^b	115 \pm 10
		1000.0	104 \pm 10	284 \pm 15 ^b	129 \pm 11

^{a–b} Levels of statistical significance as compared to the control values: ^a $P < 0.05$; ^b $P < 0.01$.

drugs. VP-16 and S30972-1 displayed the highest antitumor activity for the P388 lymphoma-like model (see “Discussion” and Table 3) and for the HS variant of the MXT mammary adenocarcinoma. However, S30972-1 and VP-16 displayed the highest antitumor activity for the aggressive HI variant of the MXT mammary adenocarcinoma (see “Discussion” and Table 3). These two compounds were able to cure several MXT-HI mammary carcinoma-bearing mice (Table 3). S30972-1 was also the most active for the B16 melanoma model, and in this model the two reference compounds (ADR and VP-16) did not increase the survival periods of the melanoma-bearing mice (Table 3). S30972-1 and VP-16 displayed very significant antitumor activity for the L1210 lymphoma-like tumor (Table 3). Thus, of the four topoisomerase II inhibitors under study, the S30972-1 olivacine derivative definitely exhibited the highest antitumor activity over all seven tumor models under study. All of the significant drug-induced increases in the survival periods of the mice bearing the five solid tumor models under study were accompanied by significant drug-induced decreases in tumor growth (data not shown).

DISCUSSION

Olivacine is the natural isomer of ellipticine (see Fig. 1) and has been extracted from a plant (*Aspidosperma olivaceum*) in 1958 (22) and synthesized in 1966 (23). Although its antitumor activity has been described since 1966, this activity has been studied less than ellipticine activity. This led the Bisagni team to synthesize different structural analogues of olivacine in the hope of modulating its antitumor activity (8). Despite the lack of studies on the relations between the structure and the activity of olivacine derivatives, some data have been obtained from the results produced by different research teams studying ellipticine.

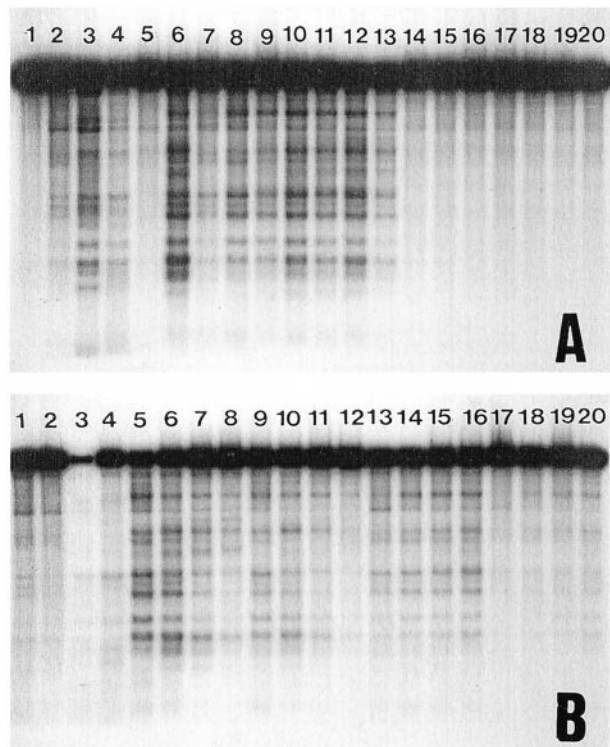


Fig. 3 *A*, yeast DNA topoisomerase II-mediated DNA cleavage in the presence or absence of ATP. Lane 1, pSP65 DNA substrate; Lane 2, cleavage reaction in the absence of drug; Lanes 3 and 4, 10 μ M etoposide; Lanes 5 and 6, 8 μ M S16020-2; Lanes 7–13, 4, 10, 30, 50, 100, 150, and 200 μ M S30972-1 in the presence of ATP; Lanes 14–20, 4, 10, 30, 50, 100, 150, and 200 μ M S30972-1 in the absence of ATP, which was present in Lanes 2, 3, and 6 and absent in Lanes 4 and 5. *B*, comparison of yeast and human DNA topoisomerase II-mediated DNA cleavage in the presence of ATP. Lanes 1, 3, 5–8, and 13–16, yeast DNA topoisomerase II; Lanes 2, 4, 9–12, and 17–20, human DNA topoisomerase II; Lanes 1 and 2, no inhibitor; Lanes 3 and 4, 100 μ M etoposide; Lanes 5–8 and 9–12, 2, 10, 20, and 40 μ M S16020-2 (in duplicate); Lanes 13–16 and 17–20, 2, 10, 20, and 40 μ M S30972-1 (in duplicate).

Hence, hydroxylation in position 9 increases the affinity of the compound for DNA (24), favors the stabilization of the cleavable complex (25) and a quinonimine formation (26), and increases the cytotoxicity of the compound and, consequently, its antitumor activity (27). However, some methoxylated derivatives in position 9 may be more efficient *in vivo* than their hydroxylated equivalents, which are more toxic generally (28). The addition of a lateral dialkylaminoalcano-type basic chain to an ellipticine (28) or an acridine (29) chromophore markedly increases the cytotoxicity of the compound and its antitumor activity. Nitrogen methylation in the indol chromophore theoretically decreases the risk of producing alkylating quinonimine derivatives *in vivo*, and thus seems to decrease the toxicity of the compound so synthesized (30). By applying these kinds of structure/activity relations to olivacine, Jaztold-Howorko *et al.* (8) and Guillonneau *et al.* (12) were able to synthesize the S16020-2 compound (NSC 659687) and different analogues including the S30972-1 derivative illustrated in Fig. 1. Three

Table 3 *In vivo* antitumor activity of S16020-2 and S30972-1 on the P388 (P388-LEU) and L1210 (L1210-LEU) leukemias, the P388 (P388-LYM) and L1210 (L1210-LYM) lymphoma-like models, the MXT-HS and MXT-HI mammary carcinomas, and the B16 melanoma

Drug	Doses ^a (mg/kg)	Experimental models ^b					
		P388-LEU	L1210-LEU	P388-LYM	L1210-LYM	MXT-HS	MXT-HI
ADR	1.25	>300 ^{c(5/9)}	>300 ^{c(9/9)}	94	121	145 ^d	118
	2.50	>300 ^{c(7/9)}	>300 ^{c(6/9)}	106	121	143 ^d	85
	5	127	166 ^d	121	104	83	98
VP-16	5	>300 ^{c(8/9)}	>300 ^{c(8/9)}	128	138 ^d	123	>300 ^{c(5/9)}
	10	>300 ^{c(7/9)}	>300 ^{c(7/9)}	170 ^e	158 ^e	135 ^d	>300 ^{c(7/9)}
	20	290 ^c	75	175 ^e	165 ^e	121	>300 ^{c(6/9)}
S16020-2	10	>300 ^{c(7/9)}	>300 ^{c(8/9)}	126	144 ^d	94	139 ^d
	20	58 ^e	85	142 ^d	133 ^d	72	81
	40	50 ^e	53 ^e	110	43 ^e	35 ^e	47 ^e
S30972-1	10	>300 ^{c(5/9)}	>300 ^{c(9/9)}	110	117	114	129
	20	>300 ^{c(8/9)}	>300 ^{c(9/9)}	136 ^d	163 ^e	153 ^e	>300 ^{c(8/9)}
	40	60 ^d	113	142 ^d	158 ^e	101	158 ^e
							148 ^e

^a The days of administration of each drug under study for each model are detailed under Materials and Methods. The two leukemia models received 4 drug injections during 1 week, starting one day after the leukemic cell inoculation into the mice, while the 5 solid tumor models were subjected to 9 drug injections for 3 weeks, starting 3 (P388-LYM), 5 (L1210-LYM) or 7 (MXT-HI, MXT-HS, B16) days post-graft.

^b The data are expressed as the T/C index, which is the ratio of the average survival time of the treated mice (the death of the 5th mouse in a given treated group of 9 mice) to the average survival time of the control mice (the death of the 5th control mouse) multiplied by 100. The values indicated as subscripts to the right of the T/C indices represent the number of mice cured (*i.e.*, surviving with T/C >300%).

Levels of significance as compared with the control group: ^c *P* < 0.001; ^d *P* < 0.05; ^e *P* < 0.01.

S16020-2 substitution sites were selected to obtain new derivatives, *i.e.*, the carbon atoms in positions 10 and 11 (methylation) and the hydroxyl function in position 9 (the addition of a hydrolyzable function) (12). Methylation in position 10 caused a slight increase in *in vitro* cytotoxicity and also more marked *in vivo* toxicity. Of the hydrolyzable derivatives, the esterification of the 9-OH group with various aliphatic diacids made it possible to obtain slightly less cytotoxic derivatives with an increased *in vivo* activity and an improved therapeutic index (12). The 9-substituted derivatives including a methyl group in position 11 maintained the same activity as the 9-unsubstituted compounds. This means that 9-substitution is much more favorable in the case of S16020-2 than in the case of the 11-methyl derivatives. The activity of the different esters can be attributed to either the cytotoxic activity of the original compound or the production of hydroxyl derivatives after hydrolysis by intra- or extracellular esterases. The glutaric ester of S16020-2 is S30972-1, selected for an extensive pharmacological study in the present paper. S16020-2 exhibits the same mechanism of action as ellipticine, and the DNA sequence specificity cleavages of S16020-2 are the same as those of the other derivatives and ellipticine (7). S16020-2 and ellipticine do not act on the rate of DNA religation, but do on the cleavage rate (7). Furthermore, S16020-2 is the sole topoisomerase II inhibitor identified to date that absolutely requires the presence of ATP to stimulate such a reaction. The data from the present study clearly indicate that S30972-1 is more active *in vivo* than S16020-2 (see Fig. 1) but is less active with respect to DNA topoisomerase II targeting *in vitro* (see Fig. 3). S30972-1 is also ATP dependent (Fig. 3).

The *in vitro* data do not enable a frank distinction to be drawn between S16020-2 and the S30972-1. Both S16020-2 and the S30972-1 induced a significant arrest of the G₂ phase of the cell cycle of proliferating cells (even in slowly proliferating ones like the human COLO 205 colon cancer model), a feature that would relate to their antitopoisomerase II activity as dem-

onstrated by the topoisomerase II targeting data. Both compounds induced marked apoptotic features in human cancer cells at a higher intensity than that observed in the reference compounds. Thus, most of the *in vitro* data show that the two olivaccine derivatives, S16020-2 and S30972-1, which are topoisomerase II inhibitors, have a higher level of antitumor activity than VP-16 and also, but to a lesser extent, than ADR. This greater efficiency of the olivaccine derivatives (in relation to the reference compounds) also manifests itself *in vivo*, but with very different activity profiles of the S16020-2 and S30972-1 compounds. However, the detection of this difference requires the use of solid tumor models which mimic clinical reality, to a certain extent at least. The leukemia models do not enable this distinction to be made. This is why the National Cancer Institute (Bethesda, MD) abandoned this kind of model for its primary drug discovery screening, after using it for about 30 years (19).

When leukemic P388 cells of lymphoblastic origin (19) are grafted s.c. instead of i.p., they develop as biologically very aggressive anaplastic lymphomas. This biological aggressiveness can be evidenced histologically in the form of a dramatic local invasion (*i.e.*, the dermis and surrounding muscles of the peritoneal cavity) and a metastatic process occurring first in the liver (as early as the third day postgraft), and then in the lungs (occurring around the 7th day postgraft) and, occasionally, in the kidneys (around the 15th day postgraft if the animals are still alive). Mice suffering from P388 lymphoma-like models usually die about 2 weeks after the cell injection. Data from the present study clearly indicate that none of the four compounds tested here was able to cure P388 lymphoma-bearing mice. The two most efficient compounds in this model were VP-16 and S30972-1, and the least efficient one was ADR.

Despite the fact that they are also of lymphoblastic origin (19), L1210 leukemia cells develop much less aggressive anaplastic lymphomas than the P388 lymphoma model. Indeed, the L1210 lymphoma-like model does not invade adjacent tissues or

metastasize. Untreated animals suffering from this L1210 lymphoma die 4 to 5 weeks postgraft. Once more, the two most efficient compounds with respect to this L1210 lymphoma model were VP-16 and S30972-1, and the least efficient one was ADR.

More than 80% of female breast cancers are invasive intraduct carcinomas, *i.e.*, NOS (31). We are therefore using the MXT tumor as an experimental model to reproduce this clinical reality because this tumor originates in the galactophorous ducts (like NOS cancers) and not in the glandular acini, as is the case of most murine mammary tumors (32, 33). Mammary cancers of the galactophorous ducts have a hormone sensitivity profile very different from the profile of glandular acini cancers; whereas the former are essentially "steroidosensitive," the latter are "prolactin-sensitive" (31–34). An experimental protocol was thus developed in our laboratory to differentiate hormone-insensitive MXT-HI tumor strains into hormone-sensitive MXT-HS strains (35). Data from the present study show that ADR and S30972-1 exhibited the highest levels of antitumor activity on the MXT-HS strain whereas S30972-1 and VP-6 actually appeared to be effective against the very aggressive MXT-HI strain (Table 3).

Experimental melanomas set up in mice by painting their skins with a carcinogen have little in common with human melanomas. In fact, even if these experimental melanomas display certain morphological characteristics close to those of human melanomas, they are actually less aggressive biologically (36). Nevertheless, there does exist an experimental model in the shape of the B16 murine melanoma which displays numerous similarities with human melanomas (37, 38). Of the four compounds under study, the two olivacine derivatives were effective against the B16 melanoma strain that we used, whereas the two reference compounds were not.

In conclusion, olivacine derivatives are promising new antitumor agents which belong to the class of topoisomerase II inhibitors. One of these (S16020-2) recently entered clinical trials. The present study shows that the glutaric ester of S16020-2, *i.e.*, S30972-1, exhibits an *in vitro* antitumor activity similar to S16020-2. In sharp contrast, S30972-1 is more efficient *in vivo* than S16020-2, a feature that could relate to the fact that S30972-1 is less toxic than S16020-2. S30972-1 exhibited an *in vivo* antitumor activity (on a panel of seven distinct tumor models) that was actually greater than the activity displayed by ADR and etoposide.

REFERENCES

- Burden, D. A., and Osheroff, N. Mechanism of action of eukaryotic topoisomerase II and drugs targeted to the enzyme. *Biochim. Biophys. Acta*, **1400**: 139–154, 1998.
- Malonne, H., and Atassi, G. DNA topoisomerase targeting drugs: mechanisms of action and perspectives. *Anticancer Drugs*, **8**: 811–822, 1997.
- Koo, H. M., Gray-Goodrich, M., Kohlhagen, G., McWilliams, M. J., Jeffers, M., Vaigro-Wolff, A., Alvord, W. G., Monks, A., Paull, K. D., Pommier, Y., Vande, and Woude, G. F. The *ras* oncogene-mediated sensitization of human cells to topoisomerase II inhibitor-induced apoptosis. *J. Natl. Cancer Inst.*, **91**: 236–244, 1999.
- Capranico, G., Binaschi, M., Borgnetto, M. E., Zunino, F., and Palumbo, M. A protein-mediated mechanism for the DNA sequence-specific action of topoisomerase II poisons. *Trends Biol. Sci.*, **18**: 323–329, 1997.
- Hande, K. R. Clinical applications of anticancer drugs targeted to topoisomerase II. *Biochim. Biophys. Acta*, **1400**: 173–184, 1998.
- Leonce, S., Perez, V., Casabianca-Pignede, M. R., Anstett, M., Bisagni, E., Pierré, A., and Atassi, G. In vitro cytotoxicity of S16020-2, a new olivacine derivative. *Invest. New Drugs*, **14**: 169–180, 1996.
- Le Mee, S., Pierré, A., Markovits, J., Atassi, G., Jacquemin-Sablon, A., and Saucier, J. M. S16020-2, a new highly cytotoxic antitumor olivacine derivative: DNA interaction and DNA topoisomerase II inhibition. *Mol. Pharmacol.*, **53**: 213–220, 1998.
- Jaztold-Howorko, R., Landras, C., Pierré, A., Atassi, G., Guilbaud, N., Kraus-Berthier, L., Leonce, S., Rolland, Y., Prost, J. F., and Bisagni, E. Synthesis and evaluation of 9-hydroxy-5-methyl-(and 5,6-dimethyl)-6H-pyrido[4,3-*b*]carbazole-1{N-(dialkylamino)alkyl}carboxamides, a new promising series of antitumor olivacine derivatives. *J. Med. Chem.*, **37**: 2445–2452, 1994.
- Guilbaud, N., Kraus-Berthier, L., Saint-Dizier, D., Rovillon, M. H., Jan, M., Burbridge, M., Pierré, A., and Atassi, G. Antitumor activity of S16020-2 in two orthotopic models of lung cancer. *Anticancer Drugs*, **8**: 276–282, 1997.
- Kraus-Berthier, L., Guilbaud, N., Jan, M., Saint-Dizier, D., Rovillon, M. H., Burbridge, M. F., Pierré, A., and Atassi, G. Experimental antitumor activity of S16020-2 in a panel of human tumors. *Eur. J. Cancer*, **33**: 1881–1887, 1997.
- Giacchetti, S., Cornez, N., Eftekhari, P., Awada, A., Cuvier, C., Bleiberg, H., Hidvegi, E., Berger, E., Gerard, B., Giroux, B., Marty, M., Calvo, F., and Piccart, M. Phase I clinical trial of the olivacine S16020. *Proc. Am. Assoc. Cancer Res.*, **39**: 324, 1998.
- Guillonneau, C., Pierré, A., Charton, Y., Guilbaud, N., Kraus-Berthier, L., Leonce, S., Michel, A., Bisagni, E., and Atassi, G. Synthesis of 9-*O*-substituted derivatives of 9-hydroxy-5,6-dimethyl-6H-pyrido[4,3-*b*]carbazole-1-carboxylic acid (2-(dimethylamino)ethyl)amide and their 10- and 11-methyl analogues with improved antitumor activity. *J. Med. Chem.*, **42**: 2191–2203, 1999.
- Camby, I., Salmon, I., Danguy, A., Pasteels, J. L., Brotchi, J., Martinez, J., and Kiss, R. Influence of gastrin on human astrocytic tumor cell proliferation. *J. Natl. Cancer Inst.*, **88**: 594–600, 1996.
- Pauwels, O., and Kiss, R. Digital morphonuclear analyses of sensitive versus resistant neoplastic cells to *Vinca*-alkaloid, alkylating and intercalating drugs. *Cytometry*, **12**: 388–397, 1991.
- Kiss, R., Salmon, I., Camby, I., Gras, S., and Pasteels, J. L. Characterization of factors in routine laboratory protocols that significantly influence the Feulgen reaction. *J. Histochem. Cytochem.*, **41**: 935–945, 1993.
- Pauwels, O., Kiss, R., Pasteels, J. L., and Atassi, G. Characterization of alkylating *versus* intercalating anticancer drug-induced effects on cell survival, cell cycle kinetic and morphonuclear pattern of three neoplastic cell lines growing *in vitro*. *Pharm. Res.*, **12**: 1011–1018, 1995.
- Sun, S. Y., Yue, P., Shroot, B., Hong, W. K., and Lotan, R. Induction of apoptosis in human non-small lung carcinoma cells by the novel synthetic retinoid CD437. *J. Cell. Physiol.*, **173**: 279–284, 1997.
- Farinelle, S., DeHauwer, C., Darro, F., Decaestecker, C., Fontaine, J., Pasteels, J. L., Van Ham, P., Atassi, G., and Kiss, R. Setting up of an original computer-assisted methodology to characterize *in vitro* drug-induced anti-angiogenic effects. *Int. J. Mol. Med.*, **2**: 545–553, 1998.
- Pihl, A. UICC Study Group on chemosensitivity testing of human tumors. Problems, applications, future prospects. *Int. J. Cancer*, **37**: 1–5, 1986.
- Lesueur-Ginot, L., Demarquay, D., Kiss, R., Kasprzyck, P. G., Dassonneville, L., Bailly, C., Camara, J., Lavergne, O., and Bigg, D. C. H. Homocamptothecin, an E-ring modified camptothecin with enhanced lactone stability, retains topoisomerase I-targeted activity and antitumor properties. *Cancer Res.*, **59**: 2939–2943, 1999.
- Farinelle, S., DeDecker, R., Malonne, H., Werry, J., Darro, F., and Kiss, R. Characterization of biological features and chemosensitivity of

- a new experimental lung metastasis model originating from the MXT mouse mammary adenocarcinoma. *Anticancer Res.*, *19*: 1171–1180, 1999.
22. Schmutz, J., and Hunzicker, F. Die Alkaloide von *Aspidosperma olivaceum* m. ar. *Aspidosperma* Alkaloid 3, mitteilung. *Pharm. Acta Helv.*, *33*: 341–347, 1958.
 23. Mosher, C. W., Crews, O. P., Acton, E. M., and Goodman, L. Preparation and antitumour activity of olivacine and some new analogs. *J. Med. Chem.*, *9*: 237–241, 1966.
 24. LePecq, J. B., Dat-Xuong, N., Gosse, C., and Paoletti, C. A new antitumoral agent: 9-hydroxyellipticine. Possibility of a rational design of anticancerous drugs in the series of DNA intercalating drugs. *Proc. Natl. Acad. Sci. USA*, *71*: 5078–5082, 1974.
 25. Fossé, P., René, B., Charra, M., Paoletti, C., and Saucier, J. M. Stimulation of topoisomerase II-mediated DNA cleavage by ellipticine derivatives: structure-activity relationship. *Mol. Pharmacol.*, *42*: 590–595, 1992.
 26. Meunier, D., De Montauzon, D., Bernadou, J., Grassy, G., Bonafous, M., Cros, S., and Meunier, B. The biooxidation of cytotoxic ellipticine derivative: a key to structure-activity relationship studies? *Mol. Pharmacol.*, *33*: 93–102, 1988.
 27. Honda, T., Kato, M., Inoue, M., Shimamoto, T., Shima, K., Nakaniishi, T., Yoshida, T., and Noguchi, T. Synthesis and antitumour activity of quaternary ellipticine glycosides, a series of novel and highly active antitumour agents. *J. Med. Chem.*, *31*: 1295–1305, 1988.
 28. Ducrocq, C., Wendling, F., Tourbez-Perrin, M., Rivalle, C., Tambourin, P., Pochon, F., Bisagni, E., and Chermann, J. C. Structure-activity relationships in a series of newly synthesized 1-amino substituted ellipticine derivatives. *J. Med. Chem.*, *23*: 1212–1216, 1980.
 29. Atwell, G. J., Newcastle, G. W., Baguley, B. C., and Denny, W. A. Potential antitumor agents. 50. In vivo solid-tumor activity of derivatives of *N*-(2-(dimethylamino)ethyl)acridine-4-carboxamide. *J. Med. Chem.*, *30*: 664–669, 1987.
 30. Braham, Y., Meunier, G., and Meunier, B. The rat biliary and urinary metabolism of the *N*6-methylated derivative of elliptinium acetate, an antitumor agent. *Drug Metab. Dispos.*, *16*: 316–321, 1988.
 31. Paridaens, R., Leclercq, G., Piccart, M., Kiss, R., Mattheiem, W., and Heuson, J. C. Comments on the treatment of breast cancer. In: R. D. Bulbrook (ed.), *Hormones of Cancer: 90 years after Beatson*. *Cancer Surv.*, *5*: 447–461, 1986.
 32. Briand, P. Hormone-dependent mammary tumors in mice and rats as a model for human breast cancer (Review). *Anticancer Res.*, *3*: 273–282, 1983.
 33. Watson, C. S., Medina, D., and Clark, J. H. Estrogen characterization in a transplantable mouse mammary tumor. *Cancer Res.*, *37*: 3344–3348, 1977.
 34. Danguy, A., Kiss, R., Leclercq, G., Heuson, J. C., and Pasteels, J. L. Morphology of MXT mouse mammary tumors. Correlation with growth characteristics and hormone sensitivity. *Eur. J. Cancer Clin. Oncol.*, *22*: 69–76, 1986.
 35. Kiss, R., de Launoit, Y., Danguy, A., Paridaens, R., and Pasteels, J. L. Influence of pituitary grafts or prolactin administrations on the hormone sensitivity of ovarian hormone-independent mouse mammary MXT tumors. *Cancer Res.*, *49*: 2945–2951, 1989.
 36. Bannasch, P., and Gössner, W. Pathology of neoplasia and preneoplasia in rodents. In: EULEP Color Atlas, Vol. 2. New York: Schattauer Stuttgart, 1997.
 37. Griswold, D. P., Jr. Consideration of the subcutaneously implanted B16 melanoma as a screening model for potential anticancer agents. *Cancer Chemother. Rep.*, *3*: 315–324, 1972.
 38. Hu, F. The developmental cycle of B16 melanoma cell in culture. *Tex. Rep. Biol. Med.*, *23*: 308–320, 1965.



Original article

Photochemical electrocyclisation of 3-vinylindoles to pyrido[2,3-*a*]-, pyrido[4,3-*a*]- and thieno[2,3-*a*]-carbazoles: Design, synthesis, DNA binding and antitumor cell cytotoxicity

Thomas Lemster ^{a,*}, Ulf Pindur ^a, Gaelle Lenglet ^{b,c}, Sabine Depauw ^{b,c}, Christelle Dassi ^{b,c}, Marie-Hélène David-Cordonnier ^{b,c,**}

^a Institute of Pharmacy, Department of Pharmaceutical and Medicinal Chemistry, Johannes Gutenberg-University, Staudingerweg 5, D-55099 Mainz, Rheinland-Pfalz, Germany

^b INSERM U837-JPARC (Jean-Pierre Aubert Research Center), Team "Molecular and Cellular Targetting for Cancer Treatment", Institut de Recherches sur le Cancer de Lille, Place de Verdun, F 59045 Lille Cedex, France

^c Université de Lille 2, IMPRT-Institut Fédératif de Recherche 114, Lille, France

ARTICLE INFO

Article history:

Received 17 October 2008

Received in revised form

13 March 2009

Accepted 19 March 2009

Available online 27 March 2009

Keywords:

DNA ligands

Pyridocarbazoles

DNA intercalation

DNA minor groove binding

ABSTRACT

In the context of the design and synthesis of DNA ligands, some new heterocyclic annulated carbazoles were synthesized. As lead structure the intercalating tetracyclic systems pyrido[2,3-*a*]- and pyrido[4,3-*a*]-carbazoles and in one case a thieno[2,3-*a*]-carbazole were taken into account. A dialkyl amino amide chain was introduced to the planar chromophoric system with the intent to generate minor groove binding properties. The cytotoxicity of some compounds was examined by the NCI antitumor screening. Furthermore, biophysical as well as biochemical studies were performed in order to get some information about the DNA-binding properties and inhibition of DNA related functional enzymes of this new series of molecules.

Crown Copyright © 2009 Published by Elsevier Masson SAS. All rights reserved.

1. Introduction

Since the discovery of the natural products ellipticine **1** and its regiosomeric olivacine **2** annelated indole and carbazole derivatives with pyrido[4,3-*b*]carbazole framework constitute an interesting class of antitumor active drugs [1–4]. Whereas ellipticine **1** as well as 9-methoxyellipticine **3** shows activity against a variety of human tumor cell lines, especially against leukaemia, the quaternary pyridinium salt ellipticinium acetate (Celliptium®) **4** was deployed against metastatic breast cancer [3,5]. The mechanism of action *in vivo* of ellipticine and variants via DNA-intercalation process, bioactivation due to oxidation at C-9 and indirect topoisomerase II-inhibition is well described [4,6]. In this context many derivatives based on the linear annelated carbazole ellipticine and olivacine were synthesized for the development of new DNA-intercalating anticancer drugs [2,3,7]. However, only a few studies

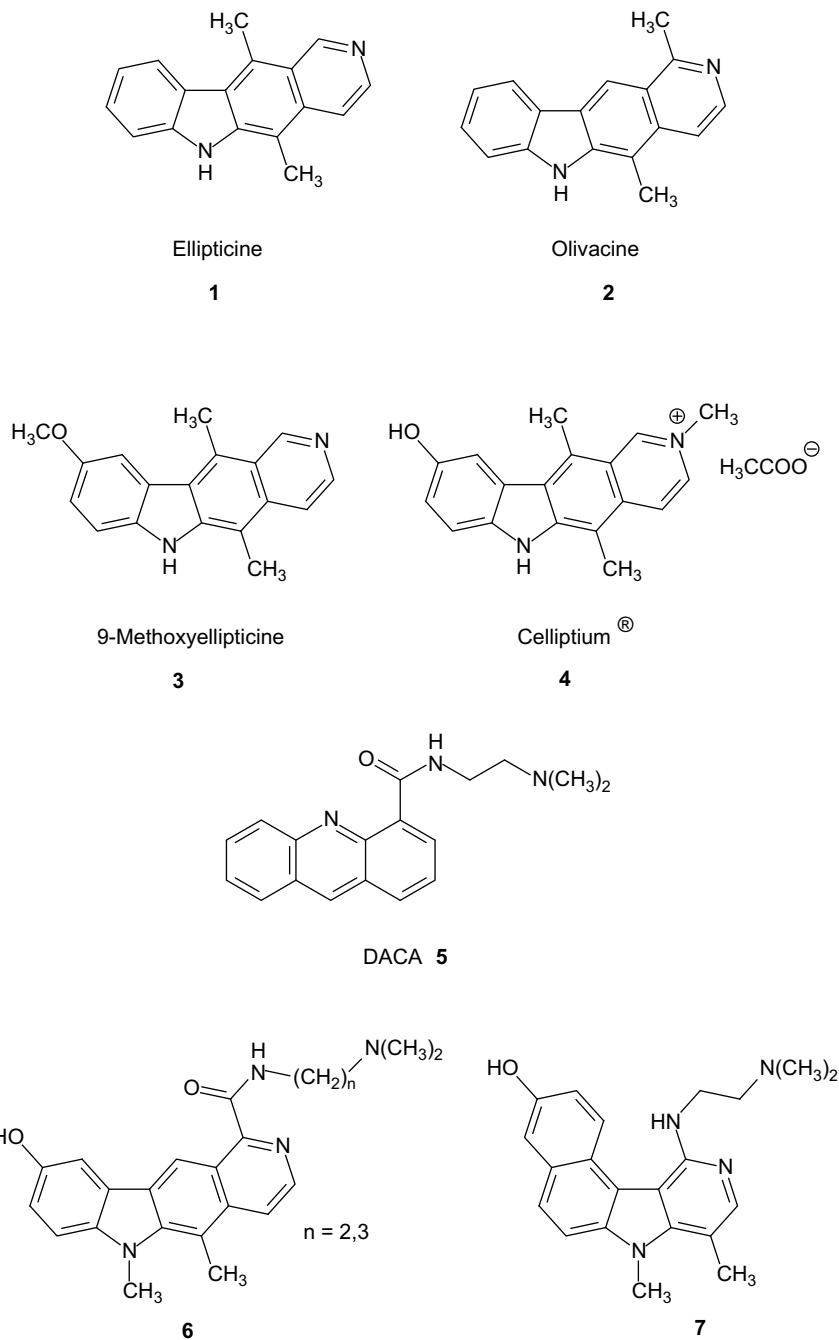
were carried out with compounds bearing an angled pyridocarbazole annellation [6,11]. Thus, in continuation of our synthetic efforts in carbazole and carbazole alkaloid chemistry [12,13], we studied new short and flexible routes to some heterocyclic-*a*-annelated carbazoles of type **10**. Moreover, derived from some literature reports [3,7,14] and from our own results in the netropsin series [15–19], the selective introduction of a dimethylaminoalkyl-carboxamide group at the coplanar chromophoric system should be of significant importance for a selective DNA binding and antitumor activity. For example DACA (*N*-[2-(dimethylamino)-ethyl]-acridine-4-carboxamide) **5** is a dual topoisomerase I/II inhibitor and DNA intercalator with potent cytotoxicity against leukaemia cell lines. Its carboxamide group is essential to the biological activity [14]. The olivacine derivatives **6** (*n* = 2: S16020-2) and the γ-carbolines **7** are further examples of drugs which bear a dimethylaminoalkylamino functionality as an important DNA-binding structure element which increases the cytotoxicity and antitumor activity (Scheme 1) [3,7–10].

On the background of these findings we describe in the present paper the preparation of new pyrido- and thieno-[*a*]-annelated carbazoles **10** bearing a dimethylaminoalkyl-carboxamide moiety at the carbazole ring C. In one case a morpholino moiety as cyclic

* Corresponding author.

** Corresponding author.

E-mail addresses: lemster@uni-mainz.de (T. Lemster), marie-helene.david@inserm.fr (M.-H. David-Cordonnier).



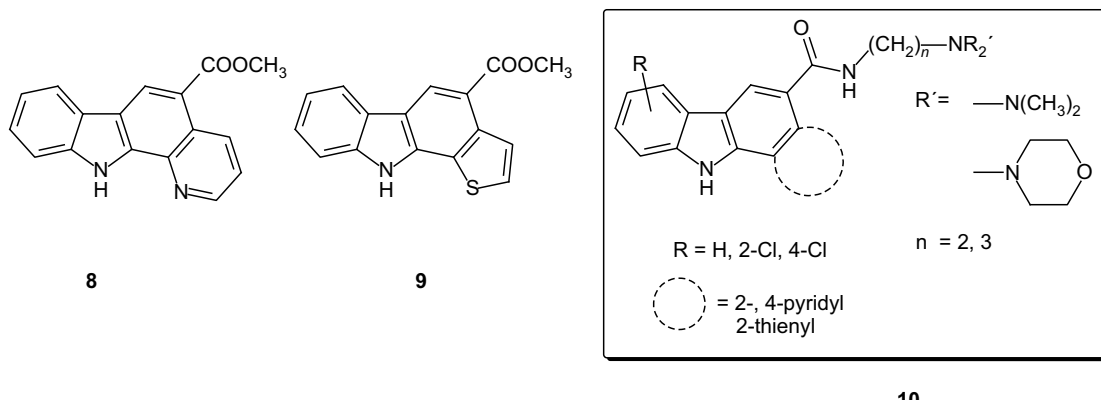
Scheme 1. Lead compounds: examples of annelated N-heterocycles as intercalating antitumor active drugs.

structural element was introduced. These products can be considered formally as regiosomeric and/or bioisosteric ellipticine derivatives combining an appropriate carboxamide structural element. The synthetical key step comprises a photochemically induced 6π -electrocyclisation, a convenient procedure derived from synthetic developments in our group [13,20]. For the establishment of primary structure–activity relationships (DNA-binding cytotoxicity) of these new functionalised carbazoles some biophysical, biochemical and cell biological studies were performed.

2. Chemistry

In former studies in our group, the synthesis of new benzo[a]-annelated carbazoles via photochemically induced

6π -electrocyclisation of 2-phenyl-3-vinylindoles has been established [20]. This convenient method has now been transferred to produce new pyrido- and thieno[a]carbazoles **8, 9** as chromophoric systems starting from the corresponding 2-hetarene-3-methyl-acrylate substituted indoles. Preorientating ΔT_m -value measurements of basic compounds **8** and **9** [18–20] exhibit no DNA binding at all. Thus, in relation to compounds **5–7** an amidic chain as potential binding element into the minor groove of DNA has been introduced (**10**) (Scheme 2). As already described above, a dimethylaminoethylamino- and the homologue dimethylamino-propylamino-function approved to have an optimal distance between the conjugated π -system and the tertiary aliphatic nitrogen as potential H-bond acceptor. Moreover the basic substituted carboxamide function comprises additional DNA-binding element (groove binding).



Scheme 2. Frameworks of the synthesized compounds (**8, 9**), general formula of the [*a*]-annelated carbazole amides (**10**).

The access to the new compounds **10** is displayed exemplarily in Scheme 3. The synthetic sequence starts with the synthesis of the corresponding hydrazones **13** readily available from the reaction of phenylhydrazines **11** with 2- and 4-acetylpyridine **12** in very good yields. Subsequent Fischer cyclization of **13** gave rise to indoles **14** in the presence of polyphosphoric acid in all cases. The obtained indoles were formylated according to Vilsmeier–Haak reaction using phosphoryl chloride in DMF. The resulting carboxaldehydes **15** were converted stereoselectively into the (*E*)-methylacrylates **16** via Wittig reaction in good yield (46–76%). In the following key step reaction the 2-hetaryl-3-vinylindoles **16** were submitted to ultraviolet irradiation ($\lambda = 200\text{--}600\text{ nm}$) for a period of 4–8 h achieving directly the desirable [*a*]-annelated carbazole derivatives **17** via 6 π -electrocyclisation and subsequent dehydrogenation. Standard hydrolysis in 20% aqueous sodium hydroxide/ethanol gave rise to the carboxylic acid **18** completely. In the last step the introduction of the dimethylaminoalkyl linker succeeded by reaction of the free acid **18** with *N,N*-dimethylalkylene diamine in DMF with EDCI/HOBt as catalysts (Scheme 3). The amides **19** were obtained in good yields. Thus, for fine tuning developments and for establishing structure–activity relationships (DNA binding, topoisomerases inhibition, cytotoxicity) structural variations were performed. In one case the tertiary amine function was implemented in morpholine ring system (**29**).

The chloro derivatives **22–27** were synthesized in order to evaluate the influence of increased polar hydrophobicity and decreased density of electrons in the chromophoric structure. Moreover the exchange of the pyridine ring against a more lipophilic and more π -electron rich thiophene ring (see compound **28** in Table 1) should expand the spectrum of structure–activity relationship. Furthermore in the planar system the position isomeric pyrido[4,3-*a*]carbazoles **24, 25** with a localized more peripheral nitrogen atom in the planar system were synthesized. These compounds should expand the activity pattern in comparison to the more lipophilic pyrido[2,3-*a*]carbazoles **20–23** relating to their biological/biophysical activities. The studies with the thiophene derivative **28** on DNA binding and topoisomerase inhibition demonstrated no significant advantage in comparison to the pyrido-derivatives, thus in the thiophene series no further synthetic variations were pursued so far (Table 1).

3. Biological and biophysical/biochemical methods

3.1. Cytotoxicity measurements

Due to restrictive criteria only three pyridocarbazole carboxamides were selected so far by the US National Cancer Institute [21] for evaluation in the *in vitro* preclinical antitumor screening

program against 60 human tumor cell lines. In the main screening, the sixty human tumor cell lines derived from the nine cancer types, leukaemia, non-small cell lung cancer, colon cancer, CNS cancer, melanoma, ovarian cancer, renal cancer, prostate cancer and breast cancer were used. The compounds' dose–response curves for each cell line were measured at a minimum of five concentrations at 10-fold dilutions in a protocol of 48 h continuous drug exposure, and a sulfurhodamine B (SRB) protein assay was used to estimate cell viability or growth. The concentration causing 50% cell growth inhibition (GI_{50}), total cell growth inhibition (TCI, 0% growth) and 50% cell death (LC_{50} , –50% growth) compared with the control was calculated. In general, $\log_{10} GI_{50}$ values (the molar concentration of the drug resulting in inhibition of cell growth to 50% of control) were used for comparative discussion.

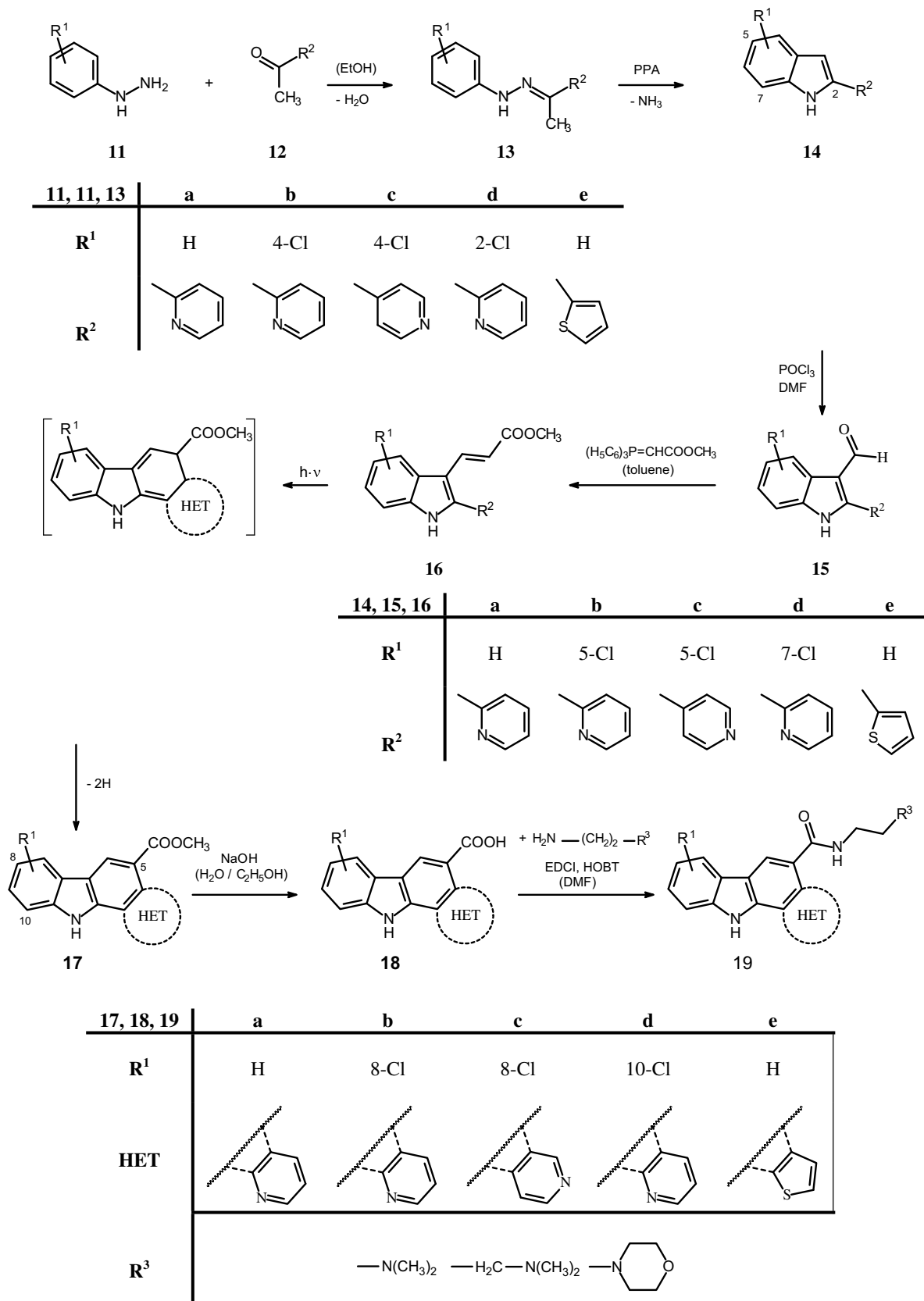
The best mean graph midpoint value MG_MID (activity is defined as a $\log_{10} GI_{50}$ of < 100 μM), which displays an averaged activity parameter over all cell lines, is –5.6 for the chloro-substituted compound **22**. The unsubstituted pyridocarbazoles display values of –5.2 for **20** and –4.9 for **21** (Table 2). From these results, it can be concluded that a C-2 side chain gives preference to the C-3 and furthermore the chloro-derivative is more active probably as a consequence of its higher lipophilicity.

It should be mentioned that compound **20** shows high potency against an ovarian (OVCAR-3; GI_{50} [M]: 2.54×10^{-8} , $\log_{10} GI_{50}$: –7.60) and a renal (CAKI-1; GI_{50} [M]: 5.15×10^{-7} , $\log_{10} GI_{50}$: –6.28) cell line suggesting that some antitumor-type cell selectivities can be adjudged to this compound.

In order to compare the whole series, the cytotoxic effect was measured on HT-29 cell line treated with increasing concentrations of the various compounds. The corresponding GI_{50} are presented in Table 3 and evidenced that compounds **24, 25** (and to a lesser extend compounds **22, 27**) are the most cytotoxic one with GI_{50} values in the micromolar range. All four compounds are chlorine-substituted molecules. Particularly, the pyrido-[4,3-*a*]carbazoles **24** and **25** are more cytotoxic than their respective pyrido[2,3-*a*]carbazole derivatives **22** and **23**. Surprisingly, in the dimethylamino-propyl series, the 10-chloro-substituted compound **27** is more cytotoxic ($GI_{50} = 4.5 \mu\text{M}$) than its 8-chloro-substituted derivative **23** ($GI_{50} = 9.2 \mu\text{M}$) whereas the opposite observation is made when the 8- or 10-chloro-substitution are present in the dimethylamino-ethyl-substituted series **26** ($GI_{50} = 14 \mu\text{M}$) and **22** ($GI_{50} = 3.2 \mu\text{M}$).

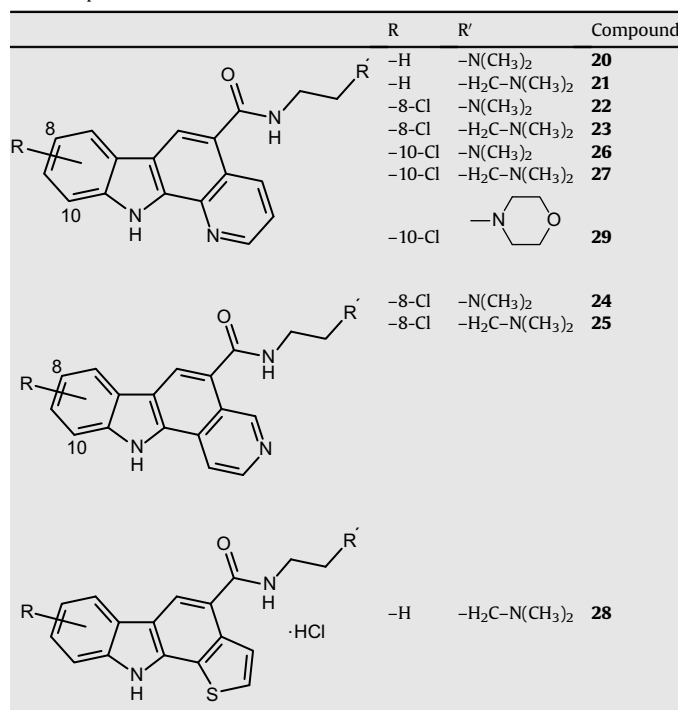
3.2. Cell cycle effect of compounds **20–29**

The effect of compounds **20–29** on cell cycle was then assessed on HT-29 colon carcinoma cells. Those cells were chosen based on the interesting result obtained on cytotoxicity measurements



Scheme 3. General synthetic route to hetarene [a]-annulated carbazole amides **19** (for the formula of the final products **20–29** see Table 1).

Table 1
The final products.



(Tables 2 and 3). Results in Fig. 1 evidenced a strong accumulation of cells in G2/M phases using the unsubstituted pyridocarbazoles **20** and **21** with a very strong reduction of cells in G1 phase. By contrast, cells treated with the chloro-pyridocarbazole compounds **22** and **23** first accumulate in G2/M phase and then in G1 phase. The increase in G2/M phase also correlate with a large decrease of the G1 phase and a smaller increase in the S phase portion from 20.4 ± 1.3 to 32.6 ± 0.3 and 31.7 ± 3.4 for $25 \mu\text{M}$ of unsubstituted compounds **20** and **21**, respectively, and to 37.0 ± 1.5 and 26.1 ± 0.8 for $10 \mu\text{M}$ of chloro-substituted pyridocarbazoles **22** and **23**. At higher concentrations ($25 \mu\text{M}$), the G2/M phase arrest observed using the chloro-pyridocarbazoles **22** and **23** is reduced with cells accumulating in G1 phase whereas using the unsubstituted pyridocarbazoles **20** and **21** cells stay in a large majority in G2/M

Table 2

Some results of the 60 panel NCI antitumor screening. GI₅₀: molar concentration of compounds, which induces inhibition of cell proliferation of 50%. MG_MID: mean graph midpoint, activity is defined as $\log_{10}\text{GI}_{50} < 100 \mu\text{M}$.

Compound	Tumor cell line	GI ₅₀ [M]	$\log_{10}\text{GI}_{50}$	MG_MID
20	OVCAR-3 (ovarian)	2.54×10^{-8}	-7.60	-5.2
	CAKI-1 (renal)	5.15×10^{-7}	-6.28	
	IGROV-1 (ovarian)	1.14×10^{-6}	-5.96	
	UO-31 (renal)	2.13×10^{-6}	-5.68	
	HT-29 (colon)	5.27×10^{-6}	-5.28	
21	CCRF-CEM (leukaemia)	4.31×10^{-6}	-5.37	-4.9
	COLO 205 (colon)	4.43×10^{-6}	-5.35	
	ACHN (renal)	5.24×10^{-6}	-5.28	
	HT-29 (colon)	1.03×10^{-5}	-5.99	
22	UO-31 (renal)	1.10×10^{-6}	-5.96	-5.6
	SK-MEL-5 (melanoma)	1.34×10^{-6}	-5.87	
	SW-620 (colon)	1.47×10^{-6}	-5.83	
	HT-29 (colon)	2.33×10^{-6}	-5.63	

Table 3
HT-29 cells cytotoxicity of the various compounds measured using MTS assays.

Compound	GI ₅₀ (μM)
20	11.5 ± 3.4
21	10.1 ± 1.4
22	3.20 ± 1.25
23	9.23 ± 3.12
24	1.08 ± 0.28
25	2.20 ± 1.07
26	14.0 ± 2.3
27	4.49 ± 1.48
28	10.8 ± 0.5
29	ND

phases. No differences were observed depending on the length of the side chain (compounds **20** and **22** versus **21** and **23**).

Using compound **24**, cells accumulate in G2/M phases and then in S phase. The cell cycle is less affected by treatment using compounds **25–27** with a much weaker accumulation in G2/M phase.

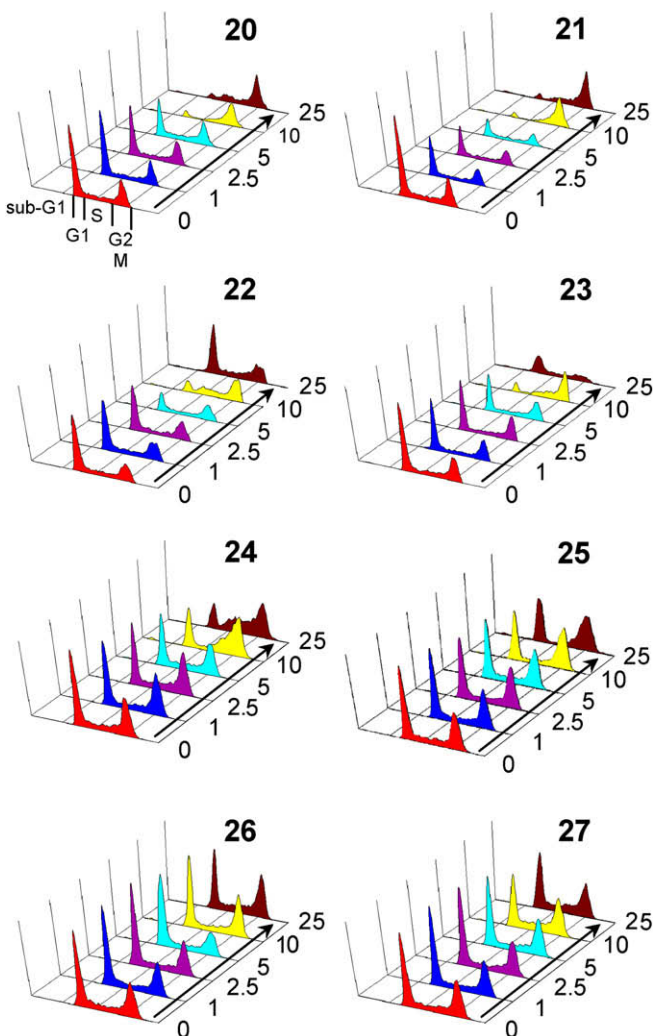


Fig. 1. Cell cycle effect of compounds **20–23** on HT-29 cells. HT-29 cells in exponential growth were exposed to the indicated concentrations of compounds **20–23** (μM) for 24 h prior to be fixed and labelled with PI for flow cytometric analysis. The various cell cycle phases and sub-G1 portion are localized in the first panel.

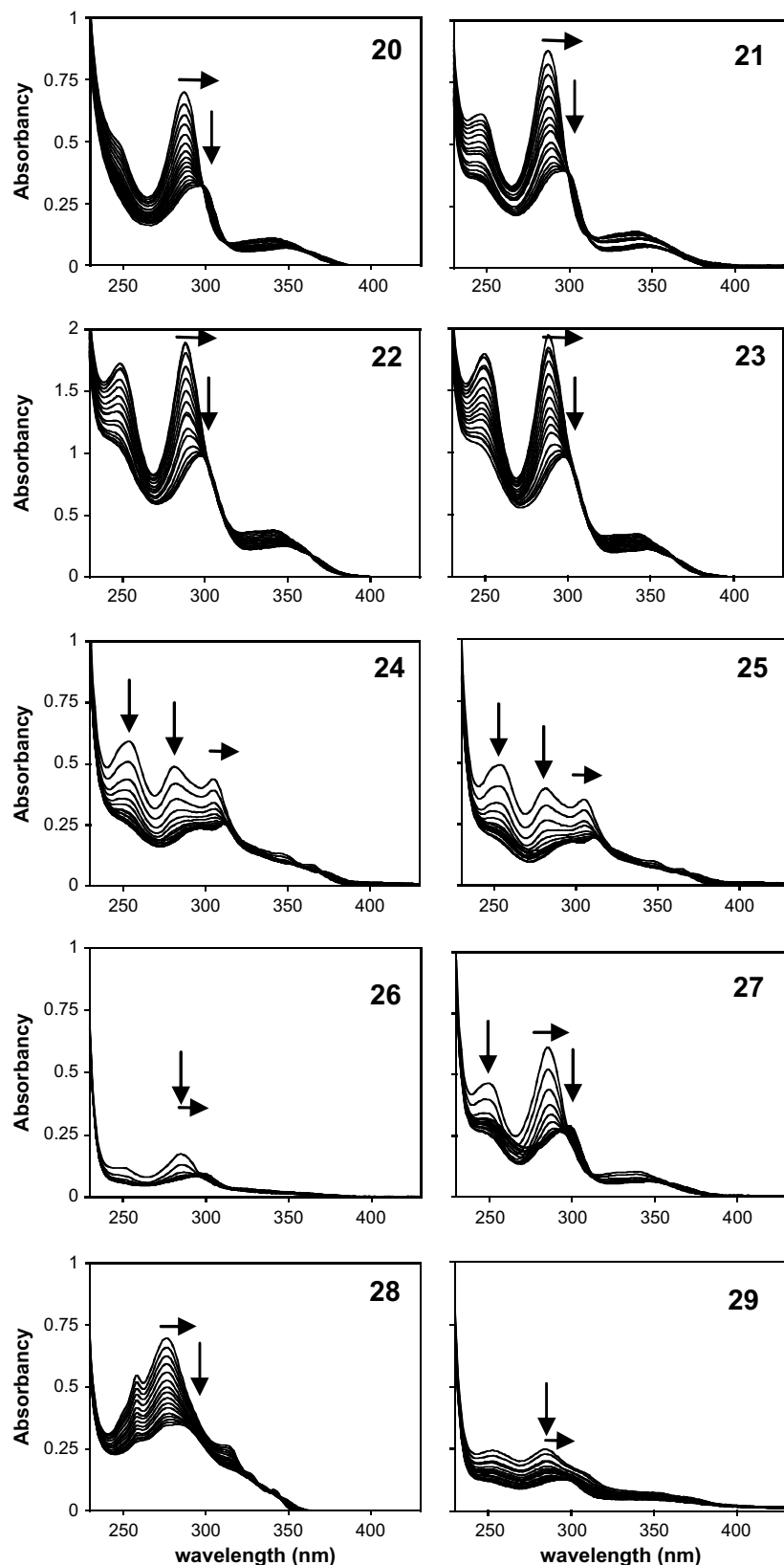


Fig. 2. UV/vis absorption spectra of pyrido[2,3-a]carbazoles in the absence (upper line) or presence of calf-thymus DNA (phosphate/drug ratio from 1 to 20). Arrows ↓ and → refer to hypochromic and bathochromic effects, respectively.

Table 4
Quantification of hypochromic and bathochromic effects.

Compound	$\lambda 1^a$ (nm)	$\lambda 2^b$ (nm)	$\Delta\lambda^c$ (nm)	H ^d %
20	287	293	+6	62
21	287	292	+5	56
22	288	298	+10	48
23	288	297	+9	51
24	254			56
	281			62
	305	309	+4	37
25	254			56
	281			65
	305	312	+7	25
26	286	298	+12	46
27	250			45 ^e
	286	291 ^e	+5	54 ^e
28	276	284	+8	50
29	284	297	+13	48

^a $\lambda 1 = \lambda_{\max}$ compound alone.

^b $\lambda 2 = \lambda_{\max}$ compound+CT-DNA.

^c $\Delta\lambda = \lambda 1 - \lambda 2$. Positive values evidenced bathochromic effects.

^d Hypochromic effect H = $[100 \times (\text{Abs}^{\text{compound alone}} - \text{Abs}^{\text{compound+CT-DNA}})/\text{Abs}^{\text{compound alone}}]$ at the specified wavelength (λ).

^e Hypochromic and bathochromic effects are measured at the minimal point regarding the following increase in the y value due to complex binding mode.

Quantification of cells in each cell cycle steps was performed as untreated cells (0) or cells treated with the increasing concentration of each compounds (arrow), as specified on the left of each graph (μM), is performed as described in the Material and methods section. The localisation of subG1, G1/G0, S, G2/M phases is specified on the first graph.

3.3. DNA binding and inhibition of topoisomerases I and II

3.3.1. UV/vis spectral absorbance

In order to address the DNA-binding ability of this series of pyridocarbazoles in the primary screening, we first looked at the modification of the absorption spectra of the various compounds in the absence and presence of increasing concentrations of calf-thymus DNA (phosphate/drug ratio from 1 to 20) based on the principle that the UV/Vis-spectra of a substance changes if it interacts with the DNA. The spectra of pyridocarbazole derivatives are presented in Fig. 2. All these compounds show hypochromic and bathochromic effects (arrows ↓ and →, respectively) that are quantified in Table 4. Comparison between compounds **20** and **21** to their corresponding chloro-containing derivatives **22** and **23** reveals similar hypochromic effects but different bathochromic shifts (Fig. 2 and Table 4). This bathochromic effect implies a stronger interaction between DNA and the chromophore using the chloro-substituted compounds from comparison with the unsubstituted pyridocarbazoles.

3.3.2. DNA-melting temperature

The DNA ligand affinity can be determined by UV measurement of the DNA-melting temperature, which is enhanced in case of ligand binding (base-pair separation). In order to confirm the DNA-binding ability of those compounds, we then looked at the stabilization of the DNA helix by the various heterocyclic annelated carbazoles using melting temperature studies. UV spectroscopic determination of the melting curve of DNA compared with the melting curve of a DNA ligand complex gives a basic information about the binding potency of a ligand to DNA [22] and is used to compare the relative affinity of a series of derivatives. The ΔT_m values ($T_m[\text{CT-DNA+drug}] - T_m[\text{CT-DNAalone}]$) were determined using calf-thymus DNA (CT-DNA) and poly(dAdT)₂ at DNA/drug ratio from 0.1 to 1. A ΔT_m value of more than 10 is a convenient sign for

a good DNA binding of the ligand. Table 5 represents the ΔT_m data of this series of the new compounds.

Derived from these data, all compounds but compound **29** reflect a significant affinity to the poly(dAdT)₂-DNA sequence (ΔT_m values > 18 °C). Comparison between ΔT_m values obtained from unsubstituted (**20**, **21**) and chloro-substituted pyridocarbazoles (**22**, **23**) clearly reveals the increase of DNA binding caused by the halogen atom. Both ΔT_m values of poly(dAdT)₂ and CT-DNA confirm this structure–activity relationship. It is mentioned that the chloro derivatives possess a higher DNA-binding affinity as the leading substance ellipticine (**1**), probably caused by their polar hydrophobicity. Concerning the length of the amidic chain, no obvious preference could be noticed from comparison of the relative affinity for DNA of compounds **20**, **22** and **24** versus **21**, **23** and **25**, respectively. However, comparison of the relative affinity for CT-DNA or poly(dAdT)₂ of compounds **26** and **27** evidenced an increase in the DNA affinity in the presence of a dimethylamino-propyl chain (**27**) instead of a dimethylamino-ethyl one (**26**). For this latter, the reduced DNA affinity could also be attributed to the orientation of the chlorine on the carbazole ring. Indeed, comparison of the relative DNA affinity for compounds **22** and **26** enlightens a decrease in DNA-binding potency when the chlorine is substituted at position 10 (**26**) instead of position 8 (**22**). The integration of a π -electron rich thiophene moiety (**28**) does not enhance the affinity for DNA compared to its pyrido analogues. Evidently, the electron density of the chromophoric system is not as determining for the DNA interaction as the introduction of a more lipophilic group. Finally, the presence of dimethyl-amine at the end of the lateral chain is, as attempted, crucial for the DNA binding as evidenced from comparison of the results using compounds **26** and **29**, in correlation with previous observation using compounds **8** and **9** lacking any side chain and that failed to induce any ΔT_m values.

3.4. Fluorescence studies

Compounds **20**–**25** and **28** present intrinsic fluorescence properties which could be used to evaluate their respective DNA-binding propensities (Fig. 3). Compounds chloro substituted in position 10 are not fluorescent. From the titration of compounds **24** and **25**, the emission maxima undergoes a clear red shift after binding to increasing concentration of CT-DNA, reflecting a more polar environments. The additional decrease of the fluorescence intensities indicates a marked quenching upon binding to the DNA. The quenching constant K_{SV} was deduced from Stern–Volmer plots to be 6.72×10^{-3} and $9.95 \times 10^{-3} \text{ M}^{-1}$ for compounds **24** and **25**,

Table 5

Variation of DNA-melting temperature ΔT_m [°C] of calf-thymus DNA and poly(dAdT)₂ from complexation with various pyridocarbazoles (**20**–**27**, **29**) and a thienocarbazole (**28**). r = molar ratio of ligand/DNA.

Compound	ΔT_m (°C)									
	CT-DN				Poly(dAdT) ₂					
	r	0.1	0.25	0.5	1	r	0.1	0.25	0.5	1
20	0	3.0	2.9	7.3	2.9	11.8	14.5	18.9		
21	0	4.4	4.4	7.3	2.9	8.9	11.6	17.5		
22	1.5	7.4	7.3	11.7	6.1	14.7	18.9	24.9		
23	3.0	7.4	8.8	13.2	6.1	9.2	20.4	27.8		
24	5.3	7.9	11.2	15.1	11.6	18.9	24.7	29.6		
25	3.6	6.6	10.7	13.9	10.3	17.3	22.7	28.3		
26	1.1	1.5	5.1	7.9	2.8	6.2	13.6	8.8		
27	2.6	5.0	10.4	13.8	9.7	17.6	23.6	29.8		
28	0	1.5	4.4	5.8	5.9	11.9	16.4	20.9		
29	0	0.7	0.4	0.6	2.1	3.9	5.3	5.3		

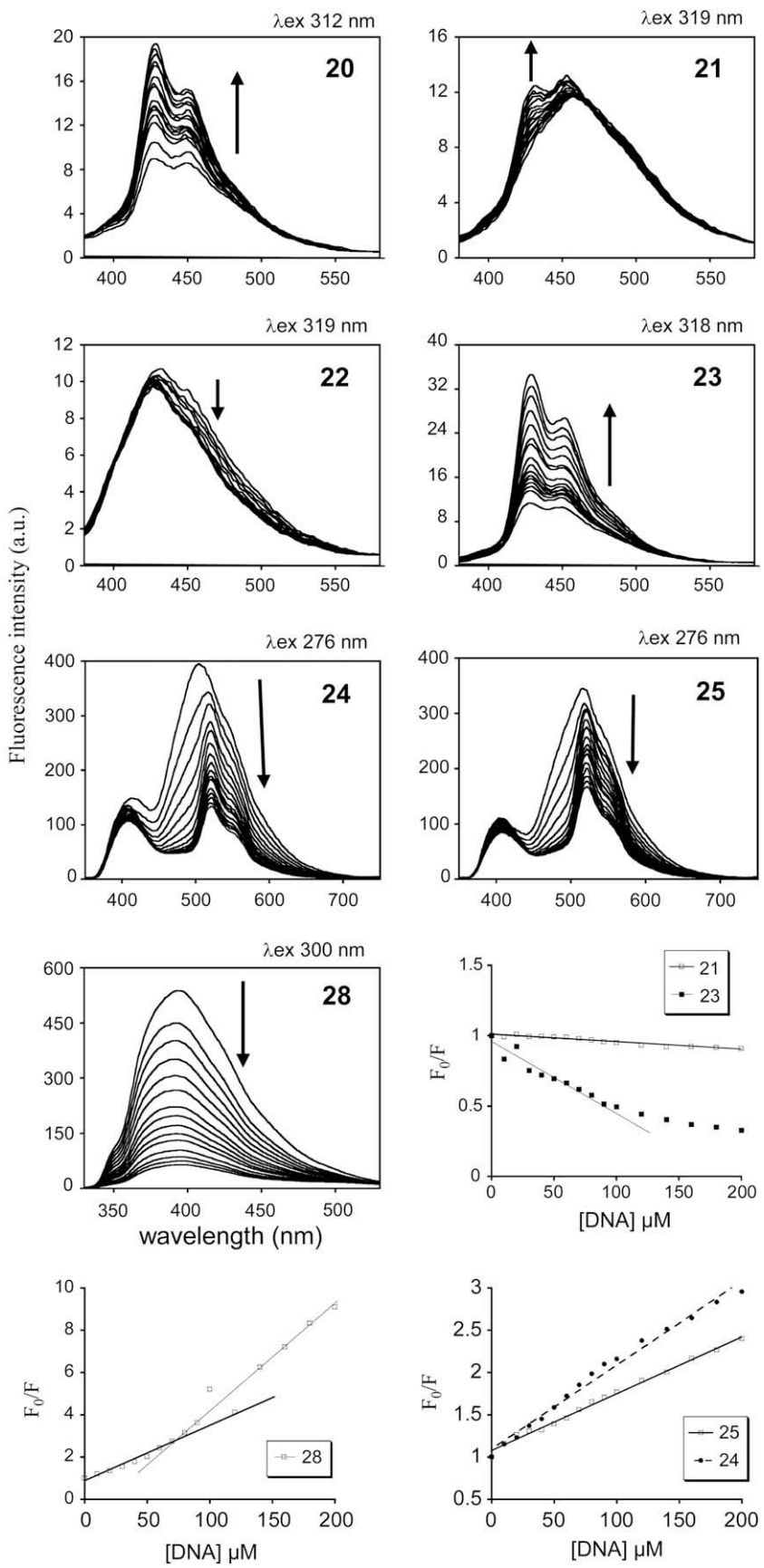


Fig. 3. Fluorescence spectra of the various pyridocarbazoles upon incubation with graded concentrations of CT-DNA. A fixed concentration of the various derivatives ($20 \mu M$) was incubated with increasing concentrations of CT-DNA from 10 to $200 \mu M$ for a phosphate/compound ratio from 0.4 to 8. Arrows indicate the orientations of the fluorescence quenching (\downarrow) or enhancement (\uparrow). The excitation wavelength peaks for the various compounds are indicated at the top of the related graphs. Stern–Volmer plots expressing F_0/F as a function of the concentration of CT-DNA is used to deduce the quenching and enhancement constants for the indicated compounds on the three bottom graphs.

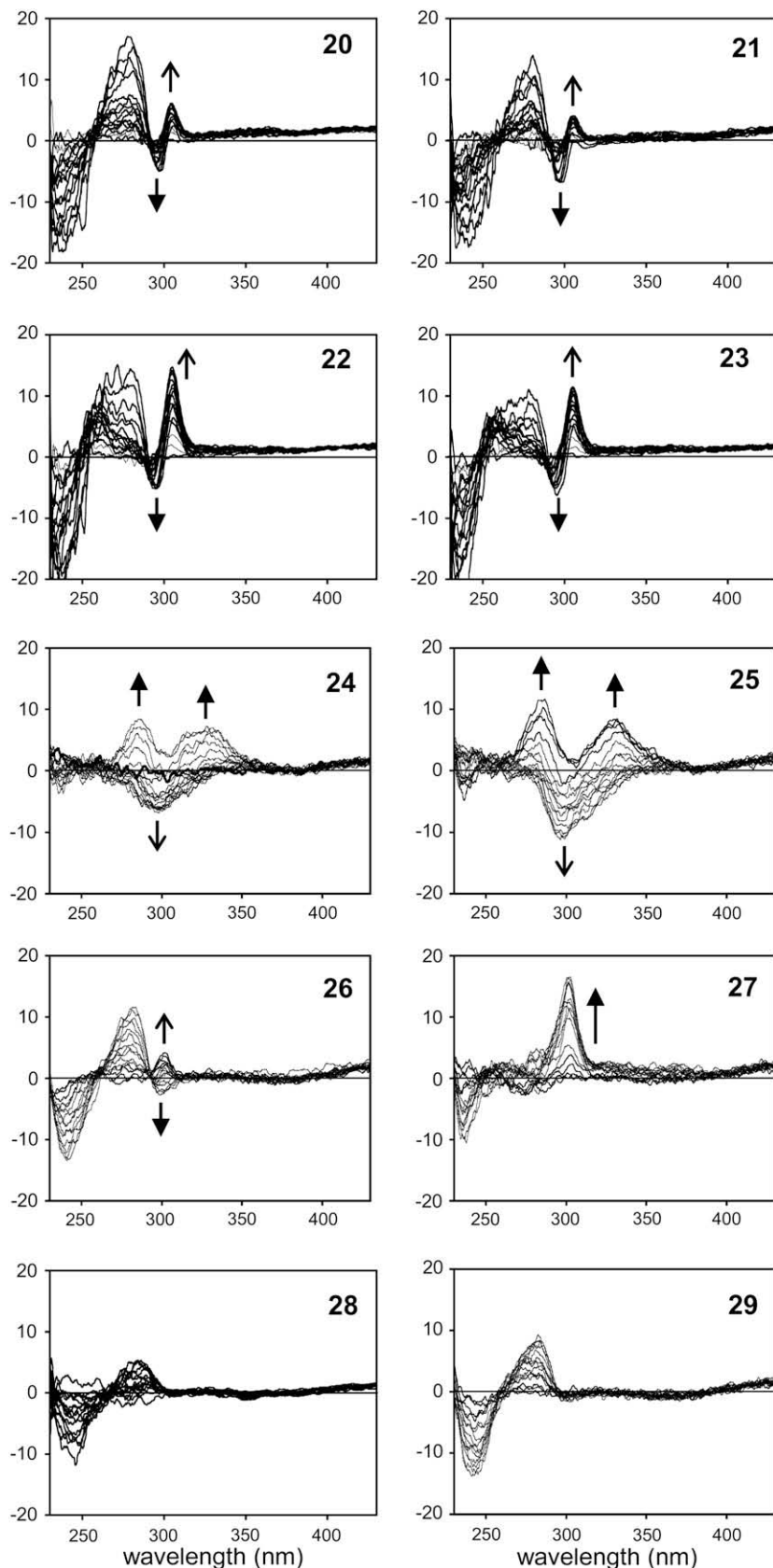


Fig. 4. Circular dichroism spectra of CT-DNA with the various pyridocarbazoles. A fixed concentration of the various derivatives (50 μ M) was incubated with increasing concentrations of CT-DNA from 10 to 200 μ M (phosphate/compound ratio from 0.4 to 8). Open and full arrows indicate the orientations of the induced CD at lower and upper CT-DNA concentrations, respectively.

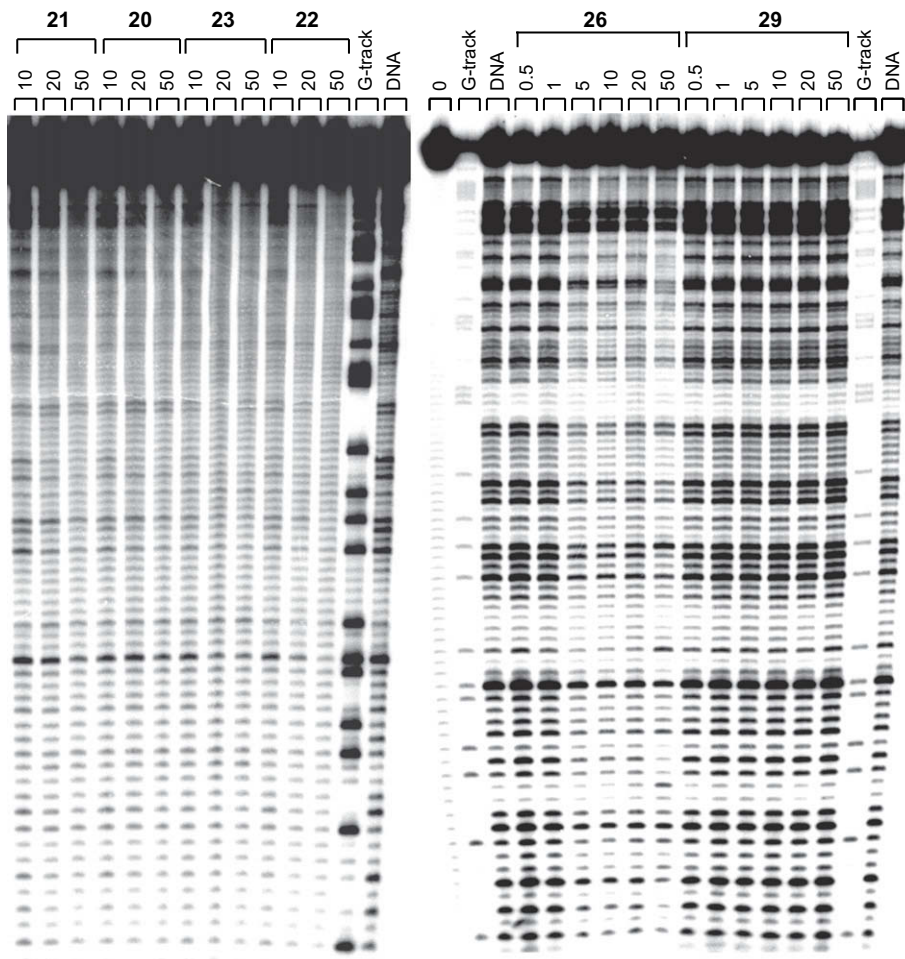


Fig. 5. Localisation of the DNA binding using DNase I footprinting analysis. The 3'-end labelled EcoRI-PvuII fragment of pBS vector was incubated with increasing amount of the drug as specified on the top of the appropriate lanes (μM) prior to be digested by DNase I. Control tracks labelled "DNA" contained no drug. Lanes labelled "G-track" were used as marker for guanine positions. Lane "0" evidenced the untreated radio-labelled DNA fragment used as quality control.

respectively. The DNA-binding mode for compound **28** appears to be more complex regarding the two slopes evidenced from Stern–Volmer plot. Such result suggests that two types of fluorophores are present in solution, one being compound **28** alone and the second being the complex formed between compound **28** and DNA base pairs. The quenching constant for compound **28** was calculated to be of $2.65 \times 10^{-4} \text{ M}^{-1}$ from the first points at CT-DNA concentrations up to $80 \mu\text{M}$. Contrasting with the fluorescence quenching through DNA interaction of those compounds, an enhancement of the fluorescent is observed using compounds **20** and **23**, as well as to a lesser extend using compound **21**. The enhancement constants for 8-chloro (**23**) or unsubstituted (**21**) derivatives were deduced from plotting F_0/F versus the concentration of CT-DNA to be $4.84 \times 10^{-3} \text{ M}^{-1}$ and $5.94 \times 10^{-2} \text{ M}^{-1}$, respectively.

3.4.1. Circular dichroism measurements

The binding of an achiral ligand to the chiral DNA causes an induced optical activity of the ligand. These measurements with CT-DNA were used to get an insight in the DNA-binding mode – intercalation and/or groove binding – of the various annulated carbazoles. The most common feature (compounds **20–23**) is a positive induced CD signal in the absorption area of the pyridocarbazole ligand around $\lambda = 310–315 \text{ nm}$ (Fig. 4) suggesting a groove binding of the compounds. This positive induced CD (ICD) occurs using the lowest CT-DNA concentrations and shifted to

a negative absorbance between $\lambda = 295–315 \text{ nm}$ (Fig. 4) for higher CT-DNA concentrations, suggesting the displacement of those compounds from DNA groove binding to an intercalation binding mode by increasing the concentration of base pairs (Fig. 2). Surprisingly, the pyrido-[4,3a]carbazoles **24** and **25** present different ICDs with a negative ICD at wavelength around 300 nm using the lowest CT-DNA concentrations shifting to a positive ICD at wavelength around 285 and 330 nm using the highest phosphate/drug ratio. A unique high positive ICD at 300 nm is observed using the 10-chloro-derivative **27** with a saturation of the effect for a phosphate/drug ratio of more than 4.8. The other 10-chloro-derivative **26** bearing a dimethyl-amino-ethyl arm instead of a dimethyl-amino-propyl (**27**) presents a positive ICD at the same wavelength for up to a phosphate/drug ratio of 1.2 followed by a negative ICD for higher CT-DNA/compound ratio. The morpholino derivative **29** which can be considered as a cyclic analogue of dimethylamino end of compound **26** to give abolished the formation of ICD at the wavelength of the compound, in agreement with the crucial role of the positively charged amino-termini for DNA-binding stabilization.

3.4.2. Localisation of DNA-binding site

The DNA minor groove is a good docking site for sequence selective DNA ligand. The sequence selectivity for a compound can be achieved using DNase I footprinting on a radio-labelled DNA

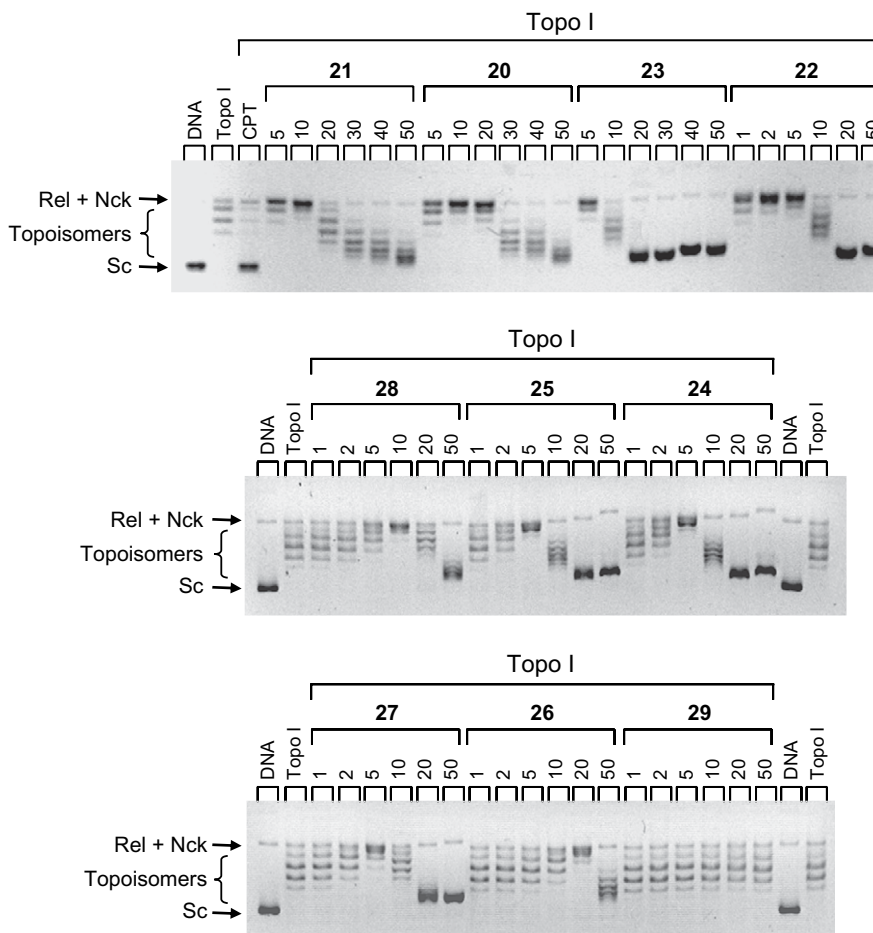


Fig. 6. Topoisomerase I-induced DNA relaxation. The effect of the various pyridocarbazoles and the thienocarbazoles on the relaxation of supercoiled plasmid DNA by topoisomerase I was established using native supercoiled pUC19 DNA (130 ng; lanes DNA) incubated with topoisomerase I in the absence (lanes Topo I) or presence of increasing concentrations (μM) of the various compounds. The different forms of plasmid DNA were separated by electrophoresis on a 1% agarose gel which was then stained with ethidium bromide. Rel, relaxed; Sc, supercoiled; Nck, nicked.

fragment. We evaluated the potential for sequence selective binding of this series of compounds on a 117 bp 3'-end labelled DNA fragment (Fig. 5). Incubation of increasing concentrations of each compounds failed to evidence any sequence selectivity but non-specific DNA interaction as attempted for DNA-intercalating compounds. The non-specific DNA binding can particularly well be seen using compounds **20–27** whereas compound **28** only weakly affect the DNase I activity and compound **29** totally failed to modify the DNA cleavage profile. Those results are in perfect correlation with previous observation from spectroscopic analysis.

The 3'-end labelled EcoRI-PvuII fragment of pBS vector was incubated with increasing amount of the drug as specified on the top of the appropriate lanes (μM) prior to be digested by DNase I. Control track labelled "DNA" contained no drug. Lanes labelled "G-track" were used as marker for guanine positions. Lane "0" evidenced the untreated radio-labelled DNA fragment used as quality control.

3.4.3. Inhibition of topoisomerases I and II

In order to get a further insight in the mode of binding of the pyridocarbazole derivative on DNA, we used the DNA relaxation properties of topoisomerase I. This method is a powerful approach to evidence DNA-intercalation process as an enhancer of DNA relaxation creating more relaxed topoisomers from topoisomerase

I-mediated cleavage of supercoiled DNA. As presented in Fig. 6, all compounds but compound **29** present a change in the topoisomer profile from negatively supercoiled to relaxed DNA (Rel) and back to (positively) supercoiled position (Sc). Those DNA relaxation profiles suggest that the compounds are potent DNA base pair intercalators thus acting on the twist of the DNA helix. The lack of DNA relaxation profile for compound **29** is in agreement with previous results evidencing no DNA double strand stabilization (Table 5), which is usually strong for DNA intercalators, and no ICD in Fig. 4. Therefore, since no groove binding could be evidenced in CD measurements, the hypochromic effect seen in UV/vis absorbance measurements with compound **29** in the presence of CT-DNA could presumably only be attributed to electrostatic binding of compound **29** to the phosphate backbone. From the DNA relaxation experiment, the intercalation efficiencies could be classified from weaker to stronger: **26 < 20 < 21**, **27, 28 < 22, 23, 24, 25** and correlate with their efficiency to stabilize the DNA helix (CT-DNA and poly(dAdT)₂) evidenced using melting temperature studies: **26 < 20, 21 < 27, 28, 22–25**.

Regarding the differences for DNA binding and DNA-intercalation potencies of the unsubstituted compounds **20** and **21** versus the chloro-substituted equivalent **22** and **23**, those four compounds were evaluated for topoisomerases I and II poisoning effect. From comparison with the respective reference compounds

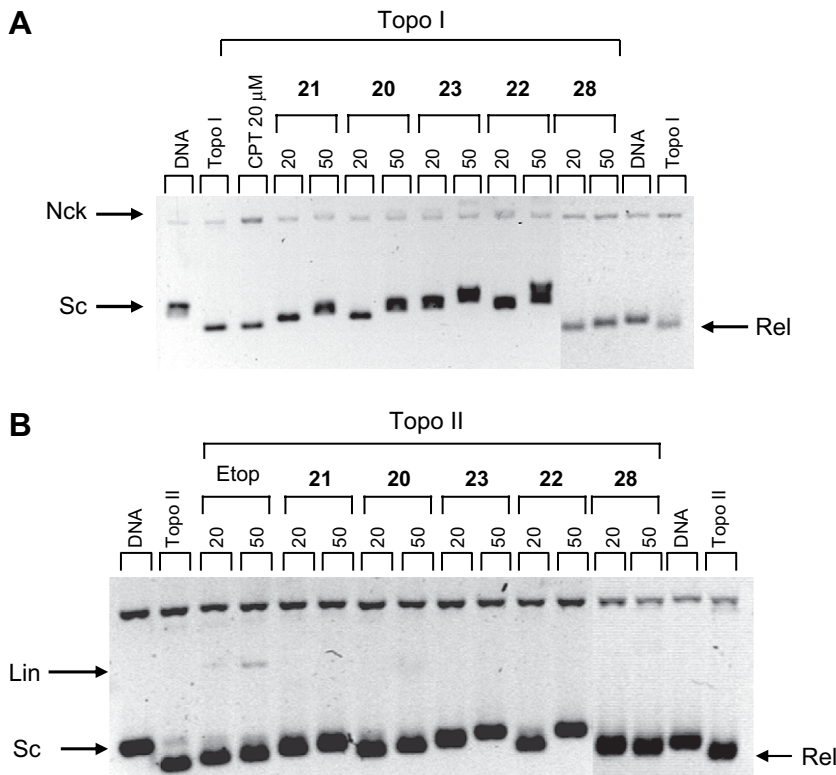


Fig. 7. Topoisomerase I (**A**) and II (**B**) poisoning effects of various pyridocarbazoles. Native supercoiled pUC19 plasmid DNA (130 ng, lanes DNA) was incubated with topoisomerase I or II in the absence (lanes Topo I or Topo II) or presence of 20 or 50 μ M of the various derivatives. Camptothecin (CPT) and etoposide (Etop) were used as specific controls. DNA samples were separated under electrophoresis on an ethidium bromide containing 1% agarose gel. The gels were photographed under UV light. Sc, supercoiled; Rel, relaxed; Nck, nicked; Lin, linear.

camptothecin (CPT, Fig. 7A) and etoposide (Etop, Fig. 7B), none of those compounds are topoisomerase I or II inhibitors as evidenced by the lack of nicking form (topoisomerase I) and double strand break form of the DNA (linear DNA, topoisomerase II). The gel shift migration of the supercoiled form correlates with the binding efficiency of the compounds: the chloro-derivatives **22** and **23** are more potent DNA-binding compounds than the unsubstituted compounds **20** and **21**, in perfect correlation with previous conclusions.

4. Discussion and conclusion

Only carbazoles **20**, **21** and the chloro derivative **22** were chosen for NCI antitumor screening. The chloro derivative **22** which displays a Mean Graph Midpoint value (MG_MID) of -5.6 proved to be the most active compound in general, whereas compound **20** shows significant activity against single ovarian (GI_{50} [M]: 2.54×10^{-8}) and renal (GI_{50} [M]: 5.15×10^{-7}) tumor cell lines (Table 2). Comparison of the cytotoxicity of the whole series of those newly synthesized carbazoles was established in the lab on the colon carcinoma cell line HT-29 and evidenced that compounds **22** but also compounds **24** and **25** (and to a lesser extend compound **27**) are the most cytotoxic agents in this series with GI_{50} in the μ M range (Table 3). The cellular effects of those compounds are associated with a major G2/M phase arrest (Fig. 1).

On the basis of the UV absorption (hypochromic and bathochromic shifts) and ΔT_m values the chloro derivatives bearing a dimethylaminoalkyl-side chain reveal a significantly stronger DNA-binding potency than the basic related compounds **20** and **21**.

This could be due to an increase of the polar hydrophobicity of the chloro-derivatives relatively to the unsubstituted pyridocarbazoles.

According to the DNA-melting temperature measurements, the ΔT_m values of chloro-pyridocarbazoles **22–25** and **27** range between about 25 and 30 °C, highlighting their potent DNA binding. Using this assay, the pyridocarbazoles **24** and **27** are the strongest DNA binders. Concerning the length of the amidic chain, no obvious preference could be noticed from comparison of the relative affinity for DNA of the ethylamides **20**, **22** and **24** versus the corresponding propylamides **21**, **23** and **25**, respectively. However, comparison of the relative DNA affinity for CT-DNA or poly(dAdT)₂ of compounds **26** and **27** evidenced an increased DNA affinity in the presence of a dimethylamino-propyl chain (**27**) instead of a dimethylamino-ethyl (**26**). For this latter, the reduced DNA affinity could also be attributed to the orientation of the chlorine on the carbazole ring. Indeed, comparison of the relative DNA affinity for compounds **22** and **26** enlightens a decrease in DNA-binding potency when the chlorine is substituted at position 10 (**26**) instead of position 8 (**22**). The integration of a π -electron rich thiophene moiety (**28**) does not enhance the affinity for DNA compared to its pyrido-analogues. Finally, the presence of dimethyl-amine at the end of the lateral chain is, as attempted, crucial for the DNA binding as evidenced from comparison of the ΔT_m results using compounds **26** and **29**, in correlation with previous observation using compounds **8** and **9** lacking any side chain and that failed to induce any ΔT_m values.

The fluorescence titration studies are throughout positively by compounds **24**, **25** and **28** with the exception of the morpholine derivative **29**. The induced CD (ICD) on drug/DNA-binding evidences a common positive ICD signal compounds **20–23** suggesting a groove binding. By contrast, the pyrido-[4,3-a]carbazoles

24 and **25** evidence negative ICD present from the lowest CT-DNA concentrations and followed by a positive ICD at the highest CT-DNA concentrations. This suggests a preliminary groove binding (amidic side chain) shifting then to an intercalation on the core of the compound between adjacent base pairs at saturating concentrations. Interestingly, the 10-chloro-derivative **27** only evidences a high positive ICD in the wavelength of the compound suggesting unique groove binding contrasting with the 10-chloro-derivative **26** presenting groove binding followed by good intercalative process. This suggests that the presence of both the chlorine and the shorter arm alters the correct positioning of the chromophore between adjacent base pairs with the chlorine protruding on one side of the DNA helix (major groove) and the dimethylaminoalkyl-side chain on the other side (minor groove), thus leading to the unique groove binding of this compound. Positioning of the chlorine at position 8 does not affect the intercalation of the chromophore within the DNA since it will be orientated properly relatively to the phosphate backbone of the DNA helix.

DNase I footprinting studies for analysing sequence selectivity of binding reveals for compounds **20–27** throughout a non-specific binding whereas carbazole **28** only weakly affects the DNase I activity and compound **29** totally failed to modify the DNA damage profile. These results are in perfect correlation with previous observations from spectroscopic analysis.

Finally, the topoisomerase I and II poisoning effects are in good correlation with other results. Indeed, the gel shift migration of the supercoiled form correlates with the binding efficiency of the compounds: the chloro derivatives **22** and **23** are more potent binding compounds than the unsubstituted compounds **20** and **21** in perfect correlation with previous conclusions.

It accomplished to synthesize a series of pyrido- and thieno-carbazole amides via photochemically induced 6π -electrocyclisation. The biological and biophysical/biochemical results reveal high DNA-binding properties especially of chlorine-substituted pyridocarbazoles which exceed considerably the DNA-binding affinity of the leading substance ellipticine. The replacement of pyridine with an electron rich thiophene does not seem to bring a benefit on DNA binding. The introduction of a cyclic residue in the amidic group as side chain (morpholine) decreases DNA binding compared to acyclic series. Concerning the binding mode of active compounds **10**, we suggest groove binding and intercalation. The synthesis of regio-isomers and particularly the introduction of a further halogen atom in the chloropyridocarbazole framework give rise to develop promising candidates as potent DNA ligands.

5. Experimental

5.1. Chemistry

Melting points were measured with a Büchi 510 instrument and are uncorrected. IR spectra were recorded on a Thermoelectron Avatar 330 FT-IR using ZnSe crystal (AMTIR) (ν in cm^{-1}). ^1H NMR, ^{13}C NMR spectra including spin echo were recorded on a Bruker AC-300 apparatus (300 MHz). The samples were dissolved in CDCl_3 or $\text{DMSO}-d_6$. pd: pseudodoublet; pt: pseudotriplet. The chemical shift values are reported in parts per million (ppm, δ units) and spin-spin coupling J were listed in hertz. 70 eV EI-mass spectra were obtained with a Mascom 311-A apparatus and FD mass spectra with a Finnigan MAT 7 instrument. Photochemical apparatus: Normag company, mercury vapour medium pressure lamp with 150 W and an area of wavelength $\lambda = 200\text{--}600$ nm. Column chromatography was performed on silica gel (Merck, silica gel 60). Petrol ether of boiling point 40–60 °C was used. Non-stoichiometric inclusion of solvent molecules gave always C, H, N analysis with divergence

>0.3%. Despite using different solvent mixtures in TLC only one spot could be detected, therefore the testing compounds were considered analytically pure.

5.2. General procedure for the synthesis of hydrazones

The acetyl hetarenies [11.2 ml (100 mmol) 2- or 4-acetylpyridine resp. 10.8 ml (100 mmol) 2-acetylthiophene] were dissolved in 300 ml ethanol and the hydrazine [9.8 ml (100 mmol) phenyl-hydrazine resp. 17.0 g (100 mmol) 2- or 4-chlorophenylhydrazine·HCl] were added. The resulting yellow suspension was refluxed for 5 h. After cooling, the precipitated hydrazone was filtered off, washed with ethanol and petrol ether and dried.

5.2.1. 2-[(1-(2-Phenylhydrazono)ethyl)pyridine] (**13a**) [23]

Yellow solid, (19.4 g) (90 mmol) (90%), m.p. 153 °C; ^1H NMR (CDCl_3): $\delta = 2.38$ (s, 3H, CH_3), 6.89 (m, 1H, phenyl-H-4), 7.16–7.31 (m, 4H, phenyl-H), 7.71 (m, 2H, pyridyl-H), 8.14 (pd, 1H, $J = 8.1$ Hz, pyridyl-H-3), 8.56 (pd, 1H, $J = 5.0$ Hz, pyridyl-H-6).

5.2.2. 2-{1-[2-(4-Chlorophenyl)hydrazono]ethyl}pyridine (**13b**)

Yellow solid, (21.3 g) (86 mmol) (86%), m.p. 238 °C; ^1H NMR ($\text{DMSO}-d_6$): $\delta = 2.40$ (s, 3H, CH_3), 7.32 (pd, 2H, $J = 8.8$ Hz, phenyl-H-2, H-6), 7.63 (pd, 2H, $J = 8.8$ Hz, phenyl-H-3, H-5), 7.77 (pt, 1H, pyridyl-H-5), 8.24 (pd, 1H, $J = 8.1$ Hz, pyridyl-H-3), 8.43 (pt, 1H, pyridyl-H-4), 8.73 (pd, 1H, $J = 5.7$ Hz, pyridyl-H-6), 10.57 (s, NH).

5.2.3. 4-{1-[2-(4-Chlorophenyl)hydrazono]ethyl}pyridine (**13c**) [24]

Yellow solid, (21.7 g) (87 mmol) (87%), m.p. 307 °C (decomposition); ^1H NMR ($\text{DMSO}-d_6$): $\delta = 2.33$ (s, 3H, CH_3), 7.34 (pd, 2H, $J = 7.6$, phenyl-H), 7.45 (pd, 2H, $J = 7.6$, phenyl-H), 8.25 (pd, 2H, $J = 5.6$, pyridyl-H-3 + 5), 8.73 (pd, 2H, $J = 5.6$, pyridyl-H-2 + 6), 10.55 (s, NH).

5.2.4. 2-{1-[2-(2-Chlorophenyl)hydrazono]ethyl}pyridine (**13d**)

Yellow solid, (21.6 g) (88 mmol) (88%), m.p. 246 °C (decomposition); ^1H NMR ($\text{DMSO}-d_6$): $\delta = 2.44$ (s, 3H, CH_3), 6.97 (m, 1H, phenyl-H), 7.34 (m, 1H, phenyl-H), 7.43 (m, 1H, phenyl-H), 7.73 (m, 1H, phenyl-H), 7.96 (pd, 1H, $J = 8.1$ Hz, pyridyl-H), 8.30 (m, 2H, pyridyl-H), 8.72 (pd, 1H, $J = 5.5$ Hz, pyridyl-H), 8.92 (s, NH).

5.2.5. 2-{1-(2-Phenylhydrazono)ethyl}thiophene (**13e**) [25]

Yellow solid, (17.5 g) (81 mmol) (81%), m.p. 94 °C; ^1H NMR ($\text{DMSO}-d_6$): $\delta = 2.25$ (s, 3H, CH_3), 6.34 (m, 1H, thiaryl-H), 7.01 (m, 1H, thiaryl-H), 7.12–7.24 (m, 5H, phenyl-H), 7.39 (pd, 1H, thiaryl-H-5), 8.92 (s, NH).

5.2.6. 2-Pyridin-2-yl-indole (**14a**) [26]

40 ml polyphosphoric acid was added into a beaker and heated under continuous stirring at 100–120 °C. 4.2 g (20 mmol) 2-[1-(2-Phenylhydrazono)ethyl]pyridine (**13a**) was added in small amounts over a period of 10 min and the brown liquid was kept at m.p. 120 °C for 30 min. After cooling the mixture was hydrolyzed carefully with ice and neutralized with aqueous sodium hydroxide. The resulting yellow solid was filtered and refluxed in 300 ml acetone for about 10 min. The hot suspension was filtrated and the solution was evaporated to dryness. The residue was chromatographed on silica gel (petrol ether/ethyl acetate (3:1)). White solid (2.0 g) (10.3 mmol) (52%), 152 °C; ^1H NMR (CDCl_3): $\delta = 7.05$ (m, 1H, indole-H-3), 7.11–7.26 (m, 3H, indole-H-5–7), 7.37 (pd, 1H, $J = 8.1$ Hz, indole-H-4), 7.67–7.75 (m, 2H, pyridyl-H-4 + 5), 7.83 (pd, 1H, $J = 8.1$ Hz, pyridyl-H-3), 8.59 (pd, 1H, $J = 4.3$ Hz, pyridyl-H-6), 10.23 (s, N-H); EI-MS: m/z 194 [M^+], $\text{C}_{13}\text{H}_{10}\text{N}_2$.

5.2.7. 5-Chloro-2-(pyridin-2-yl)-indole (**14b**)

See Section 5.3.1. 4.9 g (20 mmol) 2-{1-[2-(4-chlorophenyl)hydrazono]ethyl}pyridine (**13b**). The resulting yellow solid was filtered and refluxed in 200 ml ethanol instead of acetone for about 10 min. White solid (2.6 g) (11.4 mmol) (57%), m.p. 172 °C; ¹H NMR (CDCl₃): δ = 6.95 (m, 1H, indole-H-3), 7.13–7.28 (m, 3H, indole-H-4, 6, 7), 7.60 (m, 1H, pyridyl-H-3), 7.71–7.81 (m, 2H, pyridyl-H-4 + 5), 8.57 (m, 1H, pyridyl-H-6), 10.06 (s, N-H); EI-MS: *m/z* 228.1 [M⁺], C₁₃H₉ClN₂.

5.2.8. 5-Chloro-2-(pyridin-4-yl)-indole (**14c**)

See Section 5.3.1. 4.9 g (20 mmol) 4-{1-[2-(4-Chlorophenyl)hydrazono]ethyl}pyridine (**13c**). The temperature was kept at m.p. 140 °C for 30–45 min. The resulting yellow solid was filtered and dissolved in 100 ml dimethyl formamide. The solution was evaporated under vacuum to dryness and chromatographed on silica gel (ethyl acetate/ethanol (2:1)). White solid (2.4 g) (10.5 mmol) (53%), 260 °C (decomposition); ¹H NMR (DMSO-d₆): δ = 7.14 (m, 2H, indole-H-3 + 6), 7.45 (pd, 1H, *J* = 8.6 Hz, indole-H-7), 7.63 (pd, 1H, *J* = 1.9 Hz, indole-H-4), 7.91 (pd, 2H, *J* = 6.0, pyridyl-H-3 + 5), 8.61 (pd, 2H, *J* = 6.0, pyridyl-H-2 + 6), 12.03 (s, N-H); ¹³C NMR (DMSO-d₆): δ = 99.9 (t), 111.2 (t), 119.6 (2t), 120.2 (t), 123.5 (t), 124.6 (q), 129.7 (q), 136.3 (q), 136.6 (q), 137.2 (q), 150.8 (2t); FD-MS: *m/z* 228.3 [M⁺], C₁₃H₉ClN₂.

5.2.9. 7-Chloro-2-(pyridin-2-yl)-indole (**14d**)

See Section 5.3.1. 4.4 g (20 mmol) 2-{1-[2-(2-chlorophenyl)hydrazono]ethyl}pyridine (**13d**). The reaction time of cyclization was limited to 15 min. After neutralization the crude product is extracted three times with ethyl acetate. The combined organic solutions were dried with magnesium sulfate and after removing of the solvent the residue was recrystallized with methanol. White solid (2.8 g) (12.2 mmol) (61%), m.p. 121 °C; ¹H NMR (CDCl₃): δ = 7.02–7.07 (m, 2H, indole-H-3 + 5), 7.17–7.25 (m, 2H, indole-H-4 + 6), 7.54 (pd, 1H, *J* = 7.9 Hz, pyridyl-H-3), 7.69–7.80 (m, 2H, pyridyl-H-4 + 5), 8.59 (pd, 1H, *J* = 5.0, pyridyl-H-6), 9.76 (s, N-H); FD-MS: *m/z* 199.1 [M⁺], C₁₂H₉NS.

5.2.10. 2-Thiophen-2-yl-indole (**14e**) [27]

See Section 5.3.1. 4.0 g (20 mmol) 2-[1-(2-phenylhydrazono)ethyl]thiophene (**13e**). The reaction time of cyclization was limited to 15 min. White solid (1.9 g) (9.6 mmol) (48%), m.p. 165 °C; ¹H NMR (DMSO-d₆): δ = 6.65 (s, 1H, indole-H-3), 6.98 (m, 1H, indole-H), 7.06–7.14 (m, 2H, indole-H), 7.35 (pd, 1H, *J* = 7.9, indole-H-7), 7.50 (m, 3H, thophene-H), 11.55 (s, N-H); FD-MS: *m/z* 228.1 [M⁺], C₁₃H₉ClN₂.

5.3. General procedure for the synthesis of 2-(pyridinyl)-1H-indole-3-carbaldehydes

1.94 g of the indole **14a** resp. 2.28 g of the chloro-indoles **14b–d** (10 mmol) were dissolved in 10 ml of dry DMF under nitrogen atmosphere and cooled down to –5 °C. 1.12 ml (12 mmol) POCl₃ were added dropwise over a period of 10 min where the temperature had to be kept under 5 °C. The suspension was stirred for 30 min at 0 °C, 30 min at room temperature and further 4 h at 90 °C. Subsequent the mixture was hydrolyzed carefully with water and neutralized with aqueous sodium hydroxide solution (20%). The suspension was filtered, the filtrate extracted with ethyl acetate and the organic phase combined with the solid. The solvent of the suspension was evaporated and the precipitate was chromatographed on silica gel.

5.3.1. 2-(Pyridin-2-yl)-indole-3-carbaldehyde (**15a**) [28]

See Section 5.4. The chromatographic isolation was performed with ethyl acetate/petrol ether (2:1). Bright yellow solid (0.9 g) (41%) (4.1 mmol), m.p. 213 °C; ¹H NMR (DMSO-d₆): δ = 7.22–7.33 (m, 2H, indole-5 + 6), 7.54 (m, 2H, indole-H-7, pyridyl-H-3), 8.01–8.11 (m, 2H, pyridyl-H-4 + 5), 8.24 (pd, 1H, *J* = 7.4 Hz, indole-H-4), 8.79 (pd, 1H, *J* = 4.8 Hz, pyridyl-H-6), 10.59 (s, 1H, formyl-H), 12.22 (s, 1H, N-H); EI-MS: *m/z* 222.1 [M⁺], C₁₄H₁₀N₂O.

5.3.2. 5-Chloro-2-(pyridin-2-yl)-indole-3-carbaldehyde (**15b**)

See Section 5.4. The chromatographic isolation was performed with ethyl acetate/petrol ether (2:1). Bright yellow solid (1.2 g) (47%) (4.7 mmol), m.p. 290 °C (decomposition); ¹H NMR (DMSO-d₆): δ = 7.32 (pd, 1H, *J* = 8.8 Hz, indole-H-6), 7.53–7.58 (m, 2H), 8.06 (pd, 1H, *J* = 1.8 Hz, pyridyl-H-4), 8.11 (m, 1H), 8.21 (pd, 1H, 1H, *J* = 1.8 Hz, pyridyl-H-3), 8.80 (pd, 1H, *J* = 4.8 Hz, pyridyl-H-6), 10.55 (s, 1H, formyl-H), 12.77 (s, 1H, N-H); FD-MS: *m/z* 256.0 [M⁺], C₁₄H₉ClN₂O.

5.3.3. 5-Chloro-2-(pyridin-4-yl)-indole-3-carbaldehyde (**15c**)

See Section 5.4. The chromatographic isolation was performed with ethyl acetate/ethanol (15:1). Bright yellow solid (1.0 g) (39%) (3.9 mmol), m.p. 275 °C (decomposition); ¹H NMR (DMSO-d₆): δ = 7.33 (pd, 1H, *J* = 8.8 Hz, indole-H-6), 7.55 (pd, 1H, *J* = 8.8 Hz, indole-H-7), 7.79 (pd, 2H, *J* = 5.9 Hz, pyridyl-H-3 + 5), 8.19 (pd, 1H, *J* = 1.9 Hz, indole-H-4), 8.78 (pd, 2H, *J* = 5.9 Hz, pyridyl-H-2 + 6), 10.01 (s, 1H, formyl-H), 12.10 (s, 1H, N-H); ¹³C NMR (DMSO-d₆): δ = 114.2 (t), 114.3 (q), 120.6 (q), 124.3 (q), 124.7 (q), 127.1 (2t), 127.7 (t), 135.0 (t), 137.0 (t), 146.6 (2t), 150.6 (q), 185.7 (q); FD-MS: *m/z* 256.7 [M⁺], C₁₄H₉ClN₂O.

5.3.4. 7-Chloro-2-(pyridin-2-yl)-indole-3-carbaldehyde (**15d**)

See Section 5.4.1. The chromatographic isolation was performed with petrol ether/ethyl acetate (1:1). Bright yellow solid (1.1 g) (43%) (4.3 mmol), 256 °C (decomposition); ¹H NMR (DMSO-d₆): δ = 7.22 (m, 1H, indole-H), 7.41 (m, 1H), 7.59 (m, 1H), 8.08 (m, 1H), 8.20 (m, 2H, pyridyl-H), 8.79 (m, 1H, pyridyl-H-6), 10.49 (s, 1H, N-H), 12.67 (s, 1H, formyl-H); FD-MS: *m/z* 256.1 [M⁺], C₁₄H₉ClN₂O.

5.3.5. 2-(Thiophen-2-yl)-indole-3-carbaldehyde (**15e**) [27]

2.5 ml (26.5 mmol) POCl₃ were added dropwise to 1 ml (13 mmol) DMF at 0 °C. Subsequently a solution of 2.0 g (10 mmol) **14e** in 10 ml dry diethyl ether was added slowly at 0 °C. The mixture was stirred 30 min at 0 °C and after warming up at room temperature it was heated for 3 h at 90–100 °C. The reaction was stopped by adding 30 ml ice water and neutralized with aqueous sodium hydroxide solution (20%). The suspension was extracted three times with CH₂Cl₂ and after drying of the combined organic phases. The solvent of the suspension was evaporated and the precipitate recrystallized in ethanol. Bright yellow solid (1.4 g) (62%) (6.2 mmol), m.p. 228 °C; ¹H NMR (DMSO-d₆): δ = 7.20–7.32 (m, 3H), 7.47 (m, 1H), 7.74 (m, 1H), 7.89 (m, 1H), 8.16 (m, 1H, indole-H-4), 10.23 (s, 1H, formyl-H), 12.44 (s, 1H, N-H); ¹³C NMR (DMSO-d₆): δ = 112.2 (q), 113.8 (t), 121.2 (q), 124.4 (q), 126.2 (t), 128.8 (q), 130.2 (q), 130.8 (t), 136.1 (t), 136.3 (t), 141.5 (t), 141.7 (t), 186.1 (q); FD-MS: *m/z* 227.3 [M⁺], C₁₃H₉NOS.

5.4. General procedure for the synthesis of (E)-methyl 3-(2-hetarylindol-3-yl)acrylate

10 mmol of the carbaldehyde (2.2 g of **15a**, 2.6 g of **15b–d**, 2.3 g of **15e**) and 4.3 g (13 mmol) of (methoxycarbonylmethylen)-triphenylphosphorane are refluxed in 300 ml dry toluene for 5–6 h. The progress of the reaction was followed by TLC (silicagel, petrol

ether/ethyl acetate (2:1)). The solvent was evaporated and the residue chromatographed on silica gel.

5.4.1. (E)-Methyl-3-[2-(pyridin-2-yl)-indol-3-yl]acrylate (**16a**) [29]

See Section 5.5. The isolation was performed with petrol ether/ethyl acetate (2:1). Bright yellow solid (2.1 g) (76%) (7.6 mmol), m.p. 158 °C; ^1H NMR (CDCl_3): δ = 3.85 (s, 3H, CH_3), 6.66 (d, 1H, 3J = 16.0 Hz, =CH), 7.27–7.34, (m, 3H), 7.46 (m, 1H), 7.82–7.88 (m, 2H), 7.96 (pd, 1H, J = 7.6, pyridyl-H), 8.27 (d, 1H, 3J = 16.0 Hz, =CH), 8.70 (m, 1H), 9.97 (s, 1H, N-H); ^{13}C ($\text{DMSO}-d_6$): δ = 51.1 (p), 110.9 (q), 112.4 (t), 119.9 (t), 120.2 (t), 120.6 (t), 122.7 (t), 123.0 (t), 123.3 (t), 126.7 (q), 135.2 (q), 136.3 (q), 137.5 (2t), 149.8 (t), 150.9 (q), 166.9 (q); FT-IR (cm^{-1}): 2900–3200, 1698, 1609, 1422, 1182; FD-MS: m/z 278.6 [M^+], $\text{C}_{17}\text{H}_{14}\text{N}_2\text{O}_2$.

5.4.2. (E)-Methyl-3-[5-chloro-2-(pyridin-2-yl)-indol-3-yl]acrylate (**16b**)

See Section 5.5. The isolation was performed with ethyl acetate/petrol ether (1:1). Bright yellow solid (2.0 g) (64%) (6.4 mmol), m.p. 182 °C; ^1H NMR ($\text{DMSO}-d_6$): δ = 3.71 (s, 3H, CH_3), 6.50 (d, 1H, 3J = 16.2 Hz, =CH), 7.29 (m, 1H, indole-H-6), 7.46–7.54 (m, 2H, indole-H + pyridyl-H), 7.83 (pd, 1H, J = 7.8, pyridyl-H-3), 7.94, (m, 1H, indole-H-4), 8.03 (m, 1H, pyridyl-H), 8.46 (d, 1H, 3J = 16.2 Hz, =CH), 8.79 (pd, 1H, J = 4.0), (pyridyl-H-6), 12.38 (s, 1H, N-H); ^{13}C ($\text{DMSO}-d_6$): δ = 51.5 (p), 109.7 (q), 114.5 (t), 114.5 (t), 120.2 (t), 123.8 (t), 124.0 (t), 126.4 (q), 127.2 (q), 135.6 (q), 137.8 (t), 139.0 (2t), 140.9 (q), 149.9 (q), 150.3 (t), 167.9 (q); EI-MS: m/z 312.1 [M^+], $\text{C}_{17}\text{H}_{13}\text{ClN}_2\text{O}_2$.

5.4.3. (E)-Methyl-3-[5-chloro-2-(pyridin-4-yl)-indol-3-yl]acrylate (**16c**)

See Section 5.5. The isolation was performed with ethyl acetate/ethanol (6:1). Bright yellow solid (2.2 g) (70%) (7.0 mmol), m.p. 251 °C (decomposition); ^1H NMR ($\text{DMSO}-d_6$): δ = 4.0 (s, 3H, CH_3), 6.52 (d, 1H, 3J = 16.0 Hz, =CH), 7.31 (m, 1H, indole-H-6), 7.52 (m, 1H, indole-H-7), 7.59 (pd, 2H, J = 6.0, pyridyl-H-3 + 5), 7.77 (d, 1H, 3J = 16.0 Hz, =CH), 8.0 (m, 1H, indole-H-4), 8.79 (pd, 2H, J = 6.0, pyridyl-H-2 + 6), 12.31 (s, 1H, N-H); ^{13}C ($\text{DMSO}-d_6$): δ = 51.6 (p), 109.5 (q), 114.3 (t), 144.8 (t), 120.2 (t), 122.3 (t), 123.9 (2t), 124.1 (t), 126.6 (q), 126.9 (q), 135.8 (q), 138.2 (q), 140.9 (q), 150.6 (2t), 167.7 (q); FT-IR (cm^{-1}): 2746–3120, 1704, 1622, 1597, 1299, 1283, 998, 826; FD-MS: m/z 312.3 [M^+], $\text{C}_{17}\text{H}_{13}\text{ClN}_2\text{O}_2$.

5.4.4. (E)-Methyl-3-[7-chloro-2-(pyridin-2-yl)-indol-3-yl]acrylate (**16d**)

See Section 5.5. The isolation was performed with petrol ether/ethyl acetate (2:1). Bright yellow solid (2.1 g) (67%) (6.7 mmol), m.p. 152–155 °C; ^1H NMR (CDCl_3): δ = 3.84 (s, 3H, CH_3), 6.63 (d, 1H, 3J = 16.0 Hz, =CH), 7.17 (m, 1H, indole-H), 7.27 (m, 1H), 7.34 (m, 1H), 7.83 (m, 3H), 8.23 (d, 1H, 3J = 16.0 Hz, =CH), 8.71 (pd, 1H, J = 4.5, pyridyl-H-6), 9.91 (s, 1H, N-H); ^{13}C (CDCl_3): δ = 51.7 (p), 112.0 (2q), 117.5 (q), 117.7 (t), 119.6 (t), 122.4 (t), 123.4 (t), 123.7 (t), 124.0 (t), 128.3 (q), 133.7 (q), 137.3 (t), 37.7 (t), 148.5 (q), 149.4 (t), 168.2 (q); FT-IR (cm^{-1}): 3391, 1710, 1615, 1429, 1292, 1163; FD-MS: m/z 312.4 [M^+], $\text{C}_{17}\text{H}_{13}\text{ClN}_2\text{O}_2$.

5.4.5. (E)-Methyl 3-[2-(thiophen-2-yl)-indol-3-yl]acrylate (**16e**) [29]

See Section 5.5. The isolation was performed with chloroform/ethyl acetate (4:1). Bright yellow solid (1.3 g) (46%) (4.6 mmol), m.p. 172 °C; ^1H NMR (CDCl_3): δ = 3.82 (s, 3H, CH_3), 6.61 (d, 1H, 3J = 16.0 Hz, =CH), 7.18 (m, 1H), 7.26–7.34 (m, 3H), 7.41 (m, 1H), 7.48 (m, 1H), 7.95 (m, 1H), 8.15 (d, 1H, 3J = 16.0 Hz, =CH), 8.47 (s, 1H, N-H); FD-MS: m/z 283.5 [M^+], $\text{C}_{16}\text{H}_{13}\text{NO}_2\text{S}$.

5.5. General procedure for the synthesis of hetarene annelated [a]-carbazoles via photochemical electrocyclopisalation

2 mmol of the methyl-3-(2-hetaryl-indol-3-yl)acrylate **16** and some crystals of iodine were dissolved in 450 ml of the specified solvent and irradiated with a wavelength band λ = 200–600 nm at 17–20 °C. The reaction progress was controlled by TLC. After complete conversion the solvent was let off and evaporated to dryness. The resulting residue was purified by column chromatography on silica gel.

5.5.1. Methyl-11H-pyrido[2,3-a]carbazole-5-carboxylate (**17a**)

557 mg of **16a** was dissolved in 450 ml CH_2Cl_2 and irradiated for 6 h. The progress of reaction via TLC and the isolation of the pyridocarbazole by column chromatography on silica gel were performed with petrol ether/ethyl acetate (3:1). White solid (400 mg) (72%) (1.4 mmol), m.p. 228 °C; ^1H NMR ($\text{DMSO}-d_6$): δ = 3.97 (s, 3H, CH_3), 7.32 (m, 1H, H-8), 7.50 (m, 1H, H-9), 7.72 (m, 2H, H-4 + 10), 8.34 (m, 1H, H-7), 9.01 (m, 1H, H-3), 9.13 (m, 1H, H-6), 9.47 (m, 1H, H-2), 11.96 (s, 1H, N-H); ^{13}C ($\text{DMSO}-d_6$): δ = 52.3, 112.7, 116.3, 118.7, 120.8 (2), 122.4, 123.5, 125.4, 126.3, 126.4, 134.8, 137.1, 138.7, 139.9, 149.1, 167.4; FTIR (cm^{-1}): 3180, 2946, 1708, 1518, 1429, 1346, 1235, 1220, 1131, 1059, 727; FD-MS: m/z 276.6 [M^+], $\text{C}_{17}\text{H}_{12}\text{N}_2\text{O}_2$.

5.5.2. Methyl-8-chloro-11H-pyrido[2,3-a]carbazole-5-carboxylate (**17b**)

625 mg of **16b** was dissolved in 450 ml CH_2Cl_2 and irradiated for 6 h. The progress of the reaction via TLC and the isolation of the chloropyridocarbazole by column chromatography on silica gel were performed with petrol ether/ethyl acetate (2:1). White solid (410 mg) (66%) (1.3 mmol), m.p. 256 °C; ^1H NMR (CDCl_3): δ = 4.06 (s, 3H, CH_3), 7.45–7.55 (m, 2H), 7.66 (m, 1H), 8.15 (m, 1H), 8.92 (m, 1H), 9.06 (m, 1H), 9.75 (m, 1H), 10.69 (s, 1H, N-H); ^{13}C ($\text{DMSO}-d_6$): δ = 52.3 (p), 114.1 (t), 116.9 (q), 118.0 (q), 120.5 (t), 122.7 (t), 124.8 (q), 125.1 (q), 125.7 (q), 126.2 (t), 126.8 (t), 134.9 (t), 137.1 (q), 138.4 (q), 139.4 (q), 149.2 (t), 167.2 (q); FD-MS: m/z 310.2 [M^+], $\text{C}_{17}\text{H}_{11}\text{ClN}_2\text{O}_2$.

5.5.3. Methyl-8-chloro-11H-pyrido[4,3-a]carbazole-5-carboxylate (**17c**)

625 mg of **16c** was dissolved in 450 ml ethanol and irradiated for 6 h. The progress of reaction via TLC and the isolation of the chloropyridocarbazole by column chromatography on silica gel were performed with ethyl acetate/ethanol (3:1). White solid (390 mg) (64%) (1.3 mmol), m.p. 285–290 °C (decomposition); ^1H NMR ($\text{DMSO}-d_6$): δ = 4.00 (s, 3H, CH_3), 7.54 (m, 1H, H-9), 7.74 (m, 1H, H-10), 8.44 (m, 1H, H-1), 8.54 (m, 1H, H-7), 8.75 (m, 1H, H-2), 9.18 (m, 1H, H-6), 10.30 (m, 1H, H-4), 11.76 (s, 1H, N-H); ^{13}C ($\text{DMSO}-d_6$): δ = 52.5 (p), 114.0 (t), 115.6 (t), 117.8 (q), 118.2 (q), 120.8 (t), 124.5 (q), 124.7 (q), 125.5 (q), 126.6 (t), 127.4 (t), 137.3 (q), 138.4 (q), 143.4 (t), 143.5 (q), 150.5 (t), 167.2 (q); FD-MS: m/z 310.8 [M^+], $\text{C}_{17}\text{H}_{11}\text{ClN}_2\text{O}_2$.

5.5.4. Methyl-10-chloro-11H-pyrido[2,3-a]carbazole-5-carboxylate (**17d**)

625 mg of **16d** was dissolved in 450 ml CH_2Cl_2 and irradiated for 6 h. The progress of reaction via TLC and the isolation of the chloropyridocarbazole by column chromatography on silica gel were performed with petrol ether/ethyl acetate (2:1). White solid (425 mg) (68%) (1.4 mmol), m.p. 180 °C; ^1H NMR (CDCl_3): δ = 4.06 (s, 3H, CH_3), 7.25 (m, 1H), 7.32 (m, 1H), 7.53 (m, 1H), 7.68 (m, 1H), 8.07 (m, 1H), 8.94 (m, 1H), 9.06 (m, 1H, H-6), 9.74 (s, 1H); FD-MS: m/z 310.0 [M^+], $\text{C}_{17}\text{H}_{11}\text{ClN}_2\text{O}_2$.

5.5.5. Methyl-10H-thieno[2,3-a]carbazole-4-carboxylate (**17e**)

567 mg of **16e** was dissolved in 450 ml CH_2Cl_2 and irradiated for 3 h. The progress of reaction via TLC and the isolation of the thienocarbazole by column chromatography on silica gel were performed with petrol ether/ethyl acetate (3:1). Bright yellow solid (253 mg) (47%) (0.9 mmol), m.p. 213 °C; ^1H NMR (DMSO- d_6): δ = 3.95 (s, 3H, CH_3), 7.27 (m, 1H), 7.45 (m, 1H), 7.58 (m, 1H, H-9), 7.94 (pd, 1H, 3J = 5.5, H-3), 8.27 (m, 1H, H-6), 8.34 (pd, 1H, 3J = 5.5, H-2), 8.89 (m, 1H, H-5), 12.39 (s, 1H); ^{13}C NMR (DMSO- d_6): δ = 52.1 (p), 111.9 (t), 115.8 (q), 117.7 (q), 120.5 (t), 120.7 (t), 122.3 (t), 123.5 (q), 125.8 (t), 126.1 (t), 127.9 (t), 137.4 (q), 137.9 (q), 139.9 (q), 140.1 (q), 167.2 (q); FD-MS: m/z 281.5 [M^+], $\text{C}_{16}\text{H}_{11}\text{NO}_2\text{S}$.

5.6. General procedure for the preparation of the hetarene annelated [a]-carbazole carboxylic acids via hydrolysis

2 mmol of the hetarene annelated [a]-carbazole **17** (553 mg of **17a**, 622 mg of **17b-d**, 563 mg of **17e**) was suspended in 20 ml ethanol and 1 ml of an aqueous sodium hydroxide solution and refluxed for 2 h. The mixture was cooled down at room temperature, neutralized first with concentrated hydrochloric acid and subsequent with acetic acid. After 1 h the precipitate was filtered off, dried for 24 h by remaining at the air and then under vacuum. The purity of the free carboxylic acids was sufficient, so that they could be applied for further reactions.

5.7. General procedure for the preparation of the hetarene annelated [a]-carbazole amides by use of EDI/HOBt as coupling reagents

2.6 mmol (404 mg) 1-ethyl-3-[3-(dimethylamino)propyl]carbodiimide (EDCI), 1.045 mmol (141 mg) 1-hydroxybenzotriazole (HOBt), 1.5 mmol of the amine and 1.045 mmol of the hetarene annelated [a]-carbazole carboxylic acids **18** were dissolved in 10 ml DMF and stirred for 24 h under nitrogen atmosphere. The urea was filtered off, the filtrate was evaporated to dryness and the residue was chromatographed on silica gel (methanol/ NH_3 (25%), 97:3).

5.7.1. N-[2-(Dimethylamino)ethyl]-11H-pyrido[2,3-a]carbazole-5-carboxamide (**20**)

274 mg of **18a** and 0.2 ml N,N -dimethylethylenediamine were added. White solid (253 mg) (73%) (0.8 mmol), m.p. 217 °C; ^1H NMR (DMSO- d_6): δ = 2.29 (s, 6H, $\text{N}(\text{CH}_3)_2$), 2.58 (t, 2H, $-\text{CH}_2$ next to amine-N), 3.48 (t, 2H, $-\text{CH}_2$ next to amidic-N), 7.28 (m, 1H), 7.46 (m, 1H), 7.65 (m, 2H), 8.24 (m, 1H), 8.56 (m, 2H), 8.94 (m, 1H), 8.98 (m, 1H), 12.21 (s, 1H, indole-N-H); ^{13}C NMR (DMSO- d_6): δ = 37.6 (s), 45.4 (p), 58.4 (s), 112.5 (t), 118.7 (q), 120.1 (t), 120.5 (t), 120.8 (t), 121.4 (t), 123.5 (q), 124.5 (q), 125.1 (q), 125.8 (t), 135.1 (t), 136.6 (q), 137.2 (q), 139.8 (q), 148.9 (t), 168.7 (q); FD-MS: m/z 332.2 [M^+], $\text{C}_{20}\text{H}_{20}\text{N}_4\text{O}$.

5.7.2. N-[2-(Dimethylamino)propyl]-11H-pyrido[2,3-a]carbazole-5-carboxamide hydrochloride (**21**)

274 mg of **18a** and 0.2 ml N,N -dimethylpropylenediamine were added. White solid (280 mg) (77%) (0.8 mmol). Because of unclear correlations concerning the NMR signals of aliphatic protons in the high-field the free base had do convert into her corresponding hydrochloride. Therefore the free base was dissolved in ether and after adding some drops of ethereal HCl the salt precipitated immediately. Free base: bright yellow solid m.p. 227 °C; hydrochloride: white solid, m.p. 295 °C; ^1H NMR (DMSO- d_6) of the free base: δ = 1.75 (m, 2H, $\text{C}-\text{CH}_2-\text{C}$), 2.16 (s, 6H, $\text{N}(\text{CH}_3)_2$), 2.33 (t, 2H, $-\text{CH}_2$ next to amine-N), 3.39 (t, 2H, next to amidic-N), 7.28 (m, 1H), 7.46 (m, 1H), 7.66 (m, 2H), 8.25 (m, 1H), 8.53 (s, 1H), 8.65 (m, 1H), 8.90 (m, 1H), 8.98 (m, 1H), 12.21 (s, 1H, N-H); FD-MS: m/z 346.1 [M^+], $\text{C}_{21}\text{H}_{22}\text{N}_4\text{O}$; ^1H NMR (DMSO- d_6) of the hydrochloride:

δ = 2.03 (m, 2H, $\text{C}-\text{CH}_2-\text{C}$), 2.78 (d, 6H, $\text{N}(\text{CH}_3)_2$), 3.18 (m, 2H, $-\text{CH}_2$ next to amine-N), 3.44 (m, 2H, next to amidic-N), 7.32 (m, 1H), 7.50 (m, 1H), 7.73 (m, 2H), 8.30 (m, 1H), 8.71 (m, 1H), 8.88 (m, 1H), 9.06 (m, 2H), 10.50 (s, 1H, N-H), 12.08 (s, 1H, indole-N-H); ^{13}C NMR of the hydrochloride (methanol- d_4): 26.2 (s), 38.0 (s), 43.7 (p), 56.9 (s), 113.4 (t), 121.6 (t), 122.1 (t), 122.4 (t), 123.1 (q), 123.8 (q), 123.9 (t), 125.2 (q), 126.2 (q), 128.7 (t), 132.1 (q), 132.7 (q), 141.2 (q), 142.1 (t), 145.9 (t), 171.4 (q); FD-MS: m/z 346.1 [M^+], 347.1 [27%] $\text{C}_{21}\text{H}_{23}\text{ClN}_4\text{O}$.

5.7.3. 8-Chloro-N-[2-(dimethylamino)ethyl]-11H-pyrido[2,3-a]carbazole-5-carboxamide (**22**)

310 mg of **18b** and 0.2 ml N,N -dimethylethylenediamine were added. White solid (288 mg) (75%) (0.8 mmol), m.p. 255 °C; ^1H NMR (DMSO- d_6): δ = 2.30 (s, 6H, $\text{N}(\text{CH}_3)_2$), 2.59 (t, 2H, $-\text{CH}_2$ next to amine-N), 3.49 (t, 2H, $-\text{CH}_2$ next to amidic-N), 7.46 (m, 1H), 7.66 (m, 2H), 8.36 (m, 1H), 8.56 (m, 2H), 8.91 (m, 1H), 8.99 (m, 1H), 12.04 (s, 1H, N-H); ^{13}C NMR (DMSO- d_6): δ = 37.6 (s), 45.4 (p), 58.4 (s), 114.0 (t), 118.0 (q), 120.1 (t), 120.9 (t), 121.8 (t), 124.5 (q), 124.6 (q), 124.8 (q), 125.6 (q), 125.7 (t), 135.1 (t), 137.2 (q), 137.4 (q), 138.2 (q), 149.2 (t), 138.5 (q); FD-MS: m/z 366.2 [M^+], 368.3 [34%] $\text{C}_{20}\text{H}_{19}\text{ClN}_4\text{O}$.

5.7.4. 8-Chloro-N-[(2-(dimethylamino)propyl)-11H-pyrido[2,3-a]carbazole-5-carboxamide] (**23**)

310 mg of **18b** and 0.2 ml N,N -dimethylpropylenediamine were added. White solid (290 mg) (73%) (0.8 mmol), m.p. 256 °C; ^1H NMR (DMSO- d_6): δ = 1.75 (m, 2H, $\text{C}-\text{CH}_2-\text{C}$), 2.17 (s, 6H, $\text{N}(\text{CH}_3)_2$), 2.34 (t, 2H, $-\text{CH}_2$ next to amine-N), 3.38 (t, 2H, $-\text{CH}_2$ next to amidic-N), 7.46 (m, 1H), 7.66 (m, 2H), 8.37 (m, 1H), 8.57 (m, 1H), 8.62 (m, 1H), 8.87 (m, 1H), 8.99 (m, 1H), 12.04 (s, 1H, indole-N-H); ^{13}C NMR (DMSO- d_6): δ = 27.5 (s), 38.1 (s), 45.5 (p), 57.2 (s), 114.0 (t), 118.0 (q), 120.1 (t), 120.9 (t), 121.8 (t), 124.5 (q), 124.6 (q), 124.8 (q), 125.7 (t), 125.9 (q), 135.0 (t), 137.2 (q), 137.3 (q), 138.2 (q), 149.2 (t), 168.5 (q); FD-MS: m/z 380.2 [M^+], 382.2 [34%] $\text{C}_{21}\text{H}_{21}\text{ClN}_4\text{O}$.

5.7.5. 8-Chloro-N-[2-(dimethylamino)ethyl]-11H-pyrido[4,3-a]carbazole-5-carboxamide (**24**)

310 mg of **18c** and 0.2 ml N,N -dimethylethylenediamine were added. White solid (260 mg) (68%) (0.7 mmol), m.p. 289 °C; ^1H NMR (methanol- d_6): δ = 2.40 (s, 6H, $\text{N}(\text{CH}_3)_2$), 2.71 (t, 2H, $-\text{CH}_2$ next to amine-N), 3.68 (t, 2H, $-\text{CH}_2$ next to amidic-N), 7.48 (m, 1H), 7.62 (m, 1H), 8.19 (m, 1H), 8.25 (m, 1H), 8.57 (m, 2H), 9.77 (m, 1H); ^{13}C NMR (DMSO- d_6): δ = 7.9 (s), 45.6 (p), 58.6 (s), 113.9 (t), 115.4 (t), 118.2 (2q), 120.4 (t), 121.4 (t), 124.3 (2q), 124.8 (q), 126.2 (t), 126.7 (q), 135.2 (q), 138.2 (q), 143.5 (t), 150.9 (t), 168.3 (q); FD-MS: m/z 366.6 [M^+], 368.6 [35%] $\text{C}_{20}\text{H}_{19}\text{ClN}_4\text{O}$.

5.7.6. 8-Chloro-N-[2-(dimethylamino)propyl]-11H-pyrido[4,3-a]carbazole-5-carboxamide (**25**)

310 mg of **18c** and 0.2 ml N,N -dimethylpropylenediamine were added. White solid (271 mg) (71%) (0.8 mmol), m.p. 283 °C; ^1H NMR (DMSO- d_6): δ = 1.76 (m, 2H, $\text{C}-\text{CH}_2-\text{C}$), 2.20 (s, 6H, $\text{N}(\text{CH}_3)_2$), 2.38 (t, 2H, $-\text{CH}_2$ next to amine-N), 3.42 (t, 2H, $-\text{CH}_2$ next to amidic-N), 7.51 (m, 1H), 7.72 (m, 1H), 8.39 (m, 1H), 8.42 (m, 1H), 8.59 (m, 1H), 8.69 (m, 2H), 9.70 (m, 1H), 11.98 (s, 1H, indole-N-H); ^{13}C NMR (DMSO- d_6): δ = 27.3 (s), 28.0 (s), 45.4 (p), 57.1 (s), 113.9 (t), 115.4 (t), 118.2 (2q), 120.3 (t), 121.5 (t), 124.3 (2q), 124.8 (q), 126.2 (t), 126.6 (q), 135.3 (q), 138.2 (q), 143.5 (t), 150.8 (t), 168.3 (q); FD-MS: m/z 381.1 [M^+], 383.1 [36%] $\text{C}_{21}\text{H}_{21}\text{ClN}_4\text{O}$.

5.7.7. 10-Chloro-N-[2-(dimethylamino)ethyl]-11H-pyrido[2,3-a]carbazole-5-carboxamide (**26**)

310 mg of **18d** and 0.2 ml N,N -dimethylethylenediamine were added. Bright yellow solid (215 mg) (56%) (0.6 mmol), m.p. 199 °C;

¹H NMR (methanol-*d*₆): δ = 2.40 (s, 6H, N(CH₃)₂), 2.72 (t, 2H, –CH₂ next to amine-N), 3.69 (t, 2H, –CH₂ next to amidic-N), 7.18 (m, 1H), 7.41 (m, 2H), 7.95 (m, 1H), 8.38 (m, 1H), 8.77 (m, 2H); ¹³C NMR (DMSO-*d*₆): δ = 37.8 (s), 45.6 (p), 58.5 (s), 116.9 (q), 119.3 (q), 119.4 (t), 120.6 (t), 121.2 (t), 121.8 (t), 124.9 (q), 125.5 (q), 125.6 (t), 126.6 (q), 135.1 (t), 136.8 (q), 137.1 (q), 137.4 (q), 149.1 (t), 168.4 (q); FD-MS: *m/z* 365.8 [M⁺], 367.8 [31%] C₂₀H₁₉ClN₄O.

5.7.8. 10-Chloro-N-[2-(dimethylamino)propyl]-11H-pyrido[2,3-a]carbazole-5-carboxamide (27)

310 mg of **18d** and 0.2 ml *N,N*-dimethylpropylenediamine were added. Bright yellow solid (225 mg) (59%) (0.6 mmol), m.p. 195 °C; ¹H NMR (methanol-*d*₆): δ = 2.0 (m, 2H, C–CH₂–C), 2.42 (s, 6H, N(CH₃)₂), 2.65 (t, 2H, –CH₂ next to amine-N), 3.55 (t, 2H, –CH₂ next to amidic-N), 7.24 (m, 1H, H-8), 7.44 (m, 1H, H-9), 7.51 (m, 1H, H-3), 8.05 (m, 1H, H-7), 8.41 (s, 1H, H-6), 8.84 (m, 2H, H-2 + 4); ¹³C NMR (DMSO-*d*₆): δ = 27.3 (s), 38.0 (s), 45.4 (p), 57.1 (s), 117.0 (q), 119.3 (q), 119.4 (t), 120.6 (t), 121.2 (t), 121.8 (t), 124.9 (q), 125.5 (q), 125.6 (t), 126.6 (q), 135.1 (t), 136.8 (q), 137.1 (q), 137.5 (q), 149.1 (t), 168.4 (q); FD-MS: *m/z* 380.4 [M⁺], 382.4 [33%]; C₂₁H₂₁ClN₄O.

5.7.9. N-[3-(Dimethylamino)propyl]-10H-thieno[2,3-a]carbazole-4-carboxamide hydrochloride (28)

286 mg of **18e** and 0.2 ml *N,N*-dimethylpropylenediamine were added. The free base **28** was dissolved in ether and precipitated with ethereal HCl to generate the hydrochloride. Bright yellow solid (156 mg) (39%) (0.4 mmol), m.p. 243 °C (decomposition); ¹H NMR (DMSO-*d*₆): δ = 1.99 (m, 2H, C–CH₂–C), 2.78 (s, 6H, N(CH₃)₂), 3.16 (t, 2H, –CH₂), 3.42 (t, 2H, –CH₂), 7.26 (m, 1H), 7.43 (m, 1H), 7.58 (m, 1H), 7.82 (m, 1H), 8.15 (m, 2H), 8.56 (s, 1H), 8.71 (m, 1H), 10.15 (s, 1H, indole-N-H); ¹³C NMR (DMSO-*d*₆): δ = 24.8 (s), 36.7 (s), 42.5 (p), 55.0 (s), 111.9 (t), 117.4 (q), 118.0 (t), 120.1 (t), 120.3 (t), 122.4 (q), 134.4 (q), 123.6 (q), 125.7 (t), 125.8 (t), 126.4 (t), 135.8 (q), 137.2 (q), 140.0 (q), 168.8 (q); FD-MS: *m/z* 351.0 [M⁺]; C₂₀H₂₁N₃OS.

5.8. Cytotoxicity and cell cycle analysis on HT-29 cell line

HT-29 colon carcinoma cells were grown in DMEM-glutaMAX medium (Gibco) supplemented with 10% fetal calf serum (FCS), penicillin (100 IU/ml) and streptomycin (100 µg/ml) in a humidified atmosphere at 37 °C under 5% CO₂.

The cytotoxicity of the various compounds was assessed using the MTS cell proliferation assay developed by Promega (CellTiter 96® AQueous one solution cell proliferation assay). Briefly, 3 × 10³ exponentially growing HT-29 cells were seeded in 96-well microculture plates for 24 h prior to be subjected to treatment using graded concentrations of the tested compounds from 1 nM to 100 µM in 3 different series of duplicate or triplicate points. After 72 h of incubation at 37 °C, 20 µl of the tetrazolium dye were added to each well and the samples were incubated for a further 2 h at 37 °C. Plates were analyzed on a Labsystems Multiskan MS (type 352) reader at 492 nm. The GC₅₀ was determined as the concentration for which the number of cell is one half of that obtained in the non-treated control wells (6 individual points per plate) using graphical analyses using SoftMax Pro 4.7.1 software.

For flow cytometric analysis of DNA content, 3 × 10⁵ cells in exponential growth phase were treated with graded concentrations of the test drug for 24 h as indicated in figure legends. The cells were then washed twice with phosphate buffered saline (PBS), incubated with 100 µL of trypsin (Gibco) for 5 min at 37 °C, washed again with 500 µL of culture medium to inhibit trypsin and harvested. Cells were then fixed using 70% ethanol. Finally, 500 µL of PBS containing propidium iodide (PI, FluoProbes) at 50 µg/ml and RNase (Sigma) at 100 µg/ml were added for 30 min at room temperature in the darkness. Cell samples were analyzed on

a Becton Dickinson FACScan flow cytometer using the LYSYS II software. PI was excited at 488 nm and the emitted fluorescence was quantified at 620 nm on channel Fl-3. WinMdi software was used to determine the percentage of cells in G1, S or G2/M phases. Each experiment was performed in duplicate.

5.9. UV/vis absorption spectroscopy and DNA-melting temperature studies

CT-DNA and double stranded poly(dAdT)₂ oligonucleotide were purchased from Sigma. CT-DNA was prepared as previously described [12]. The synthesized compounds were prepared as 10 mM solutions in DMSO and further freshly diluted in the appropriate aqueous buffer.

UV/vis spectral absorption measurement was conducted using 20 µM of the various tested drugs incubated in 1 ml of BPE buffer (6 mM Na₂HPO₄, 2 mM NaH₂PO₄, 1 mM EDTA, pH 7.1) in the presence or absence of increasing concentrations of CT-DNA (10, 20, 30, 40, 50, 60, 70, 80, 90, 100, 120, 140, 160, 180, 200 µM of base pairs) in a quartz cuvette of 10 mm path length. The UV/vis spectra were recorded from 230 nm to 430 nm using an Uvikon 943 spectrophotometer and are referenced against a cuvette containing DNA at the same concentration than in the sample cuvette to directly substrate intrinsic DNA absorption.

The variation of melting temperature was calculated from the melting temperature measurement of 20 µM of CT-DNA or poly(dAdT)₂ incubated alone (control T_m) or with increasing concentration of the various compounds (drug/base pair ratio of 0.1, 0.25, 0.5 or 1) in 1 ml BPE buffer. The absorbency of DNA at 260 nm was measured in quartz cells using the Uvikon 943 spectrophotometer thermostated with a Neslab RTE111 cryostat. Absorption value was measured every minute over a range of 20–100 °C with an increment of 1 °C/min. The T_m values were obtained from the midpoint of the hyperchromic transition. ΔT_m values = T_m[Drug+DNA] – T_m[DNA alone].

5.10. Fluorescence spectroscopy

Fluorescence spectral measurement was recorded using 20 µM of the fluorescent drugs incubated in 1 ml of BPE buffer in the presence or absence of increasing concentrations of CT-DNA (10, 20, 30, 40, 50, 60, 70, 80, 90, 100, 120, 140, 160, 180, 200 µM of base pairs) in a quartz cuvette of 10 mm path length. The excitation wavelengths were 312 (compound **20**), 319 (compounds **21**, **22**), 318 (compound **23**), 276 (compounds **24**, **25**) and 300 nm (compound **28**). The quenching constant K_{sv} was deduced from Stern–Volmer method where the ratio of fluorescence of the compound alone (F₀) over the fluorescence of the compound in the presence of CT-DNA (F) is presented as a function of CT-DNA concentration. In this configuration, F₀/F = 1 + K_{sv}[CT-DNA]. The slope K_{sv} is considered as an equilibrium constant for the static quenching process.

5.11. Circular dichroism

The different drugs (50 µM) were incubated in 1 ml of sodium cacodylate (1 mM, pH 7.0) with or without (control) increasing concentration of CT-DNA (10, 20, 30, 40, 50, 60, 70, 80, 90, 100, 120, 140, 160, 180, 200 µM). The CD spectra were collected from 430 to 230 nm with a resolution of 0.1 nm, in a quartz cell of 10 mm path length, using a J-810 Jasco spectropolarimeter at 20 °C controlled by a PTC-424S/L peltier type cell changer (Jasco).

5.12. DNase I footprinting

DNase I footprinting experiments were performed essentially as described in Ref. [30]. A 117 bp DNA fragment was obtained from double digestion of the pBS plasmid (Stratagene, La Jolla, CA) at EcoRI and PvuII restriction sites for 1 h with the corresponding enzymes in their respective buffers. The generated DNA fragment was 3'-end labelled by incubation with α -[³²P]-dATP (3000 Ci/mmol, GE Healthcare, Buckinghamshire, England) and 10 units of Klenow enzyme (BioLabs) for 30 min at 37 °C. The 117 bp radio-labelled DNA fragment was then isomated on a 6% polyacrylamide gel under native conditions in TBE buffer (89 mM Tris base, 89 mM boric acid, 2.5 mM Na₂EDTA, pH 8.3), cut off from the gel, crushed and dialyzed overnight against 400 µl of elution buffer (10 mM Tris-HCl pH 8.0, 1 mM EDTA, 100 mM NaCl). This suspension was separated from polyacrylamide gel by filtration through a Millipore 0.22 µm membrane. The DNA was precipitated with cold ethanol followed by centrifugation. The radio-labelled DNA fragment was then dried and the pellet dissolved in water. Appropriate concentrations of the various ligands (as indicated in the figure legends) were incubated with the 117-bp radio-labelled DNA fragment 15 min incubation at 37 °C to ensure equilibrium prior to digestion of the DNA by the addition of DNase I (final concentration 0.001 unit/ml) in 20 mM NaCl, 2 mM MgCl₂, 2 mM MnCl₂, pH 7.3. After 3 min of digestion, the reaction was stopped by freeze-drying. Samples were lyophilized and subsequently dissolved in 4 µL of denaturing loading buffer (80% formamide solution containing tracking dyes). The DNA samples were heated at 90 °C for 4 min and chilled on ice for 4 min prior to electrophoresis. DNA cleavage products were resolved under polyacrylamide electrophoresis in denaturing conditions (0.35 mm thick, 8% polyacrylamide containing 8 M urea). After a 90 min electrophoresis at 65 W in TBE buffer, gels were soaked in 10% acetic acid for 10 min, transferred to Whatman 3 MM paper and dried under vacuum at 80 °C. A Molecular Dynamics STORM 860 was used to collect data from storage screens exposed to dried gels overnight at room temperature. The identity of the bases was established from comparison of the relative position of the bands to the guanines sequencing standard (G-track) classically obtained using dimethyl-sulfate and piperidine treatment of the same DNA fragment.

5.13. Topoisomerase I-mediated DNA relaxation, topoisomerases I or II cleavage assays

Topoisomerase I-mediated DNA relaxation experiments were performed as previously described in Ref. [15] with the following modifications. Graded concentrations of the tested compounds were incubated in the presence of supercoiled pUC19 plasmid DNA (130 ng) prior to the addition of 4 units of human topoisomerase I (Topogen, USA) at 37 °C for 45 min in relaxation buffer [50 mM tris(hydroxymethyl)aminomethane (pH 7.8), 50 mM KCl, 10 mM MgCl₂, 1 mM dithiothreitol, 1 mM EDTA and 1 mM ATP]. The reactions were stopped upon addition of SDS to 0.25% and proteinase K to 250 µg/ml and incubation of the samples for 30 min at 50 °C. 3 µl of the electrophoresis dye mixture were added to the DNA samples which were then loaded on a 1% agarose gel. The various DNA forms were separated by electrophoresis at room temperature for 2 h at 120 V in TBE buffer (89 mM Tris-borate pH 8.3, 1 mM EDTA). Gels

were run without ethidium bromide and then stained using a bath containing ethidium bromide. For topoisomerase I DNA cleavage assays, the samples were treated as for the relaxation assays but loaded on a 1% agarose gel that was prepared with ethidium bromide. Camptothecin (CPT, 20 µM) was used as a control for topoisomerase I poisoning effect. For topoisomerase II DNA cleavage assays, supercoiled pUC19 plasmid (130 ng) was incubated with 20 or 50 µM of compounds **20–24**, or etoposide as a control, prior to the addition of 4 units of human topoisomerase II (Topogen, USA) at 37 °C for 45 min in the appropriate cleavage buffer. SDS (0.25%) and proteinase K (250 µg/ml) were then added to stop the reaction during 30 min at 50 °C. DNA samples were loaded on 1% agarose gels containing ethidium bromide for 2 h at 120 °C in TBE buffer. After migration, both gels were washed and photographed under UV light.

Acknowledgments

This work was supported by grants from the Ligue Nationale contre le Cancer (Comité du Nord) and the IRCL to M.-H.D.-C. G.L. thanks the Université de Lille 2 and the Conseil Régional Nord/Pas-de-Calais for a Ph.D. fellowship.

References

- H. Mastalarz, R. Jasztold-Howorko, F. Rulko, A. Croisy, D. Carrez, Arch. Pharm. Pharm. Med. Chem. 337 (2004) 434–439.
- M.M. Harding, A.R. Grummitt, Mini Rev. Med. Chem. 3 (2003) 67–76.
- A. Pierré, G. Atassi, M. Devissaguet, E. Bissagli, Drugs Future 22 (1997) 53–59.
- G.W. Gribble, The Alkaloids, , In: Synthesis and Antitumor Activity of the Ellipticine Alkaloids and Related Compounds, vol. 39 (1990).
- J. Rouessé, M. Spielman, F. Turpin, T. Le Chevalier, M. Azab, J.M. Mondésir, Eur. J. Cancer 29A (1993) 856–859.
- U. Pindur, Pharm. Unserer Zeit. 16 (1987) 47–52.
- M.F. Brana, M. Cacho, A. Gradillas, B. de Pascual-Teresa, A. Ramos, Curr. Pharm. Des. 7 (2001) 1745–1780.
- C. Guillonneau, A. Nault, E. Raimbaud, S. Léonce, L. Kraus-Berthier, A. Pierré, S. Goldstein, Bioorg. Med. Chem. 13 (2005) 175–184.
- R. Jasztold-Howorko, C. Landras, A. Pierré, G. Atassi, N. Guibaud, L. Kraus-Berthier, S. Léonce, Y. Rolland, J.F. Prost, E. Bisagni, J. Med. Chem. 37 (1994) 2445–2452.
- C. Asche, M. Demeunynck, Anti-cancer agents, Med. Chem. 7 (2007) 247–267.
- D. Pelaprat, R. Oberlin, I. Le Guen, B.P. Roques, J.B. Pecq, J. Med. Chem. 23 (1980) 1330–1335.
- U. Pindur, T. Lemster, Recent Res. Dev. Org. Bioorg. Chem. 1 (1997) 33–53.
- T. Lemster, U. Pindur, Recent Res. Dev. Org. Bioorg. Chem. 5 (2002) 99–115.
- R. Martinez, L. Chacon-Garcia, Curr. Med. Chem. 12 (2005) 127–151.
- M.H. David-Cordonnier, M.P. Hildebrand, B. Baldeyrou, A. Lansiaux, C. Keuser, K. Benzschawel, T. Lemster, U. Pindur, Eur. J. Med. Chem. 42 (2007) 752–771.
- C. Keuser, U. Pindur, Pharmazie 4 (2006) 261–268.
- U. Pindur, M. Jansen, T. Lemster, Curr. Med. Chem. 12 (2005) 2805–2847.
- C. Hotzel, A. Marotto, U. Pindur, Eur. J. Med. Chem. 36 (2003) 189–197.
- U. Pindur, T. Lemster, Recent Res. Dev. Org. Bioorg. Chem. 5 (2002) 99–115.
- C. Perlick, Dissertation: 2,3-Divinyl- und 2-Aryl-3-vinylindole als Bausteine zu Carbazolen und Versuche zur photochemischen und Ultraschall-induzierten 1,6-Eletrocyclisierung, 2003.
- National Cancer Institute (NCI). Bethesda. [http://ntp.nci.nih.gov](http://.dtp.nci.nih.gov).
- C.H. Spink, S.E. Wellman, Methods Enzymol. 340 (2001) 193–211.
- Muth, et al., J. Heterocycl. Chem. 9 (1972) 1299.
- Zhaiwei Lin, Pankaja Kadaba, Heterocycl. Commun. 8 (2002) 565–568.
- A.Y. Hassan, M.M. Ghorab, O.M. Nassar, Phosphorus, Sulfur Silicon Relat. Elem. 134 (1998) 77–86.
- K.B. Prasad, G.A. Swan, J. Chem. Soc. (1958) 2024–2038.
- H.B. Shivarama, A. Sarvottam, J. Ind. Chem. Soc. 51 (1974) 965–966.
- M. Somei, S. Sayama, K. Naka, F. Yamada, Heterocycles 27 (1988) 1585–1587.
- I. Fernandez, C. Galvez, L. Urpi, An. Quim. 87 (1991) 936–939.
- C. Bailly, M.J. Waring, J. Biomol. Struct. Dyn. 12 (1995) 869–898.
- T. Lemster, U. Pindur, Recent Res. Dev. Org. Bioorg. Chem. 1 (1997) 33–53.
- T. Lemster, U. Pindur, Recent Res. Dev. Org. Bioorg. Chem. 5 (2002) 99–115.
- R. Martinez, L. Chacon-Garcia, Curr. Med. Chem. 12 (2005) 127–151.
- M.H. David-Cordonnier, M.P. Hildebrand, B. Baldeyrou, A. Lansiaux, C. Keuser, K. Benzschawel, T. Lemster, U. Pindur, Eur. J. Med. Chem. 42 (2007) 752–771.
- C. Keuser, U. Pindur, Pharmazie 4 (2006) 261–268.
- U. Pindur, M. Jansen, T. Lemster, Curr. Med. Chem. 12 (2005) 2805–2847.
- C. Hotzel, A. Marotto, U. Pindur, Eur. J. Med. Chem. 36 (2003) 189–197.
- U. Pindur, T. Lemster, Recent Res. Dev. Org. Bioorg. Chem. 5 (2002) 99–115.
- C. Perlick, Dissertation: 2,3-Divinyl- und 2-Aryl-3-vinylindole als Bausteine zu Carbazolen und Versuche zur photochemischen und Ultraschall-induzierten 1,6-Eletrocyclisierung, 2003.
- National Cancer Institute (NCI). Bethesda. <http://ntp.nci.nih.gov>.
- C.H. Spink, S.E. Wellman, Methods Enzymol. 340 (2001) 193–211.
- Muth, et al., J. Heterocycl. Chem. 9 (1972) 1299.
- Zhaiwei Lin, Pankaja Kadaba, Heterocycl. Commun. 8 (2002) 565–568.
- A.Y. Hassan, M.M. Ghorab, O.M. Nassar, Phosphorus, Sulfur Silicon Relat. Elem. 134 (1998) 77–86.
- K.B. Prasad, G.A. Swan, J. Chem. Soc. (1958) 2024–2038.
- H.B. Shivarama, A. Sarvottam, J. Ind. Chem. Soc. 51 (1974) 965–966.
- M. Somei, S. Sayama, K. Naka, F. Yamada, Heterocycles 27 (1988) 1585–1587.
- I. Fernandez, C. Galvez, L. Urpi, An. Quim. 87 (1991) 936–939.
- C. Bailly, M.J. Waring, J. Biomol. Struct. Dyn. 12 (1995) 869–898.



Review article

Heterocyclic scaffolds as promising anticancer agents against tumours of the central nervous system: Exploring the scope of indole and carbazole derivatives

Chris Sherer, Timothy J. Snape*

School of Pharmacy and Biomedical Sciences, University of Central Lancashire, Preston, Lancashire, PR1 2HE, UK

ARTICLE INFO

Article history:

Received 7 September 2014

Received in revised form

30 October 2014

Accepted 3 November 2014

Available online 5 November 2014

Keywords:

Indole
Carbazole
Indolocarbazole
CNS
Cancer
Heterocycle

ABSTRACT

Tumours of the central nervous system are intrinsically more dangerous than tumours at other sites, and in particular, brain tumours are responsible for 3% of cancer deaths in the UK. Despite this, research into new therapies only receives 1% of national cancer research spend. The most common chemotherapies are temozolomide, procarbazine, carmustine, lomustine and vincristine, but because of the rapid development of chemoresistance, these drugs alone simply aren't sufficient for long-term treatment. Such poor prognosis of brain tumour patients prompted us to research new treatments for malignant glioma, and in doing so, it became apparent that aromatic heterocycles play an important part, especially the indole, carbazole and indolocarbazole scaffolds. This review highlights compounds in development for the treatment of tumours of the central nervous system which are structurally based on the indole, carbazole and indolocarbazole scaffolds, under the expectation that it will highlight new avenues for research for the development of new compounds to treat these devastating neoplasms.

© 2014 Elsevier Masson SAS. All rights reserved.

1. Introduction

Despite continued research efforts, cancer remains one of the biggest threats to human health, and it was estimated to be responsible for 15% of all deaths internationally in 2010 [1]. More recently, in 2014 in the USA, it is expected that there will be 1,665,540 new incidences of cancer, of which 23,380 would be of the "brain and other nervous system" (1.4%), yet such cancers would result in 14,320 of the 585,720 cancer-related deaths (2.4%) [2]. Tumours of the brain and central nervous system, unlike many other tumour types, can occur in people regardless of sex, race and age, as well as generally being unpreventable [3]. This means that continued research, specifically into curative therapies, is paramount.

In particular, tumours of the central nervous system (CNS) are intrinsically more dangerous than tumours at other sites. In the case of brain tumours, they are responsible for 3% of cancer deaths in the UK, yet research into cures receives only 1% of national cancer research spend [4]. Current treatment for brain tumours generally involves surgical resection (if possible), followed by radiotherapy and chemotherapy, with the most common chemotherapies,

according to Cancer Research UK, being temozolomide, procarbazine, carmustine, lomustine and vincristine. Because of the rapid chemoresistance developed by many brain cancers, these drugs alone simply aren't sufficient for long-term treatment [5].

The indole moiety has been described as a privileged structure [6] as it is a structure that appears extensively in many unrelated areas of biology and medicine, and depending on substituents can have a diverse range of effects. The indole nucleus can be found in compounds as diverse as the hormone serotonin, the amino acid tryptophan, the psychedelic drug LSD and the antimigraine drug rizatriptan (Fig. 1). It is believed by many to be the most ubiquitous and important privileged structure known [6,7].

Just as indoles can be diverse in structure, there are a wide range of biological targets that indoles have been shown to affect. This review discusses ways in which indoles have been shown to prevent cell signalling (PKC inhibitors, PDGF signal transduction inhibitors), prevent normal cell cycle progression (G2/M abrogators, CK2 inhibitors, Trk inhibitors, topoisomerase inhibitors), induce oxidative stress to cells (reactive oxygen species generators), prevent vascularisation in tumours (angiogenesis inhibitors), prevent DNA repair (PARP inhibitors, CK2 inhibitors), and induce the form of cell death known as methiosis.

This review focuses on the development of drugs for the treatment of tumours of the central nervous system which are

* Corresponding author.

E-mail address: tjsnape@uclan.ac.uk (T.J. Snape).

Acronyms/initialisms

AML	Acute myeloid leukaemia
CK2	Casein kinase 2
CNS	Central nervous system
PARP	Poly ADP ribose polymerase
PDGF	Platelet-derived growth factor
PKC	Protein kinase C
ROS	Reactive oxygen species
VEGF	Vascular endothelial growth factor

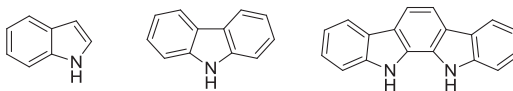


Fig. 2. From left to right: indole, carbazole and indolocarbazole.

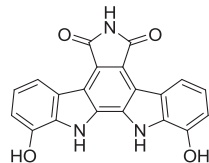


Fig. 3. The topoisomerase inhibitor BE-13793C.

structurally based on the indole, carbazole and indolocarbazole scaffolds (Fig. 2). In doing so, the literature was searched using Thomson Reuters' Web of Knowledge™ for articles containing both a classification of tumours of the central nervous system and either the term “*indol*” or “*carbazol*”, and no restraint on publication date was used. In the interest of ensuring comprehensiveness, this review focuses solely on indole-based structures, so related structures such as isoindoles, indolenes, indazoles and azaindoles are not included, but will be the focus of a separate review. As this is a review of the effect of the indole moiety on biological activity, molecules where the inclusion of an indole moiety does not appear to be the important structural factor, such as in large natural products, are also not included.

2. Topoisomerase inhibitors

Topoisomerase enzymes regulate how wound the double helical structure of DNA is, since they are capable of changing the topology of a DNA strand. Topoisomerases work by binding to the DNA and clipping the phosphate backbone, then either overwinding or underwinding the helix before reforming the backbone. They are particularly active during DNA replication, when the DNA helix can become overwound and then relaxed by topoisomerases.

Topoisomerases are split into two main categories; type I and type II. Type I topoisomerase (often referred to as topo I) acts by clipping one of the two strands of DNA, underwinding or overwinding the strand once (i.e. changing the linking number by ± 1) and then reannealing the strand. This differs to Type II topoisomerase (topo II), which simultaneously clips both strands of the DNA helix in order to undo tangles and supercoils, and in the process change the linking number by ± 2 .

Topoisomerase inhibitors have been of interest as anticancer agents for the past 30 years [8], and the first potential anticancer drug underwent Phase I clinical testing over 20 years ago [9]. They are of pharmacological interest because of the strand breaks that occur in the absence of topoisomerases. These strand breaks render the DNA irreparably damaged, leading to cell death. Indole-containing topoisomerase inhibitors have been worked on by multiple research groups (see below), and many of these

compounds have strong structural similarities, in particular those containing an indolocarbazole group.

During a screening programme for antitumour substances at Banyu Pharmaceutical Company, a group lead by Suda discovered that the bacteria *Streptomyces mobaraensis* (strain BA13793) produced a topoisomerase I and II inhibitor which they named BE-13793C (Fig. 3) [10]. BE-13793C is an indolocarbazole, an indole fused to a carbazole (Fig. 2), which is a moiety that appears commonly in topoisomerase inhibitors [11].

Although initially BE-13793C wasn't tested on any brain tumour cell lines, it was shown to inhibit the growth of certain leukaemia cell lines, and was used as a lead compound for subsequently developed compounds, which ultimately were active against various brain tumour cell lines. During this lead development process one such compound identified was ED-110 (Fig. 4), a derivative first described in 1993 by many of the same people who discovered BE-13793C [12]. This analogue was found to induce topoisomerase I-mediated DNA cleavage, but not topoisomerase II-mediated cleavage [13]. ED-110 was produced by selectively glucosating one of the nitrogens of BE-13793C [12], and was tested on the tumour cell lines MKN-45 (human stomach), LS-180 (colon) and PC-13 (lung), and was found to have IC₅₀ values of 0.28 µg/mL, 1.65 µg/mL and 1.70 µg/mL respectively. It was also shown to help prevent metastases of the CNS tumour fibrosarcoma [14].

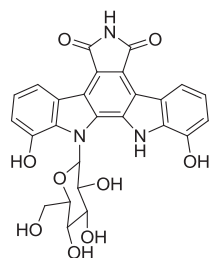


Fig. 4. The structure of ED-110.

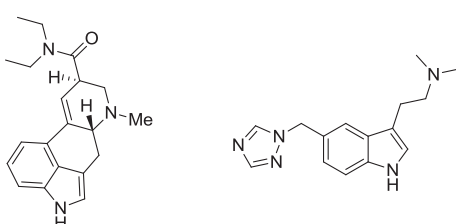
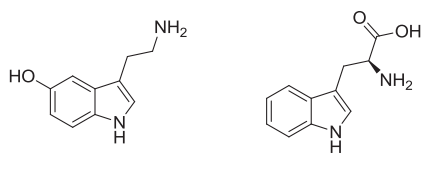
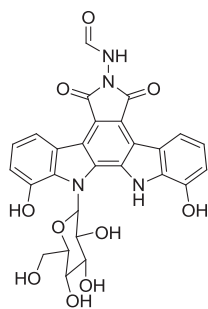


Fig. 1. From left to right: serotonin, tryptophan, LSD and rizatriptan.

**Fig. 5.** The structure of NB-506.

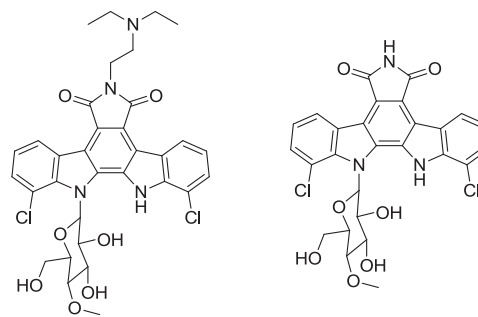
Another derivative of BE-13793C, which also used ED-110 as a lead compound, is NB-506 (Fig. 5), a compound created by a group lead by Yoshinari and published in 1995 [15].

NB-506 was shown to cause DNA breaks in a wide range of cell lines, and in some cases caused DNA breaks at concentrations below $0.1 \mu\text{M}$. It was outperformed by the positive controls camptothecin and adriamycin in the preclinical trials, however due to its cell line selectivity, research continued into developing further derivatives of this compound.

Furthermore, in 1999, a group lead by Fukasawa synthesised a range of derivatives, the most successful of these being J-1007088 (aka edotecarin, Fig. 6) [16]. The activity of edotecarin was described by Arakawa et al. in the same year [17], and was shown to work by stabilising the DNA-topoisomerase I complex. This resulted in cells being incapable of unwinding DNA and therefore preventing them from dividing. Edotecarin also induces single-strand DNA breaks in the presence of topoisomerase I at lower concentrations than its lead compound NB-506 and the widely investigated topoisomerase I inhibitor camptothecin. It was tested on CNS xenografts in mice by Friedman et al. in 2001 [18], and was found to be comparable to topotecan and CPT-11 (irinotecan), but has the distinct advantage of not interacting disfavourably with anticonvulsants.

To date, a number of Phase I and Phase II clinical trials have been carried out on edotecarin, with one of the Phase II trials investigating the effect of the drug on glioblastoma multiforme [19–24], the most aggressive malignant primary brain tumour in humans [25]. Edotecarin unfortunately showed no improvement over the blockbuster control drug, temozolomide, but such is the promise that this compound must show, it has nevertheless been entered into a Phase III clinical trial on the effect of this compound against glioblastoma multiforme [26].

In a 1990 paper by Kaneko et al., the rebeccamycin analogue NSC 655649 (later known as becatecarin, Fig. 7) was synthesised as a water-soluble derivative of rebeccamycin [27], a natural product and topoisomerase I inhibitor first isolated and characterised in

**Fig. 7.** Structure of becatecarin (left) and its lead compound rebeccamycin (right).

1985 [28,29]. Bocatecarin is an indolocarbazole, like edotecarin (Fig. 6), and indeed has a remarkably similar structure. However, coincidentally, its development began from a different lead compound, yet nevertheless convergently arrived at this similar compound.

During *in vitro* studies, bocatecarin was shown to be active against cell lines of Ewing sarcoma, medulloblastoma, neuroblastoma and rhabdomyosarcoma [30], and it appeared to be a more potent anticancer drug than rebeccamycin itself when tested on a leukaemia cell line [27].

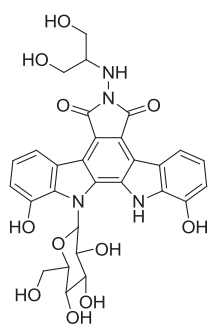
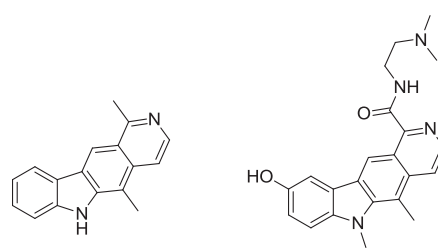
A range of promising Phase I clinical trials were carried out on bocatecarin between 1996 and 2002 [31–36], but in a 2008 Phase II clinical study by Langevin et al. on the effects of the drug on children with solid CNS tumours, it was revealed that myelosuppression was a significant side effect [37], effectively halting the development of this drug for use on this demographic.

Indolocarbazoles aren't the only class of indole derivatives capable of inhibiting topoisomerases. During the synthesis and evaluation of olivacine derivatives [38], the cytotoxic compound S16020 (aka NSC 659687) was found (Fig. 8) [39], which was later discovered to be a potent and selective topoisomerase II inhibitor [40].

S16020 has since completed a Phase I clinical study [41], and more recently has been tested on xenografts of medulloblastoma and glioblastoma [42], where it unfortunately showed lower activity than the positive control, doxorubicin. The reason for this reduced activity was associated with the compound having difficulties crossing the blood–brain barrier.

3. PKC inhibitors

There are currently nine known protein kinase C (PKC) isotypes encoded by the human genome [43], a family of enzymes which regulate the activity of other proteins by phosphorylating specific exposed hydroxyl groups on tyrosine, serine or threonine [44]. PKCs are often involved in cell signal transduction pathways, regulating cell growth, differentiation and proliferation [45], thus making them attractive targets in the fight against cancer.

**Fig. 6.** The topoisomerase inhibitor edotecarin.**Fig. 8.** Left: Olivacine. Right: S16020.

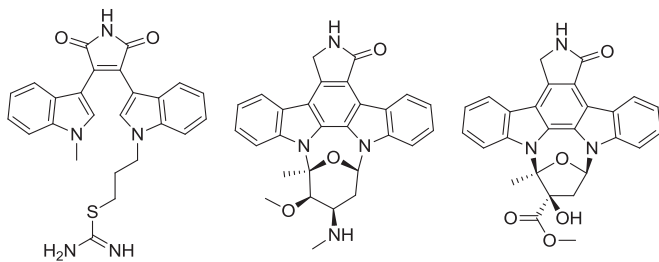


Fig. 9. The PKC inhibitors Ro 31-8220 (left), staurosporine (centre) and K252a (right).

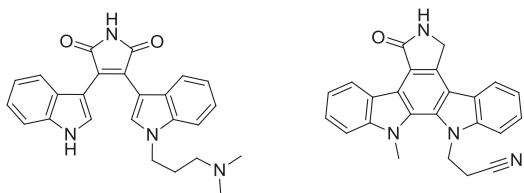


Fig. 10. The structurally related PKC inhibitors GF109203X (left) and Gö 6976 (right).

One compound that has shown promise against two glioblastoma muliforme cell lines is the bisindolylmaleimide Ro 31-8220 (Fig. 9, commercially available as the methanesulfonate salt and also known as bisindolylmaleimide IX). It was first synthesised by Davis et al. in 1989 as part of a small series of analogues of the natural products staurosporine and K252a [46], which are also PKC inhibitors.

In 1995, Ro 31-8220, along with the structurally related PKC inhibitors GF109203X [47] and Gö 6976 (Fig. 10), were tested on the mouse neuroblastoma Neuro-2A cell line (aka N2A) [48]. Apoptosis was induced by all three compounds when added in concentrations between 2 and 12 μ M, with Gö 6976 showing to be the most potent.

Ro 31-8220 is more specifically a PKC α inhibitor, and because PKC α is particularly highly expressed in glioblastoma cells, Glazer and Shen tested it on the glioblastoma cell lines U87 and A172 in 1998 [49]. They found that after the addition of 2.5 μ M of Ro 31-8220, this compound leads to an accumulation of p53 which upregulates IGFBP3, which further leads on to DNA fragmentation and apoptosis, killing the cell. Although this series of compounds didn't make it to clinical testing, it is used experimentally to determine the role of PKC in biological specimens [50].

The structurally related LY-317615 (now known as enzastaurin, Fig. 11), first described by Faul et al. in 2003 [51], is a PKC β inhibitor [52] that underwent promising preclinical studies [53] as well as in a Phase I/II clinical trial [54], but faired disappointingly in Phase III clinical trials [55,56]. The conclusion made was that enzastaurin is "unlikely to be a useful agent as a monotherapy". Enzastaurin has thus been investigated as a concomitant therapy with

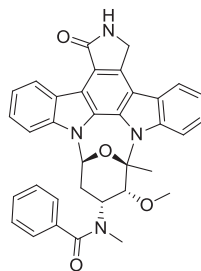


Fig. 12. The structure of midostaurin.

temozolamide on gliomas in a Phase I trial with positive results [5], with temozolamide and radiotherapy on glioblastoma in a Phase II clinical trial with results comparable to an existing therapy [57], and with radiotherapy on glioblastoma with poor results [58]. It has not yet been ruled out as a possible therapy, but as of yet, it has not received approval for use on brain tumours.

A further PKC suppressor, which like Ro 31-8220 is a staurosporine derivative, is midostaurin (aka CGP 41251 and PKC 412), shown in Fig. 12. As a multi-targeted protein kinase suppressor, it has reached Phase III clinical trials as a therapy for acute myeloid leukaemia (AML), [59] but has also been shown to suppress PKC in the glioblastoma cell line U373 MG [60]. Midostaurin has also been shown to have antiproliferative activity against 29 cell lines, including 5 glioblastoma cell lines, for which it had IC₅₀ values in the sub-micromolar range [61].

A further suspected inhibitor of a PKC, specifically PKC δ , was found in 2011 by the Shen group in the extracts of the Asian shrub *Clausena vestita* [62]. Of the 13 carbazoles that were extracted in quantities suitable for further study, clauszoline-I (Fig. 13) had a particularly low IC₅₀ growth inhibitory value against the cancerous liver cell line HepG2 of 15.8 μ M, and also showed almost no cytotoxicity against the normal liver cell line LO2. Clauszoline-I underwent further testing on a variety of cell lines including the glioblastoma cell line T98G. Unfortunately, the IC₅₀ growth inhibitory value against the T98G cell line was a much higher 71.6 μ M, suggesting that this compound is unlikely to be investigated further as a potential glioblastoma therapy.

4. PDGF signal transduction inhibitor

Inhibiting the signal transduction of the protein platelet-derived growth factor (PDGF) works in a similar way to the inhibition of PKC, in that the signals required for cell growth and division are inhibited, resulting in reduced cell proliferation.

The natural product K-252a (Fig. 9), a metabolite of, and originally isolated from, the culture broth of the bacteria *Nocardiopsis* sp., was originally described as an extremely potent inhibitor of PKC, having a recorded IC₅₀ value of just 32.9 nM [63].

In 1997, K-252a was tested on the glioblastoma cell lines U87 and T98G, and was found to inhibit proliferation in both (IC₅₀ = 1170 nM and 529 nM respectively), as well as inducing apoptosis in the U87 cell line, but not the T98G cell line, at a concentration of 1000 nM. Interestingly, K-252a was found not to inhibit PKC but to inhibit PDGF signal transduction [64]. Research

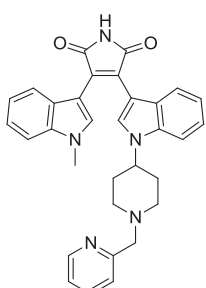


Fig. 11. The structure of the PKC inhibitor enzastaurin.

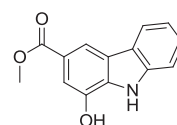


Fig. 13. Structure of the PKC δ inhibitor, clauszoline-I.

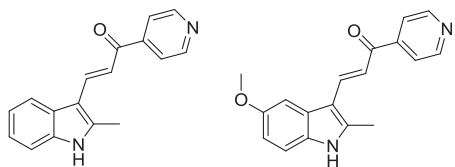


Fig. 14. Methuosis-initiating indoles MIPP (left) and MOMIPP (right).

into K-252a is ongoing, although not as a potential chemotherapy for CNS tumours.

5. Methuosis initiators

In 2008, Maltese et al. published a paper on a novel form of cell death they termed “methuosis”, which is categorised by an accumulation of vacuoles which eventually lead to cell rupture [65]. In 2011 the same group reported an indole named MIPP (Fig. 14) which induced methuosis in a glioblastoma cell line [66]. In 2012 they reported on a small library of MIPP analogues, and attempted to elucidate structure–activity relationships when tested against the glioblastoma cell line U251 [67]. MOMIPP (Fig. 14) was found to have the highest activity against the glioblastoma cell line used, and only differed from MIPP in the addition of a 5-methoxy group, implying that this structural change is responsible for the improvement in activity. Similar improvements in activity have been reported due to inclusion of a 5-methoxy group on an indole scaffold elsewhere [68–70].

The same group has recently published a paper on the synthesis and activity of a series of MOMIPP analogues [71], which shows that increasing the size of the aliphatic substituent at the 2-position does not reduce vacuolisation but does reduce the cytotoxicity of the compounds. Work on this form of cell death *via* the use of indoles is still ongoing by this group.

6. G2/M abrogators

During the cell cycle, the G2/M checkpoint ensures that cells don't enter the mitotic phase (M-phase) from the G2 phase without repairing any damaged DNA. Arresting the cell cycle at the G2/M checkpoint has been a consistently active area of research for the past 30 years [72].

In 1998, research was published describing the discovery of a G2/M checkpoint inhibitor, granulatimide, isolated from the ascidian *Didemnum granulatum*, as well as the synthesis of an active analogue, isogranulatimide (Fig. 15). Roberge et al. synthesised a library of granulatimide and isogranulatimide analogues in an effort to elucidate structure–activity relationships in work published in 2004 [73], and determined that the imide group as well as a basic nitrogen at the 14 or 15 position is essential for G2/M checkpoint inhibition activity in these molecules. It was also shown that these compounds acted by inhibiting Chk1 kinase, a key enzyme in the G2/M checkpoint [74].

A series of granulatimide and isogranulatimide analogues were synthesised in 2009 by Delfourne et al. [75], which were

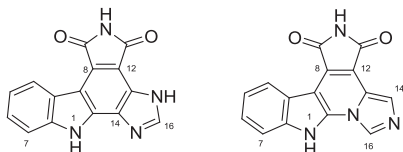


Fig. 15. The G2/M checkpoint abrogators granulatimide (left) and isogranulatimide (right).

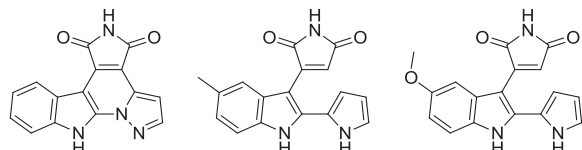


Fig. 16. The three most active analogues of granulatimide, as found by Delfourne et al.

subsequently tested on a range of cancerous cell lines including oligodendrogloma and glioblastoma lines (Hs683 and U373 respectively) [70]. Delfourne showed that, contrary to the SAR published by Roberge, the most active compound had a basic nitrogen at position-16 instead of position-14 or -15. The indole moiety was however still present in the most active compounds (Fig. 16).

In 2001, Mahboobi et al. produced a library of 2-aryl indoles, differing greatly in structure from the G2/M abrogators described so far, and screened them against a range of cancerous cell lines. Of these analogues, three of them were tested on the glioblastoma cell line U373, and were found to be cytostatic with IC₅₀s in the range of 10.7–62.7 nM (Fig. 17) [69]. The antiproliferative IC₅₀s were also reported, and ranged from 28 to 74 nM with the same trend as with the cytostatic IC₅₀s. Antiproliferative activity was noticed to coincide with the inhibition of tubulin polymerisation.

7. Trk inhibitors

Trk receptors are a class of receptor that affect cell differentiation as well as neuronal survival, and by inhibiting them, the cell is often driven to apoptosis.

As well as being a PDGF inhibitor, K252a (Fig. 9) has been shown to be trk family tyrosine kinase inhibitor [76], although this activity does not translate to anticancer activity *via* this mechanism [77]. In order to find a trk family tyrosine kinase inhibitor which had anticancer activity, a family of analogues, including CEP-751 (aka KT-6587) and CEP-701 (aka lestaurtinib) (Fig. 18), were synthesised and tested, both of which were shown to have anti-tumour activity [78,79]. The only structural difference between these compounds is the reduction of the ester at the 2'-position to a hydroxymethyl group, indicating that a 2'-hydroxymethyl group is important to the activity of these compounds.

Camoratto et al. showed, in 1997, that CEP-751 specifically inhibits the receptors trkA, trkB and trkC [78], and in 1999, Brodeur

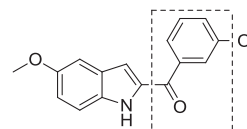


Fig. 17. The most active indole tested on the U373 cell line by Mahboobi et al., with the 2-aryl group highlighted.

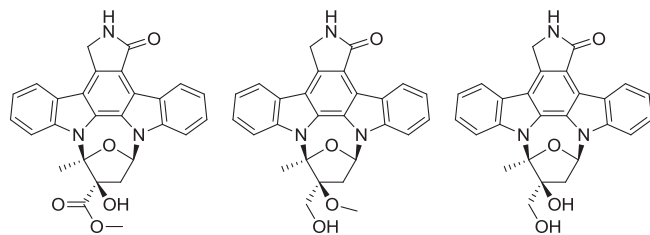


Fig. 18. Trk inhibitors K252a (left), CEP-751 (centre) and CEP-701 (right).

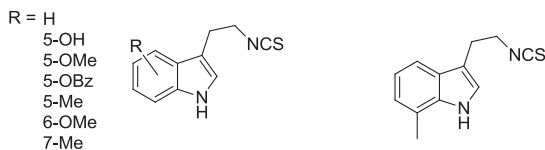


Fig. 19. Left: The ROS-producing compounds tested. Right: The most active compound tested, 7Me-IEITC.

et al. tested it on a range of neuroblastoma and medulloblastoma cell lines as xenografts in mice. It was shown that CEP-751 reduced the *in vivo* growth of neuroblastoma and medulloblastoma xenografts with high and borderline significance respectively, and also showed no toxicity in the mice used. The same group reported in 2001 that this activity is likely due to the inhibition of the trkB receptor [80].

CEP-751 was further studied on four neuroblastoma and three medulloblastoma cell lines as xenografts by the Brodeur group [81]. A significant decrease in tumour size was observed in three of the neuroblastoma cell lines and one of the medulloblastoma cell lines, which was attributed to neurblastoma cells generally expressing at least one tyrosine kinase receptor. It was concluded that CEP-751 may be a viable chemotherapy for neuroblastomas, but would be less well suited to treating medulloblastomas. Despite some early promise, this drug appears to have fallen out of development as both a neuroblastoma and medulloblastoma treatment.

Contrastingly, CEP-701 has received more attention. Since being shown to be well tolerated in a Phase I clinical trial in 2005 [82], it has shown promise in preclinical trials as a combinatorial drug for neuroblastomas [83,84]. Despite this, its use as a trk inhibitor against neuroblastomas no longer appears to be an active area of research.

8. ROS producers

A reactive oxygen species (ROS) is an umbrella term given to a wide range of reactive, oxygen containing, often small molecules that have been found to be active in many biological functions, ranging from cellular homeostasis to cell death [85]. Examples of ROS are often given as superoxide (O_2^- or $O_2^{\cdot -}$), hydrogen peroxide ($HOOH$), the hydroxyl radical (HO^\bullet), ozone (O_3) and singlet oxygen (1O_2) [86], and can be generated endogenously by the cell, or

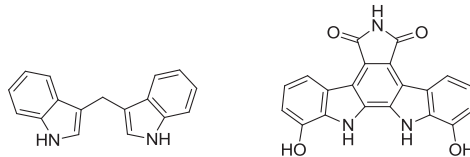


Fig. 21. Structural comparison of DIM (left) and BE-13793C (right), the simplest indolocarbazole described in this review.

exogenously by so-called ROS generators. When ROS are produced by an exogenous source, the aim is for them to kill cells.

During their investigations into the effects of isothiocyanates as anti-tumour agents, Brard et al. synthesised a library of seven indole ethyl isothiocyanates (Fig. 19) and screened them for activity against four neuroblastoma cell lines [87]. Indole ethyl isothiocyanates were investigated due to their similarity to benzyl isothiocyanates and phenyl ethyl isothiocyanates, both of which have been reported to have anti-cancer activity in a range of cancers [6,88–90].

Of all the indole ethyl isothiocyanates tested, 7-methyl-indole-3-ethyl isothiocyanate (7Me-IEITC, Fig. 19) was found to be the most active, and when tested on a range of neuroblastoma cell lines was found to have an IC_{50} in the range of 2.5–5 μM , while not affecting the primary control cells. 7Me-IEITC activates the apoptotic markers caspase-3, caspase-8 and caspase-9, activates the pro-apoptotic p38 mitogen-activated protein kinases and signalling pathway SAPK/JNK, and downregulates AKT. This compound was also shown to display antiproliferative activity and cell cycle arrest at higher doses ($IC_{50} = 600$ nM). During a study of the therapeutic potential of 7Me-IEITC on uterine endometrial cells, it was shown that apoptosis correlated with the production of ROS [91].

Indole-3-carbinol (I3C) and its derivatives (Fig. 20) are a class of compounds that have received considerable attention over the past 30 years [92,93]. I3C has been shown to be effective against a range of cancers including those of the breast [94], colon [95–97] and prostate [98–100]. The activity of I3C is believed to be due to its intrinsic instability in acidic media, and the subsequent formation of its metabolites (Fig. 20) [101]. The major metabolite, 3,3'-diindolylmethane (DIM), is responsible for the majority of the observed activity, but collectively all the metabolites have a range of broad targets and activities [98].

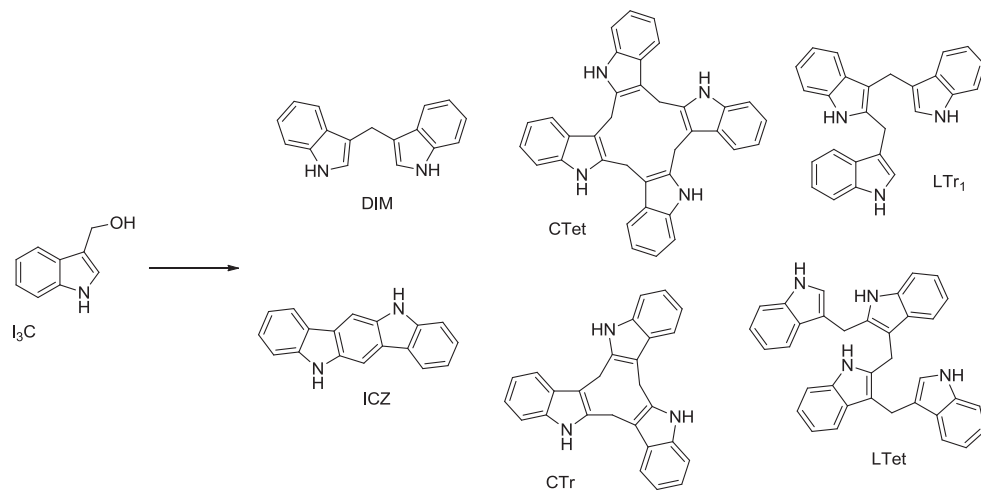


Fig. 20. Indole-3-carbinol (I3C) and its metabolites 3,3'-diindolylmethane (DIM), a cyclic tetramer (CTet), the first linear trimer (LTr₁), indolo[3,2-b]carbazole (ICZ), a cyclic trimer (CTr) and a linear tetramer (LTet).

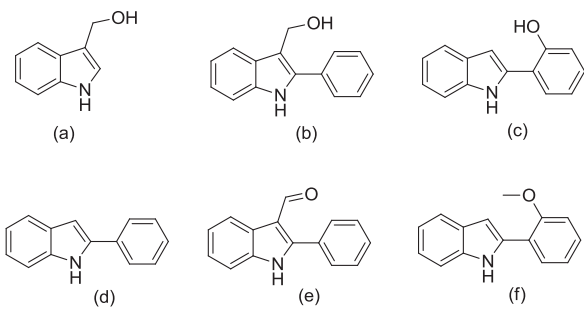


Fig. 22. Active (top row) and inactive (bottom row) species tested by Snape et al.

There are structural comparisons that can be drawn between the major metabolite DIM and many of the indolocarbazoles discussed previously (Fig. 21), with the indolocarbazoles being structurally more rigid and planar. Such observations may be useful in rationally designing new compound classes of these indole-containing scaffolds, and may prove to be especially useful in the preparation and evaluation of hybrid structures.

In a related research area, in 2013, Snape and Prabhu also found that I3C, as well as a small series of analogues (Fig. 22), had activity against glioblastoma cell lines [102]. In particular, these analogues gave some indications as to the structure–activity relationship of this class of indoles against glioblastoma, most notably that a protonated heteroatom (e.g. a hydroxyl group) is necessary for activity, as well as suggesting that phenyl groups at the 2-position of the indole nucleus improve activity.

The activity of these compounds was originally hypothesised to be due to ROS formation, a hypothesis supported by the observation that cells were under oxidative stress when in the presence of indoles (**b**) and (**c**), but not indoles (**d**) and (**f**).

9. Angiogenesis inhibitors

Angiogenesis inhibitors were once one of the most hotly researched areas in oncology, and are still of interest due to their ability to inhibit the growth of new blood vessels in a tumour. A common way of inhibiting angiogenesis is by inhibiting the vascular endothelial growth factor (VEGF), the signalling protein that is responsible for initiating vasculogenesis and angiogenesis.

The carbazole derivative CEP-7055 and its prodrug CEP-5214 have been shown to be potent angiogenesis inhibitors that act by inhibiting the VEGF receptor kinase [103]. Although CEP-7055 is the active compound, the ester derivative (CEP-5214) was required in order to improve aqueous solubility and allow for an oral route of administration (Fig. 23).

CEP-7055 had successfully been through a preclinical trial (including showing promise against glioblastoma xenografts) [103], and has shown to be a viable co-therapy along with temozolamide against glioblastoma in mice [104]. Development of this compound was however dropped in 2006, after it showed no activity during a Phase I clinical trial [105].

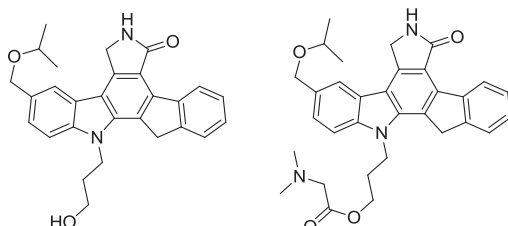


Fig. 23. The structures of CEP-7055 (left) and its prodrug CEP-5214 (right).

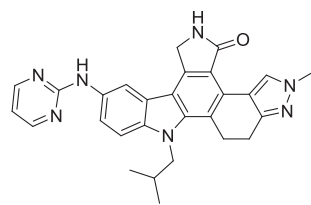


Fig. 24. The structure of CEP-11981.

In 2012, the same group published research with the intention of finding a compound that inhibited “multiple, complementary and nonredundant angiogenic targets”, using CEP-7055 as their lead compound [106]. To this end, the group synthesised and tested 11 CEP-7055 analogues, and found that CEP-11981 (Fig. 24), an antiangiogenic compound, was a potent inhibitor of the receptors TIE-2, VEGF-R1, 2 and 3, and FGF-R1.

The melanoma cell line A375 and the glioblastoma cell line U251 MG were used as murine xenografts to assess the antitumour efficacy of CEP-11981. Growth inhibition and tumour regression was observed with both cell lines, but a higher efficacy was observed against the melanoma cell line. A reportedly successful Phase I clinical trial of this compound has also been completed [107].

10. PARP inhibitors

Poly(ADP-ribose) polymerase (PARP) works by helping repair DNA that is damaged either through natural processes (such as replication) or otherwise. PARP inhibitors therefore work by preventing this repair from occurring, and are becoming an ever more popular research area due to their potential for selectivity, especially in tumours with BRCA mutations [108] or in rapidly growing tumours that become oxygen-deficient [109].

Due to their mode of activity, PARP inhibitors are particularly suited to being a co-therapy along with a drug that damages DNA. In 2007, the PARP inhibitor CEP-8983 and its more soluble prodrug CEP-9722 (Fig. 25) were tested on a small range of chemoresistant CNS xenografts as co-therapies. CEP-8983 was shown to sensitise the glioblastoma xenograft (RG2), rhabdomyosarcoma xenograft (RH18) and the neuroblastoma xenograft (NB1691) to both temozolamide and camptothecin in mice. CEP-9722, which was only tested on the glioblastoma xenograft as a co-therapy with temozolamide, was shown to be an improvement over temozolamide alone without potentiating myelotoxicity [110]. Although the structure of CEP-8983 has been published, the structure of the more soluble prodrug CEP-9722 has not been disclosed, presumably because it is currently under development by Cephalon Inc. Cephalon Inc. have however patented a series of CEP-8983 analogues, one of which may be CEP-9722 [111].

11. Casein kinase 2 inhibitors

Casein kinase 2 (CK2), a protein kinase, is an uncommon but promising target for anticancer drugs. As a kinase, it has been implicated in almost 500 processes [112], including DNA repair [113] and cell cycle processes [114].

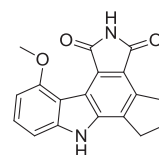
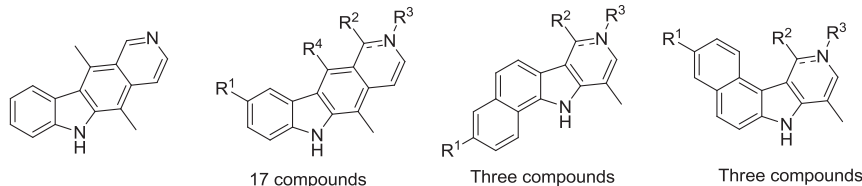
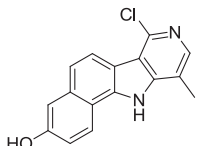


Fig. 25. Structure of CEP-8983. The structure of CEP-9722 has not been disclosed.

**Fig. 26.** Ellipticine (left) and its derivatives.**Fig. 27.** The most successful compound tested by Cochet et al.

Cochet et al., who have developed a series of ellipticine derivatives (Fig. 26), found that this class of compound competitively inhibited ATP from binding, in turn inhibiting CK2 and inducing apoptosis and cell cycle arrest [115].

It was found that hydroxyl groups at the R¹ position tended to lead to much greater CK2 inhibition, and a C=N double bond led to a slight improvement over a single C—N bond in inhibitory activity. The most active CK2 inhibitor tested (Fig. 27) had both of these features, however some of the other compounds tested showed greater inhibition of c-Kit (a protein involved in many cellular processes including cell survival) [116] and topoisomerase II α , as well as greater DNA intercalation.

12. Conclusion

As this review has shown, the privileged structure of the indole and the carbazole and indolocarbazole nucleus appears in the structure of anticancer drugs with widely varying modes of activity. Nevertheless, the quantity of indoles for each mode of activity that are making it through to clinical trials does not reflect this ubiquity. As structure–activity relationships for such compounds as anti-cancer agents are built up, the fact that such versatile syntheses have already become well established will surely improve the rate at which such drugs can be synthesised and subsequently tested for anticancer activity.

Acknowledgements

The authors wish to thank the Sydney Driscoll Neuroscience Foundation, Brain Tumour North West (BTNW) and The School of Pharmacy and Biomedical Sciences, UCLan for funding this PhD studentship (CS).

References

- [1] R. Lozano, M. Naghavi, K. Foreman, S. Lim, K. Shibuya, V. Aboyans, J. Abraham, T. Adair, R. Aggarwal, S.Y. Ahn, et al., Lancet 380 (2013) 2095–2128.
- [2] R. Siegel, J. Ma, Z. Zou, A. Jemal, CA. Cancer J. Clin. 64 (2014) 9–29.
- [3] T. de Cresci Braga Montelli, M. Terezinha Serrao Peracoli, S. Regina Rogatto, R. Kaneno, C. Helena Braga Montelli do Prado, P. de Medeiros Cardassi Rocha, Cent. Nerv. Syst. Agents Med. Chem. Former. Curr. Med. Chem.-Cent. Nerv. Syst. Agents 11 (2011) 8–30.
- [4] Brain Tumour Research, Report on National Research Funding July 2013, 2014 can be found under www.braintumourresearch.com.
- [5] R. Rampling, M. Sanson, T. Gorlia, D. Lacombe, C. Lai, M. Gharib, W. Taal, C. Stoffregen, R. Decker, M.J. van den Bent, Neuro-Oncology 14 (2012) 344–350.
- [6] S. Lal, T.J. Snape, Curr. Med. Chem. 19 (2012) 4828–4837.
- [7] D.A. Horton, G.T. Bourne, M.L. Smythe, Chem. Rev. 103 (2003) 893–930.
- [8] E.M. Nelson, K.M. Tewey, L.F. Liu, Proc. Natl. Acad. Sci. 81 (1984) 1361–1365.
- [9] E.K. Rowinsky, L.B. Grochow, C.B. Hendricks, D.S. Ettinger, A.A. Forastiere, L.A. Hurowitz, W.P. McGuire, S.E. Sartorius, B.G. Lubejko, S.H. Kaufmann, J. Clin. Oncol. 10 (1992) 647–656.
- [10] K. Kojiri, H. Kondo, T. Yoshihara, H. Arakawa, S. Nakajima, F. Satoh, K. Kawamura, A. Okura, H. Suda, M. Okanishi, J. Antibiot. (Tokyo) 44 (1991) 723–729.
- [11] H. Nakano, S. Omura, J. Antibiot. (Tokyo) 62 (2009) 17–26.
- [12] S. Tanaka, M. Ohkubo, K. Kojiri, H. Suda, J. Antibiot. (Tokyo) 45 (1992) 1797–1798.
- [13] T. Yoshihara, A. Yamada, D. Uemura, K. Nomura, H. Arakawa, K. Kojiri, E. Yoshida, H. Suda, A. Okura, Cancer Res. 53 (1993) 490–494.
- [14] H. Arakawa, T. Iguchi, T. Yoshihara, K. Kojiri, H. Suda, A. Okura, Jpn. J. Cancer Res. 84 (1993) 574–581.
- [15] T. Yoshihara, M. Matsumoto, H. Arakawa, H. Okada, K. Noguchi, H. Suda, A. Okura, S. Nishimura, Cancer Res. 55 (1995) 1310–1315.
- [16] T. Yoshihara, M. Ohkubo, K. Fukasawa, S. Egashira, Y. Hara, M. Matsumoto, K. Nakai, H. Arakawa, H. Morishima, S. Nishimura, Cancer Res. 59 (1999) 4271–4275.
- [17] H. Arakawa, M. Morita, T. Kodera, A. Okura, M. Ohkubo, H. Morishima, S. Nishimura, Cancer Sci. 90 (1999) 1163–1170.
- [18] C. Cavazos, S. Keir, T. Yoshihara, D. Bigner, H. Friedman, Cancer Chemother. Pharmacol. 48 (2001) 250–254.
- [19] H.I. Hurwitz, R.B. Cohen, J.P. McGovern, S. Hirawat, W.P. Petros, Y. Natsumeda, T. Yoshihara, Cancer Chemother. Pharmacol. 59 (2006) 139–147.
- [20] M.W. Saif, R.B. Diasio, Clin. Colorectal Cancer 5 (2005) 27–36.
- [21] M. Gilbert, M. Capone, A.A. Brandes, S. Gertler, S. Green, C. Fost, J. Caulkins, A. Ingrosso, M. Foley, Eur. J. Cancer Suppl. 3 (2005) 136.
- [22] R. Peck, Proceeds Am. Soc. Clin. Oncol. 19 (2000). Abstract #767.
- [23] L. Lewis, R. Perez, W. Petros, Proceeds Am. Soc. Clin. Oncol. 19 (2000). Abstract #688.
- [24] Y. Yamada, N. Yamamoto, T. Shimoyama, Proceeds Am. Soc. Clin. Oncol. 21 (2002). Abstract #385.
- [25] D.W. Parsons, S. Jones, X. Zhang, J.C.-H. Lin, R.J. Leary, P. Angenendt, P. Mankoo, H. Carter, I.-M. Siu, G.L. Gallia, et al., Science 321 (2008) 1807–1812.
- [26] Pfizer, Study of IV Edotecarin Vs Temozolomide or Carmustine (BCNU) or Lomustine (CCNU) in Patients with Glioblastoma Multiforme, National Library of Medicine (US), Bethesda (MD), 2008. ClinicalTrials.gov.
- [27] T. Kaneko, H. Wong, J. Utzig, J. Schurig, T.W. Doyle, J. Antibiot. (Tokyo) 43 (1990) 125–127.
- [28] Y. Yamashita, N. Fujii, C. Murakata, T. Ashizawa, M. Okabe, H. Nakano, Biochemistry (Mosc.) 31 (1992) 12069–12075.
- [29] D.E. Nettleton, T.W. Doyle, B. Krishnan, G.K. Matsumoto, J. Clardy, Tetrahedron Lett. 26 (1985) 4011–4014.
- [30] S. Weitman, R. Moore, H. Barrera, N.K. Cheung, E. Izicka, D.D. Von Hoff, J. Pediatr. Hematol. Oncol. 20 (1998) 136–139.
- [31] J. Merchant, K. Tutsch, A. Dresen, R. Arzomanian, D. Alberti, C. Feierabend, K. Binger, R. Marnocha, J. Thomas, J. Cleary, et al., Clin. Cancer Res. 8 (2002) 2193–2201.
- [32] A.W. Tolcher, S.G. Eckhardt, J. Kuhn, L. Hammond, G. Weiss, J. Rizzo, C. Aylesworth, M. Hidalgo, A. Patnaik, G. Schwartz, et al., J. Clin. Oncol. 19 (2001) 2937–2947.
- [33] A. Dowlati, C.L. Hoppel, S.T. Ingalls, S. Majka, X. Li, N. Sedransk, T. Spiro, S.L. Gerson, P. Ivy, S.C. Remick, J. Clin. Oncol. 19 (2001) 2309–2318.
- [34] S.G. Eckhardt, J. Kuhn, J. Rizzo, S. Sharma, E. Campbell, P. Ivey, G. Weiss, L. Hammond, M. Kraynak, D.D. Von Hoff, et al., Ann. Oncol. 9 (1998) 66.
- [35] J. Cleary, K.D. Tutsch, J. Berlin, R.Z. Arzomanian, D. Alberti, C. Feierabend, K. Sinon, P. Hutson, J. Steward, G. Silding, Proc. Am. Assoc. Cancer Res. Annu. Meet. 37 (1996) 164.
- [36] K.D. Tutsch, J.F. Cleary, J.D. Berlin, R.Z. Arzomanian, D. Alberti, C. Feierabend, K. Simon, K. Morgan, A. Wahamaki, R. Marnocha, et al., Proc. Am. Assoc. Cancer Res. Annu. Meet. 39 (1998) 322.
- [37] A.-M. Langevin, M. Bernstein, J.G. Kuhn, S.M. Blaney, P. Ivy, J. Sun, Z. Chen, P.C. Adamson, Pediatr. Blood Cancer 50 (2008) 577–580.
- [38] R. Jaszfeld-Howorko, C. Landras, A. Pierre, G. Atassi, N. Guillaud, L. Kraus-Berthier, S. Leonce, Y. Rolland, J.-F. Prost, E. Bisagni, J. Med. Chem. 37 (1994) 2445–2452.
- [39] S. Leonce, V. Perez, M.-R. Casabianca-Pigneau, M. Anstett, E. Bisagni, A. Pierré, G. Atassi, Invest. New Drugs 14 (1996) 169–180.
- [40] S. Le Mée, A. Pierré, J. Markovits, G. Atassi, A. Jacquemin-Sablon, J.-M. Saucier, Mol. Pharmacol. 53 (1998) 213–220.

- [41] A. Awada, S. Giacchetti, B. Gerard, P. Eftekhar, C. Lucas, D. de Valeriola, M.G. Poullain, J. Soudon, C. Dosquet, M.-H. Brillianceau, et al., *Ann. Oncol.* 13 (2002) 1925–1934.
- [42] G. Vassal, J.-L. Merlin, M.-J. Terrier-Lacombe, J. Grill, F. Parker, C. Sainte-Rose, G. Aubert, J. Morizet, N. Sévenet, M.-G. Poullain, et al., *Cancer Chemother. Pharmacol.* 51 (2003) 385–394.
- [43] L.V. Dekker, *Protein Kinase C*, Kluwer Academic/Plenum Publishers, Texas, 2004.
- [44] H. Hug, T.F. Sarre, *Biochem. J.* 291 (1993) 329–343.
- [45] T. Leppänen, R.K. Tuominen, E. Moilanen, *Basic Clin. Pharmacol. Toxicol.* 114 (2014) 37–43.
- [46] P.D. Davis, C.H. Hill, E. Keech, G. Lawton, J.S. Nixon, A.D. Sedgwick, J. Wadsworth, D. Westmacott, S.E. Wilkinson, *FEBS Lett.* 259 (1989) 61–63.
- [47] D. Toullec, P. Pianetti, H. Coste, P. Bellevergue, T. Grand-Perret, M. Ajakane, V. Baudet, P. Soissin, E. Boursier, F. Loriolle, et al., *J. Biol. Chem.* 266 (1991) 15771–15781.
- [48] M.M. Behrens, J.L. Martinez, C. Moratilla, J. Renart, *Cell Growth Differ.* 6 (1995) 1375–1380.
- [49] L. Shen, R.I. Glazer, *Biochem. Pharmacol.* 55 (1998) 1711–1719.
- [50] P. Pundir, A. Catalli, C. Leggiadro, S.E. Douglas, M. Kulka, *Mucosal Immunol.* 7 (2014) 177–187.
- [51] M.M. Faul, J.R. Gillig, M.R. Jirousek, L.M. Ballas, T. Schotten, A. Kahl, M. Mohr, *Bioorg. Med. Chem. Lett.* 13 (2003) 1857–1859.
- [52] E. Galanis, J.C. Buckner, *J. Clin. Oncol.* 28 (2010) 1097–1098.
- [53] J.R. Graff, A.M. McNulty, K.R. Hanna, B.W. Konicek, R.L. Lynch, S.N. Bailey, C. Banks, A. Capen, R. Goode, J.E. Lewis, et al., *Cancer Res.* 65 (2005) 7462–7469.
- [54] T.N. Kreisl, S. Kotliarova, J.A. Butman, P.S. Albert, L. Kim, L. Musib, D. Thornton, H.A. Fine, *Neuro-Oncology* 12 (2010) 181–189.
- [55] W. Wick, V.K. Puduvalli, M.C. Chamberlain, M.J. van den Bent, A.F. Carpenter, L.M. Cher, W. Mason, M. Weller, S. Hong, L. Musib, et al., *J. Clin. Oncol.* 28 (2010) 1168–1174.
- [56] H.A. Fine, V.K. Puduvalli, M.C. Chamberlain, A.F. Carpenter, L. Cher, W.P. Mason, M.J. van den Bent, S. Hong, D. Thornton, W. Wick, *ASCO Meeting Abstr.* 26 (2005).
- [57] N. Butowski, S.M. Chang, K.R. Lamborn, M.-Y. Polley, R. Pieper, J.F. Costello, S. Vandenberg, R. Parvataneni, A. Nicole, P.K. Sneed, et al., *Neuro-Oncology* 13 (2011) 1331–1338.
- [58] W. Wick, J.P. Steinback, M. Platten, C. Hartmann, F. Wenz, D.D. von Deimling, P.P. Shei, C. Moreau-Donnet, S.E. Combs, *Neuro-Oncology* 15 (2013) 1405–1412.
- [59] Alliance for Clinical Trials in Oncology, Daunorubicin, Cytarabine, and Midostaurin in Treating Patients with Newly Diagnosed Acute Myeloid Leukemia, National Library of Medicine (US), Bethesda (MD), 2014. [ClinicalTrials.gov](#).
- [60] W. Luo, T.R. Sharif, P.J. Houghton, M. Sharif, *Cell Growth Differ.* 8 (1997) 1225–1240.
- [61] D. Fabbro, E. Buchdunger, J. Wood, J. Mestan, F. Hofmann, S. Ferrari, H. Mett, T. O'Reilly, T. Meyer, *Pharmacol. Ther.* 82 (1999) 293–301.
- [62] W. Lin, Y. Wang, S. Lin, C. Li, C. Zhou, S. Wang, H. Huang, P. Liu, G. Ye, X. Shen, *Eur. J. Med. Chem.* 47 (2012) 214–220.
- [63] H. Kase, K. Iwahashi, M. Yuzuru, *J. Antibiot. (Tokyo)* 39 (1986) 1059–1065.
- [64] L.S. Chin, S.F. Murray, K.M. Zitnay, B. Rami, *Clin. Cancer Res.* 3 (1997) 771–776.
- [65] J.H. Overmeyer, A. Kaul, E.E. Johnson, W.A. Maltese, *Mol. Cancer Res.* 6 (2008) 965–977.
- [66] J.H. Overmeyer, A.M. Young, H. Bhanot, W.A. Maltese, *Mol. Cancer* 10 (2011) 69–85.
- [67] M.W. Robinson, J.H. Overmeyer, A.M. Young, P.W. Erhardt, W.A. Maltese, *J. Med. Chem.* 55 (2012) 1940–1956.
- [68] I.V. Magedov, F. Lefranc, L.V. Frolova, L.M.Y. Banuls, A.S. Peretti, S. Rogelj, V. Mathieu, R. Kiss, A. Kornienko, *Bioorg. Med. Chem. Lett.* 23 (2013) 3277–3282.
- [69] S. Mahboobi, H. Pongratz, H. Hufsky, J. Hockemeyer, M. Frieser, A. Lyssenko, D.H. Paper, J. Bürgermeister, F.-D. Böhmer, H.-H. Fiebig, *J. Med. Chem.* 44 (2001) 4535–4553.
- [70] S. Deslandes, D. Lamoral-Theys, C. Frongia, S. Chassaing, C. Bruyère, O. Lozach, L. Meijer, B. Ducommun, R. Kiss, E. Delfourne, *Eur. J. Med. Chem.* 54 (2012) 626–636.
- [71] C.J. Trabucco, H.M. Dietisch, E.M. Alexander, P.I. Nagy, M.W. Robinson, J.H. Overmeyer, W.A. Maltese, P.W. Erhardt, *ACS Med. Chem. Lett.* 5 (2014) 73–77.
- [72] G.R. Stark, W.R. Taylor, *Mol. Biotechnol.* 32 (2006) 227–248.
- [73] X. Jiang, B. Zhao, R. Britton, *Mol. Cancer Ther.* 3 (2004) 1221–1227.
- [74] R. Boutros, V. Lobjois, B. Ducommun, *Nat. Rev. Cancer* 7 (2007) 495–507.
- [75] S. Deslandes, S. Chassaing, E. Delfourne, *Mar. Drugs* 7 (2009) 754–786.
- [76] M. Ohmichi, S.J. Decker, L. Pang, A.R. Saltiel, *Biochemistry (Mosc.)* 31 (1992) 4034–4039.
- [77] S. Akinaga, T. Ashizawa, K. Gomi, H. Ohno, M. Morimoto, C. Murakata, M. Okabe, *Cancer Chemother. Pharmacol.* 29 (1992) 266–272.
- [78] A.M. Camoratto, J.P. Jani, T.S. Angeles, A.C. Maroney, C.Y. Sanders, C. Murakata, N.T. Neef, L.L. Vaught, J.T. Isaacs, C.A. Dionne, *Int. J. Cancer* 72 (1997) 673–679.
- [79] S.J. Miknyoczki, H. Chang, A. Klein-Szanto, C.A. Dionne, B.A. Ruggeri, *Clin. Cancer Res.* 5 (1999) 2205–2212.
- [80] A.E. Evans, K.D. Kisselbach, X. Liu, A. Eggert, N. Ikegaki, A.M. Camoratto, C.A. Dionne, G.M. Brodeur, *Med. Pediatr. Oncol.* 36 (2001) 181–184.
- [81] A.E. Evans, K.D. Kisselbach, D.J. Yamashiro, N. Ikegaki, A.M. Camoratto, C.A. Dionne, G.M. Brodeur, *Clin. Cancer Res.* 5 (1999) 3594–3602.
- [82] J.L. Marshall, H. Kindler, J. Deeken, P. Bhargava, N.J. Vogelzang, N. Rizvi, T. Luhatala, S. Boylan, M. Dordal, P. Robertson, *Invest. New Drugs* 23 (2005) 31–37.
- [83] R.E. Norris, J.E. Minturn, G.M. Brodeur, J.M. Maris, P.C. Adamson, *Cancer Chemother. Pharmacol.* 68 (2011) 1469–1475.
- [84] R. Iyer, A.E. Evans, X. Qi, R. Ho, J.E. Minturn, H. Zhao, N. Balamuth, J.M. Maris, G.M. Brodeur, *Clin. Cancer Res.* 16 (2010) 1478–1485.
- [85] C. Nathan, A. Cunningham-Bussel, *Nat. Rev. Immunol.* 13 (2013) 349–361.
- [86] C. Nathan, A. Ding, *Cell* 140 (2010) 951, 951.e2.
- [87] R.K. Singh, T.S. Lange, C. Lieb, G.L. Sholler, L. Brard, K. Kim Kyu, Y. Zouo, *Bioorg. Med. Chem. Lett.* 17 (2007) 5846–5852.
- [88] K.S. Satyan, N. Swamy, D.S. Dizon, R. Singh, C.O. Granai, L. Brard, *Gynecol. Oncol.* 103 (2006) 261–270.
- [89] S. Kalkunte, N. Swamy, D.S. Dizon, L. Brard, *J. Exp. Ther. Oncol.* 5 (2006) 287–300.
- [90] P. Barraja, L. Caracaus, P. Diana, A. Montalbano, A. Carbone, A. Salvador, P. Brun, I. Castagliuolo, S. Tisi, F. Dall'Acqua, et al., *ChemMedChem* 6 (2011) 1238–1248.
- [91] K. Kristjansdottir, K. Kim, J.S. Choi, T.C. Horan, L. Brard, R.G. Moore, R.K. Singh, *Gynecol. Oncol.* 126 (2012) 252–258.
- [92] H.L. Bradlow, *In Vivo* 22 (2008) 441–445.
- [93] J.-R. Weng, C.-H. Tsai, S.K. Kulp, C.-S. Chen, *Cancer Lett.* 262 (2008) 153–163.
- [94] L.M. Howells, B. Gallacher-Horley, C.E. Houghton, M.M. Manson, E.A. Hudson, *Mol. Cancer Ther.* 1 (2002) 1161–1172.
- [95] H.R. Frydoonfar, D.R. McGrath, A.D. Spigelman, *Colorectal Dis.* 4 (2002) 205–207.
- [96] E.A. Hudson, L.M. Howells, B. Gallacher-Horley, L.H. Fox, A. Gescher, M.M. Manson, *BMC Cancer* 3 (2003) 2.
- [97] Q. Zheng, Y. Hirose, N. Yoshimi, A. Murakami, K. Koshimizu, H. Ohigashi, K. Sakata, Y. Matsumoto, Y. Sayama, H. Mori, *J. Cancer Res. Clin. Oncol.* 128 (2002) 539–546.
- [98] M. Nachshon-Kedmi, S. Yannai, A. Haj, F.A. Fares, *Food Chem. Toxicol.* 41 (2003) 745–752.
- [99] S.R. Chinni, Y. Li, S. Upadhyay, P.K. Koppolu, F.H. Sarkar, *Oncogene* 20 (2001) 2927–2936.
- [100] H.R. Frydoonfar, D.R. McGrath, A.D. Spigelman, *ANZ J. Surg.* 73 (2003) 154–156.
- [101] K.R. Grose, L.F. Bjeldanes, *Chem. Res. Toxicol.* 5 (1992) 188–193.
- [102] S. Prabhu, Z. Akbar, F. Harris, K. Karakoula, R. Lea, F. Rowther, T. Warr, T. Snape, *Bioorg. Med. Chem.* 21 (2013) 1918–1924.
- [103] B. Ruggeri, J. Singh, D. Gingrich, T. Angeles, M. Albom, H. Chang, C. Robinson, K. Hunter, P. Dobrzanski, S. Jones-Bolin, et al., *Cancer Res.* 63 (2003) 5978–5991.
- [104] S. Jones-Bolin, H. Zhao, K. Hunter, *Mol. Cancer Ther.* 5 (2006) 1744–1753.
- [105] R. Williams, *Expert Opin. Investig. Drugs* 17 (2008) 1791–1816.
- [106] R.L. Hudkins, N.C. Becknell, A.L. Zulli, T.L. Underiner, T.S. Angeles, L.D. Aimone, M.S. Albom, H. Chang, S.J. Miknyoczki, K. Hunter, et al., *J. Med. Chem.* 55 (2012) 903–913.
- [107] Cephalon, Open-label Study to Determine the Maximum Tolerated Oral Dose of the Kinase Inhibitor CEP-11981 in Patients with Advanced Cancer, National Library of Medicine (US), Bethesda (MD), 2012. [ClinicalTrials.gov](#).
- [108] A.J. Chalmers, *Br. Med. Bull.* 89 (2008) 23–40.
- [109] N. Chan, I.M. Pires, Z. Bencokova, C. Coackley, K.R. Luoto, N. Bhogal, M. Lakshman, P. Gottipati, F.J. Oliver, T. Helleday, et al., *Cancer Res.* 70 (2010) 8045–8054.
- [110] S. Miknyoczki, H. Chang, J. Grobelny, S. Pritchard, C. Worrell, N. McGann, M. Ator, J. Husten, J. Diebold, R. Hudkins, et al., *Mol. Cancer Ther.* 6 (2007) 2290–2302.
- [111] J. Diebold, R.L. Hudkins, S.J. Miknyoczki, B. Ruggeri, Method of Radio-Sensitizing Tumors Using A Radio-Sensitizing Agent (Cephalon, Inc.), 2007. WO2008/63644 A1.
- [112] F. Meglio, L.A. Pinni, *FASEB J.* 17 (2003) 349–368.
- [113] J. Walter, A. Schindzielorz, B. Hartung, C. Haass, *J. Biol. Chem.* 275 (2000) 23523–23529.
- [114] J.L. Milhon, T.J. Albert, E.A. Vande Waa, K.A. O'Leary, R.N. Jackson, M.A. Kessler, L.A. Schuler, J.W. Tracy, *Mol. Biochem. Parasitol.* 108 (2000) 225–236.
- [115] R. Prudent, V. Moucadel, C.-H. Nguyen, C. Barette, F. Schmidt, J.-C. Florent, L. Lafanechere, C.F. Sautel, E. Duchemin-Pelletier, E. Spreux, et al., *Cancer Res.* 70 (2010) 9865–9874.
- [116] L. Ronstrand, *Cell Mol. Life Sci.* 61 (2004) 2535–2548.



Research Article

Crude alkaloid extract of *Rhazya stricta* inhibits cell growth and sensitizes human lung cancer cells to cisplatin through induction of apoptosis

Ayman I. Elkady

Department of Biological Sciences, Faculty of Sciences, King Abdulaziz University, Jeddah, Kingdom of Saudi Arabia.

Abstract

There is an urgent need to improve the clinical management of non-small cell lung cancer (NSCLC), one of the most frequent causes of cancer-related deaths in men and women worldwide. *Rhazya stricta*, an important medicinal plant used in traditional Oriental medicine, possesses anti-oxidant, anti-carcinogenic and free radical scavenging properties. This study was done to explore the potential anticancer activity of a crude alkaloid extract of *R. stricta* (CAERS) against the NSCLC line A549. CAERS markedly suppressed the growth of A549 cells and considerably enhanced the anti-proliferative potential of cisplatin. CAERS-mediated inhibition of A549 cell growth correlated with the induction of apoptosis that was accompanied by numerous morphological changes, DNA fragmentation, an increase in the Bax/Bcl-2 ratio, the release of mitochondrial cytochrome *c*, activation of caspases 3 and 9 and cleavage of poly(ADP-ribose)-polymerase. CAERS reduced the constitutive expression of anti-apoptotic proteins (Bcl-2, Bcl-X_L, Mcl-1 and Survivin) and cell cycle regulating proteins (cyclin D1 and c-Myc), but enhanced expression of the proapoptotic proteins Noxa and BAD. These observations indicate that CAERS induced apoptosis and sensitized NSCLC to cisplatin via a mitochondria-mediated apoptotic pathway. These data provide a rationale for using a combination of CAERS and CDDP to treat NSCLC and other CDDP-resistant tumors.

Keywords: apoptosis, lung cancer, medicinal plant, RT-PCR, western blot.

Received: June 13, 2012; Accepted: September 28, 2012.

Introduction

Lung cancer is one of the most common cancers in many countries and accounts for 28% of all cancer-related deaths (Bilello *et al.*, 2002; Jemal *et al.*, 2008). Clinically, lung cancer is classified into two groups, namely, small cell and non-small cell lung cancer (NSCLC). The latter is more prevalent, accounting for almost 85% of lung cancers (Jemal *et al.*, 2004). Although early detection and treatment can improve the prognosis, only 15% of patients with NSCLC are diagnosed at an early stage since most lung cancer begins to grow silently without any symptoms until the cancer is in an advanced stage (Gargiullo *et al.*, 2002; Beadsomore and Screamton, 2003; Jemal *et al.*, 2004), at which point the treatment options are generally limited to surgery or radiation. Currently, the most active chemotherapeutic agent for the treatment of NSCLC is cisplatin (cis-diamminedichloroplatinum(II); CDDP) and CDDP-based combinations have remained the standard first-line chemotherapy for advanced NSCLC for more than two decades (Johnson, 2000; Wang *et al.*, 2004). Unfortunately, despite its great efficacy, CDDP is associated with several

major problems, including a number of side effects and the development of resistance that tend to limit the therapeutic potential of CDDP (Rom *et al.*, 2000; Gridelli *et al.*, 2003; Wang *et al.*, 2004). Consequently, new approaches such as novel effective drugs with low toxicities or excellent combination regimens are needed to overcome CDDP-resistance in NSCLC therapy.

During the past decade, various studies have shown that current cancer therapies (for example, chemotherapy, γ -irradiation, immunotherapy or suicide gene therapy) exert their antitumor effect primarily by triggering apoptosis in cancer cells (Makin and Dive, 2001). Consistent with this evidence, most tumor cells, including NSCLC, are naturally resistant to apoptotic-related cell death and to non-apoptotic cell death such as necrosis, autophagy, senescence, mitotic catastrophe and paraptosis (Okada and Mak, 2004; Debatin and Krammer, 2004). To date, three apoptotic pathways have been identified, *i.e.*, mitochondrial-, death receptor- and endoplasmic reticulum stress-mediated apoptosis (reviewed in Wong, 2011). Of these, the mitochondrial pathway initiates apoptosis in most physiological and pathological situations. A variety of stimuli such as stress and drugs induce disruption of the mitochondrial membrane and the release of mitochondrial proteins such as cytochrome *c* (cyt *c*).

The release of cyt *c* from mitochondria is tightly regulated by Bcl-2 family proteins that include anti-apoptotic (*e.g.*, Bcl-2) and pro-apoptotic (*e.g.*, Bax) members (Reed, 2000; Wong, 2011). Bcl-2 can stabilize mitochondrial permeability to prevent the release of cyt *c* whereas Bax increases the membrane permeability leading to the release of cyt *c* from mitochondria (Reed, 2000; Wong, 2011). Upon release from mitochondria into the cytosol, cyt *c*, together with Apaf-1, activates caspase-9 and the latter then activates caspases 3 and 7 (Cruchten and Den Broeck, 2002; Wong, 2011). Subsequently, active caspase-3 cleaves downstream substrates such as poly-(ADPribose) polymerase (PARP), which are responsible for the morphological and biochemical changes that are the hallmarks of apoptosis (Cruchten and Den Broeck, 2002; Wong, 2011). However, tumor cells do not undergo apoptosis easily because of defects in their ability to activate the death signaling pathway. Consequently, one effective strategy for the treatment/prevention of cancer is to search for agents that can activate apoptotic pathways in tumor cells (Call *et al.*, 2008; Liu *et al.*, 2011).

Members of the plant family Apocynaceae have been used in folk medicine for centuries and many of their constituents have been isolated and are now in clinical use, *e.g.*, vinblastine, vincristine and reserpine (Neuss, 1970). *Rhazya stricta* (harmal) is an important medicinal species of the Apocynaceae used in indigenous medicinal herbal drugs to cure various diseases in southern Asia (Pakistan, India and Afghanistan) and the Middle East (Saudi Arabia, Qatar, United Arab Emirates, Iran and Iraq) (Gilani *et al.*, 2007). Indeed, extracts of *R. stricta* leaves are prescribed in folklore medicine for the treatment of various disorders such as diabetes, sore throat, helminthesis, inflammatory conditions and rheumatism (Ali *et al.*, 2000, 1995, 1998). Some of the chemical constituents of *R. stricta* and their pharmacological activities have been reviewed (Ali *et al.*, 2000). The plant extract contains many alkaloids, glycosides, flavonoids, tannins and triterpenes (Ahmed *et al.*, 1983; Al-Yahya *et al.*, 1990). The effective uses of *R. stricta* described in traditional medicine have been attributed to the presence of indole alkaloids. Indeed, activity-guided phytochemical analysis of *R. stricta* extract has shown that the alkaloidal fraction has the highest biological activity (Tanira *et al.*, 2000). In addition, two indole alkaloids, 16-epi-Z-isositsirikine and didemethoxycarbonyl-tetrahydrosecamine, isolated from *R. stricta* have antineoplastic activity (Mukhopadhyay *et al.*, 1981, 1983; Attar-Rahman and Zaman, 1986).

Previously work has shown that an aqueous extract of *R. stricta*, acting as a single agent, inhibits cell proliferation in the breast cancer cell lines MCF-7 and MDA MB-231 (Baeshen *et al.*, 2012). In contrast, no detailed studies have addressed the effect of a crude alkaloid extract of *R. stricta* (CAERS) on cancers. The present study was undertaken to assess the impact of CAERS on the growth of NSCLC

A549 cells and to examine the mechanism of action. The results described here clearly show that CAERS suppressed the growth of A564 cells and increased the sensitivity to and cytotoxicity of CDDP. CAERS sensitized A549 cells to CDDP through a mitochondria-dependent apoptotic pathway. These data provide a basis for using a combination of CAERS and CDDP to treat lung carcinoma and other tumors.

Materials and Methods

Preparation of crude alkaloid extract from *R. stricta*

A crude alkaloid extract of *R. stricta* leaves was prepared essentially as described elsewhere (Tanira *et al.*, 2000), with some modifications. Briefly, air-dried leaves of *R. stricta* (350 g) were soaked in 80% methanol (1 L) at ambient temperature for seven days after which the methanolic extract was evaporated in a rotatory evaporator and the remaining residue was suspended in water and filtered. The aqueous extract was then acidified with 10% glacial acetic acid and extracted with chloroform. This chloroform fraction contained weakly basic alkaloids and neutral compounds. The remaining aqueous solution was alkalinized using NaOH and the pH was adjusted to 11. The alkaline aqueous layer was extracted with chloroform to yield a chloroform fraction enriched in strongly basic alkaloids (Tanira *et al.*, 2000). The chloroform layer was evaporated to dryness and the resulting residue was re-dissolved in DMSO to the desired concentrations.

Cell culture

The human NSCLC cell line A549 and non-malignant human foreskin fibroblasts (HF-5 cells) were obtained from King Fahd Center for Medical Research, King Abdulaziz University, Saudi Arabia. The A549 cells were maintained in Dulbecco's modified Eagle's medium (DMEM, Promega) supplemented with 10% of FBS (Promega) and 1% penicillin-streptomycin antibiotics (Promega) and were grown at 37 °C in a humidified atmosphere with 5% CO₂.

Cell growth assay

Cell viability and the effects of drugs on the growth of NSCLC cells were assessed with the trypan blue dye exclusion assay. Briefly, A549 cells were seeded onto 24-well plates (50 x 10³ cells/well) and grown overnight. The cells were then treated with increasing concentrations of CAERS (0, 3, 6, 15, 30, 45 and 60 µg/mL) or CDDP (0, 5, 10, 25, 50, 75 and 100 µg/mL) and incubated for 24, 48 or 72 h. At the end of each incubation, the floating and adherent cells were collected (with care being taken that none of the floating cells were lost during washes) and pelleted by centrifugation (700 g, 5 min). The cells were re-suspended in 25 µL of phosphate-buffered saline (PBS), mixed with 5 µL of 0.4% trypan blue solution and counted using a hemocytometer under an inverted microscope. Cell growth

rates were determined by counting the number of viable cells in each CAERS-/CDDP-treated well and expressing this as a percentage of the total number of viable cells in the control well (no drugs added).

Clonogenic assay

The clonogenic assay was done by seeding 1000 cells/well onto 6-well plates. After incubation for 24 h, the cells were treated with increasing concentrations of CAERS (0, 3, 6, 15, 30, 45 and 60 µg/mL) for 72 h and then washed twice with PBS to remove any remaining CAERS before adding fresh medium. The cells were subsequently incubated for another 12 days after which the colonies were stained the 0.4% trypan blue solution. Colonies with > 50 cells were scored as surviving and the percentage survival was determined using the equation: percentage of survival = (colonies with drug treatment/colonies without drug treatment, *i.e.*, control) x 100.

Assessment of cell morphological changes

Cells were seeded (50×10^3 /well) onto 24-well plates and treated for 24 h with increasing concentrations (0, 3, 6, 15, 30, 45 and 60 µg/mL) of CAERS after which they were washed in PBS and fixed and permeabilized in 3.7% paraformaldehyde (Sigma) in PBS for 10 min at room temperature. Fixed cells were washed with PBS and stained with ethidium bromide solution (20 µg/mL) for 20 min at room temperature. The cells were washed twice more with PBS and analyzed. Representative images were captured with an inverted fluorescence microscope (Carl Zeiss, Germany) using the magnification indicated in the figures.

DNA fragmentation assay

Cells were seeded (20×10^4 /well) onto 6-well plates and treated for 24 h with different concentrations (0, 3, 6, 15 and 30 µg/mL) of CAERS after which the cells were harvested, washed in PBS and purified using a DNA purification kit (DNeasy Blood and Tissue kit, QIAGEN), according to the manufacturer's recommendations. The concentration of DNA was determined spectrophotometrically and DNA was electrophoresed on a 1% agarose gel at 100 V for 2 h and analyzed. The gel was stained with ethidium bromide (0.5 µg/mL) and DNA was visualized with a UV trans-illuminator (Bio-Rad).

RNA extraction and reverse transcriptase-PCR

Cells were seeded (20×10^4 /well) onto 6-well plates and treated with different concentrations (0, 3, 6, 15 and 30 µg/mL) of CAERS for 24 h. After this period, floating and adherent cells were collected (with care being taken that none of the floating cells were lost during washes) and pelleted by centrifugation (700 g, 5 min). RNA extraction and reverse transcriptase-PCR were done as previously described (Elkady, 2012). Briefly, total RNA was extracted,

reverse transcribed and amplified by PCR using QIAamp RNA Blood mini kits (QIAGEN) according to the manufacturer's instructions. The polymerase chain reaction (PCR) was done using gene-specific primers. The primer sequences for Bcl-2, Bcl-x_L, Mcl-1, survivin (BIRC5), Bad, Noxa, c-Myc, cyclin D1 and HPRT1 were described earlier (El-Kady *et al.*, 2011). Amplification products obtained by PCR were separated electrophoretically on 1% agarose gels and visualized by ethidium bromide (0.5 µg/mL) staining (Elkady, 2012).

Preparation of mitochondrial and cytosolic extracts

To detect cyt *c* release by western immunoblotting, mitochondrial and cytosolic extracts were obtained as described previously (Elkady, 2012). Briefly, cells were seeded (20×10^4 /well) onto 6-well plates, treated with the indicated concentrations of CAERS and CDDP and incubated for 24 h. After this incubation, the cells were collected by centrifugation, washed twice with cold PBS, re-suspended in 500 µL of ice-cold cytosol extraction buffer (20 mM HEPES, pH 7.5, 10 mM KCl, 1.5 mM MgCl₂, 1 mM EDTA and 1 mM EGTA) containing a protease inhibitor cocktail (1 mM PMSF, 1% aprotinin, 1 mM leupeptin and 1 µg of pepstatin A/mL). After a 30 min incubation on ice, the cells were homogenized in the same buffer using a dounce homogenizer (30 strokes) and centrifuged (1000 x g, 10 min, 4 °C). The supernatant was collected and centrifuged again (14,000 x g, 30 min) to collect the mitochondria-rich (pellet) and cytosolic (supernatant) fractions. The supernatant was used as cytosolic lysate while the pellet was suspended in lysis buffer (137 mM NaCl, 20 mM Tris, pH 7.9, 10 mM NaF, 5 mM EDTA, 1 mM EGTA, 10% (v/v) glycerol and 1% Triton X-100) supplemented with a protease inhibitor cocktail (Protease Inhibitor Cocktail Set III, Calbiochem) before being centrifuged to obtain the mitochondrial lysate. Proteins concentrations were determined with a BCA protein assay kit (Pierce) and equal amounts of protein fractions were subjected for further analyses as described below.

Western blot analysis

After treatment with CAERS and CDDP, the cells were harvested, washed three times with PBS and lysed in cold lysis buffer containing 0.05 mM Tris-HCl, 0.15 mM NaCl, 1 M EGTA, 1 M EDTA, 20 mM NaF, 100 mM Na₃VO₄, 0.5% NP40, 1% Triton X-100 and 0.5 mM phenylmethylsulfonyl fluoride, pH 7.4, with freshly added protease inhibitor cocktail (Protease Inhibitor Cocktail Set III, Calbiochem). The amount of protein was quantified using a BCA protein assay kit (Pierce). Western immunoblotting was done essentially as described elsewhere (Elkady, 2012). Briefly, equal amounts (20 µg per treatment) of protein from control and CAERS/CDDP-treated cells were boiled for 5 min in Laemmli buffer and separated by SDS-PAGE on 10% polyacrylamide gels. The proteins were sub-

sequently transferred to PVDF membranes that were then blocked and probed with primary antibodies (Spring Bioscience) against the desired proteins followed by incubation with secondary HRP-conjugated antibodies (Spring Bioscience). In all experiments, the blots were stripped with stripping buffer (62.5 mM Tris, pH 6.7, 2% SDS and 90 mM 2-mercaptoethanol) and reprobed with anti- β -actin (Spring Bioscience) antibody as a control for protein loading. Signals were detected with an enhanced chemiluminescence detection kit (Amersham).

Statistical analysis

All assays were done at least three times and the results were expressed as the mean \pm SD unless otherwise stated. Statistical comparisons were done by using Student's *t*-test. Probability values of $p < 0.05$ indicated statistical significance.

Results

CAERS suppresses cell growth and colony formation and sensitizes A549 cells to CDDP

Initially, the effect of CAERS on the death of A549 cells was evaluated by trypan blue dye exclusion, with the viability being expressed as a percentage of that of untreated (control) cells (assumed to be 100%). Figure 1 shows that continuous exposure to increasing concentrations of CAERS (0, 3, 6, 15, 30, 45 and 60 μ g/mL) for 24, 48 and 72 h resulted in a concentration- and time-dependent decrease in cell viability relative to control cultures. The IC₅₀ (inhibitory concentration 50%) for CAERS-induced cell death was ~28, 15 and 8 μ g at 24, 48 and 72 h, respectively. To assess whether CAERS-dependent growth inhibition was selective for cancer cells, the effect of CAERS on the viability of non-malignant human foreskin fibroblasts (HF-5 cells) was also assessed. Figure 1B shows that HF-5 cells were significantly more resistant to growth inhibition by CAERS than were A549 cells. The strongest effect was seen at the highest concentration of CAERS, where the survival of HF-5 cells was inhibited by only ~15% after 72 h, indicating that CAERS is not toxic to normal, non-transformed cells. These results suggest that CAERS may selectively target A549 cancer cells but spare normal fibroblasts, which is a highly desirable property of potential anticancer agents.

CDDP is one of the most effective chemotherapeutic drugs for treating NSCLC but it has a narrow therapeutic window between efficacy and unacceptable toxicity (Rom *et al.*, 2000; Gridelli *et al.*, 2003). Since CAERS effectively inhibited the growth of A549 cells and had little effect on the growth of normal HF-5 fibroblasts, the ability of CAERS to enhance the cell killing effect of CDDP was examined. For this, the effect of CDDP alone or in combination with CAERS on the growth of A549 cells was assessed. Figure 1C shows the effect of increasing concen-

trations (0, 5, 10, 25, 50, 75 and 100 μ g/mL) of CDDP alone on A549 cells; the IC₅₀ values were 70, 60 and 40 μ g/mL at 24, 48 and 72 h, respectively. On the other hand, combined treatment with CAERS (6 μ g/mL) and increasing concentrations of CDDP markedly increased the inhibition of A549 cell growth by CDDP. In this case, there was a decrease in the IC₅₀ values of CDDP to 15, 8 and 4 μ g/mL at 24, 48 and 72 h, respectively, in the presence of CAERS (Figure 1D). Pair-wise comparisons between the IC₅₀ values shown in panels C and D showed that, in general, CDDP alone had an approximately half-maximal inhibitory effect on cell growth at all concentrations over 24, 48 and 72 h. These results indicate that CAERS strongly enhances the inhibition of cell proliferation by CDDP in the human NSCLC A549 cell line.

Subsequently, a clonogenic assay was done to confirm the potential of CAERS to suppress the growth of A549 cells. As shown in Figure 1E, the clonogenic survival of A549 cells was significantly affected by exposure to CAERS for 72 h, with CAERS causing a concentration-dependent decrease in the number and size of growing colonies when compared to the untreated controls (100%). These results demonstrate that CAERS had a cytostatic effect on long-term colony formation by A549 cells.

CAERS induces apoptosis in A549 cells

The major goal of cancer chemotherapy is to commit tumor cells to apoptosis following exposure to anticancer agents, and it is generally believed that the induction of apoptosis is the primary cytotoxic mechanism of phytochemicals (Khan *et al.*, 2007). To determine whether CAERS inhibited the cell growth of A549 cells by inducing apoptosis and whether CAERS-induced apoptosis accounts for its ability to enhance CDDP-induced inhibition of cell growth and proliferation, cells were treated with increasing concentrations of CAERS for 24 h and frequency of apoptotic cell death was assessed by phase microscopy. As seen under an inverted phase microscope (Figure 2A), untreated A549 cells grew well to form confluent monolayers with a homogenous morphology containing lightly and evenly stained nuclei. In contrast, CAERS-treated cells showed marked morphological changes compared to untreated cells. Most of the cells treated with CAERS concentrations $\geq 30 \mu$ g/mL had densely stained nuclear granular bodies containing highly condensed chromatin ('apoptotic bodies'). The nuclear changes and apoptotic body formation characteristic of apoptosis were visualized by incubating A549 cells with CAERS for 24 h followed by staining with ethidium bromide (Figure 2B).

DNA fragmentation to yield DNA ladders is a characteristic feature of apoptosis (Nagata, 2000). To examine whether CAERS might provoke such fragmentation in A549 cells, genomic DNA from A549 cells treated with CAERS was extracted and separated by agarose gel electrophoresis. Figure 2C shows that there were clear DNA

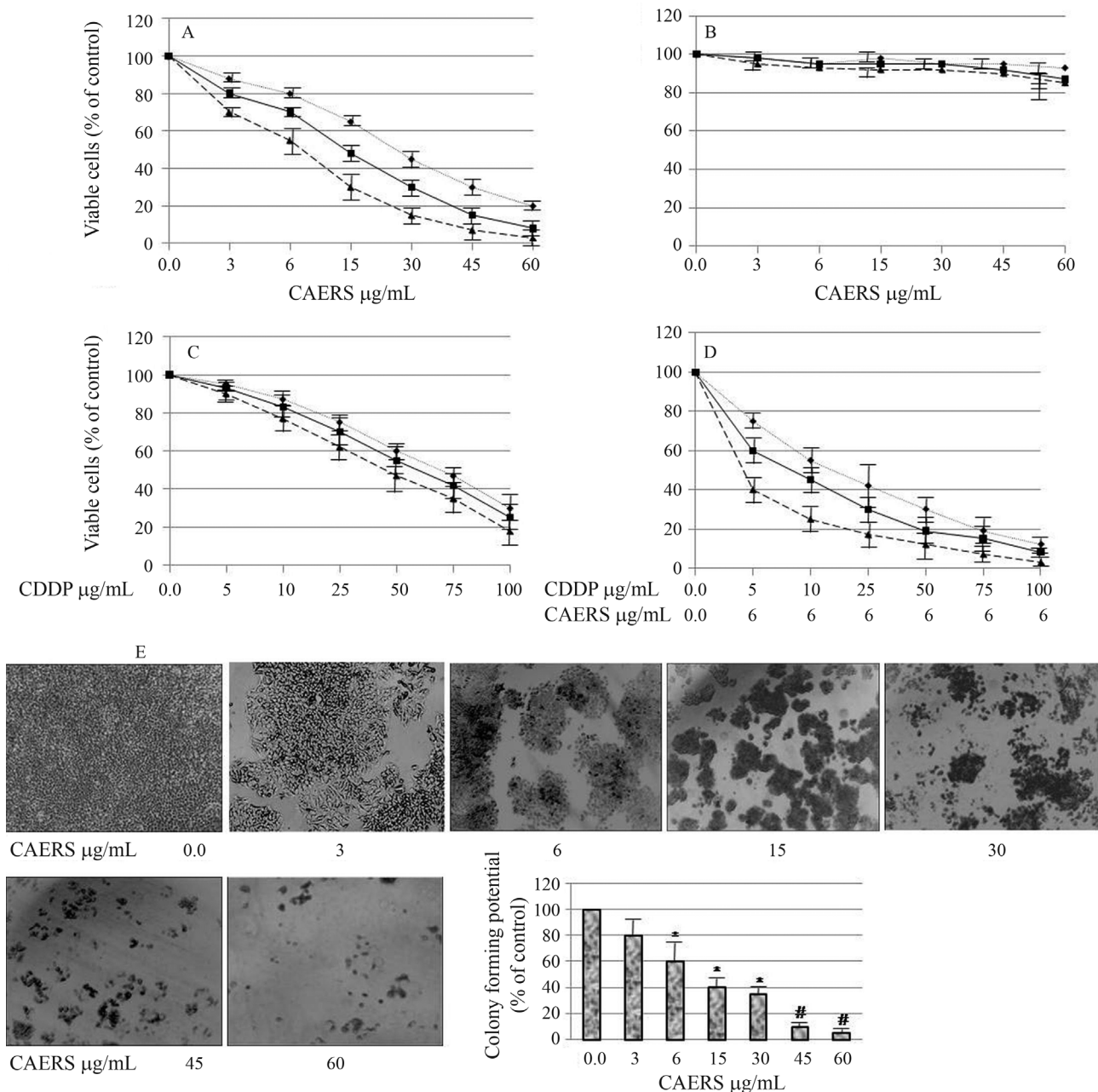


Figure 1 - CAERS suppresses cell growth and colony formation and sensitizes A549 cells to CDDP. A549 (A) and HF-5 (B) cells (50×10^3 cells/well) were seeded onto 24-well plates and treated with the indicated concentrations of CAERS alone for 24 h (dotted line), 48 h (solid line) and 72 h (dashed line). (B and C) A549 cells (50×10^3 cells/well) were seeded onto 24-well plates and treated with the indicated concentrations of CDDP alone (C) or CDDP + CAERS (D) for 24, 48 and 72 h. The inhibition of cell proliferation was assessed by the trypan blue dye exclusion assay. Cell viability was expressed as a percentage of control (no drug treatment) cell viability. The points are the mean \pm SD of at least three independent experiments. (E) Effects of CAERS on clonogenicity of A549 cells. Cells were seeded onto a 6-well plate at 1000 cells/well and treated with the indicated concentrations of CAERS as detailed in Materials and Methods. The colonies were counted under a dissection microscope. A survival of 100% corresponded to the number of colonies obtained with cells that were not treated with CAERS. The experiment was repeated three times and the colony forming potential of the cells at each concentration of CAERS is expressed as a percent of the control and is reported as the mean \pm SD. *p < 0.05 and #p < 0.001 compared to control cells (100%).

fragmentation ladders in samples from cells treated with all concentrations of CAERS. The comet assay was used to confirm DNA fragmentation after incubation with CAERS. This assay is a sensitive method for monitoring single strand (ss) DNA breaks at the single cell level (reviewed in

Tice *et al.*, 2000). When A549 cells were treated with 3, 6 and 15 μg of CAERS/mL for 24 h there was significant ssDNA damage, as indicated by the increased tail length in the CAERS-treated cells compared with the controls (data not shown). Thus, these two independent methods of as-

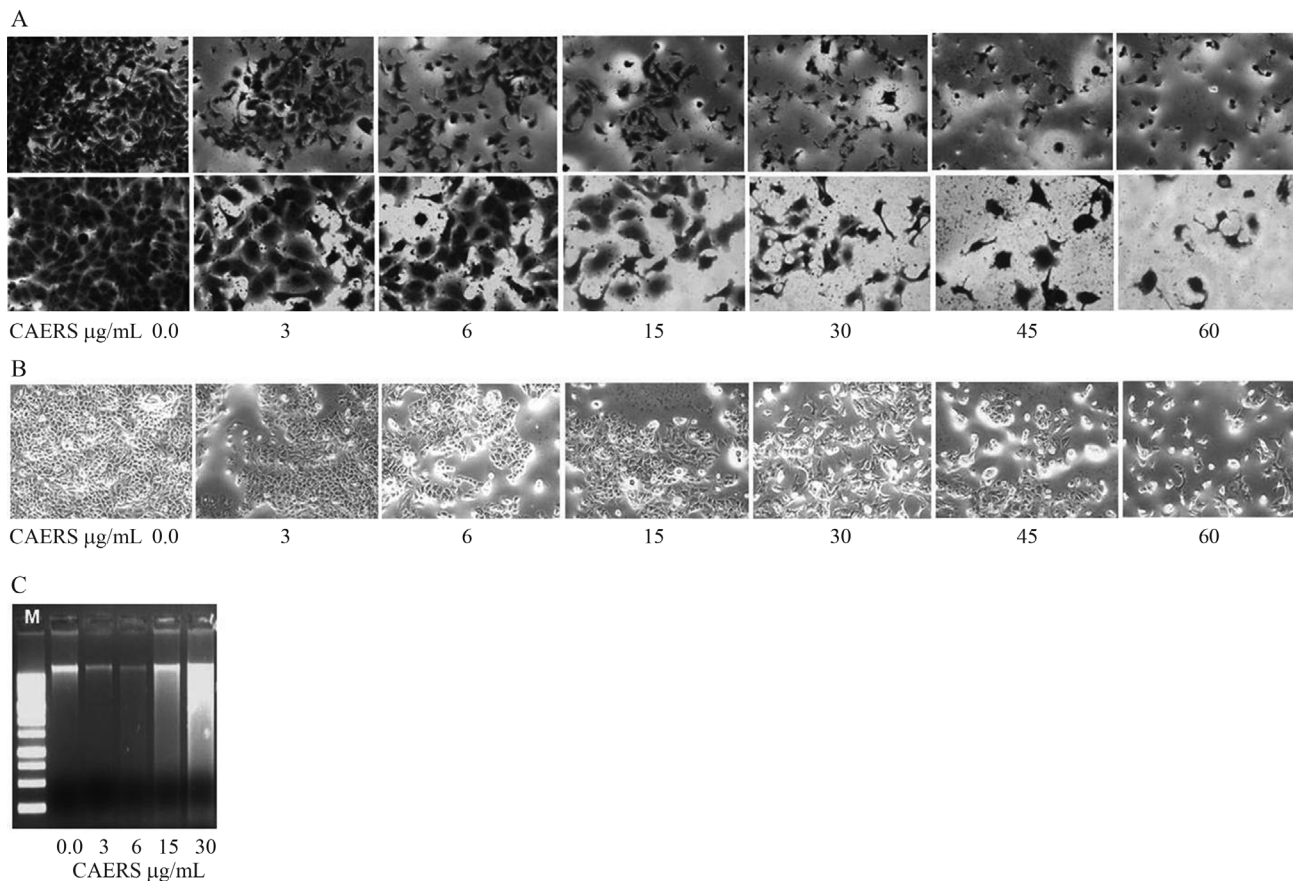


Figure 2 - CAERS induces apoptosis in A549 cells. (A) Morphological changes in A549 cells after incubation with CAERS. (A) The cells were treated with the indicated concentrations of CAERS for 24 h after which they were examined using an inverted microscope (first row: magnification - 200x; second row: magnification - 400x). (B) The cells were stained with ethidium bromide for 20 min and photographed with a fluorescence microscope using a red filter (magnification: 200x). (C) Fragmentation of DNA isolated from A549 cells incubated with CAERS. The cells were incubated with the indicated concentrations of CAERS for 24 h after which DNA fragmentation was assessed as described in Materials and Methods. Lane 'M' indicates the DNA marker ladder. The data are representative of three independent experiments with similar results.

sessing apoptosis provided similar results, suggesting that the anti-proliferative potential of CAERS was linked to its ability to induce apoptosis in A549 cells.

CAERS modulates the expression of apoptotic regulatory proteins and their activation in A549 cells

To elucidate how CAERS induced A549 cell apoptosis, changes in the expression of several key apoptosis-related proteins, including Bcl-2, Bax, cyt c, caspases 9 and 3, and poly(ADPribose) polymerase (PARP) were examined. Bcl-2 and Bax play critical roles in the regulation of cyt c release from the mitochondria into the cytosol; the released cyt c initiates caspase activation and apoptotic cell death. PARP is an early marker of chemotherapy-induced apoptosis (Reed, 2000; Cruchten and Den Broeck, 2002; Wong, 2011). A549 cells were treated with increasing concentrations of CAERS for 24 h after which the levels of Bcl-2, Bax, cyt c, caspases 9 and 3, and cleaved PARP were analyzed by western blotting. Figure 3 shows that incubation with CAERS significantly reduced the level of Bcl-2 and increased those of Bax (A) and cytosolic cyt c (B), as

well as the activation of caspases 9 and 3 and cleavage of PARP (C). These results demonstrate that CAERS induced A549 cell apoptosis at the molecular level, possibly by activating an intrinsic apoptotic pathway.

CAERS modulates the expression of antiapoptotic- and cell cycle-regulating genes in A549 cells

To assess the significance of the expression patterns of antiapoptotic and cell cycle regulating genes in response to CAERS, A549 cells were treated with CAERS for 24 h and then possible alterations in the mRNA expression levels of various apoptosis-/cell cycle-related genes were analyzed by RT-PCR using gene-specific primers. The proteins examined included the anti-apoptotic proteins Bcl-2, Bcl-X_L and Mcl-1, a member of the IAP family of proteins, Survivin (Reed, 2000) and the cell cycle-regulating proteins cyclin D1 and c-Myc (Liao *et al.*, 2007). In addition, the expression levels of the proapoptotic BH3-only protein, Noxa (Reed, 2000; Wong, 2011), and a positive regulator of cell death, Bad (Danial, 2009), were also examined. Figure 4 shows that incubation with CAERS consistently mod-

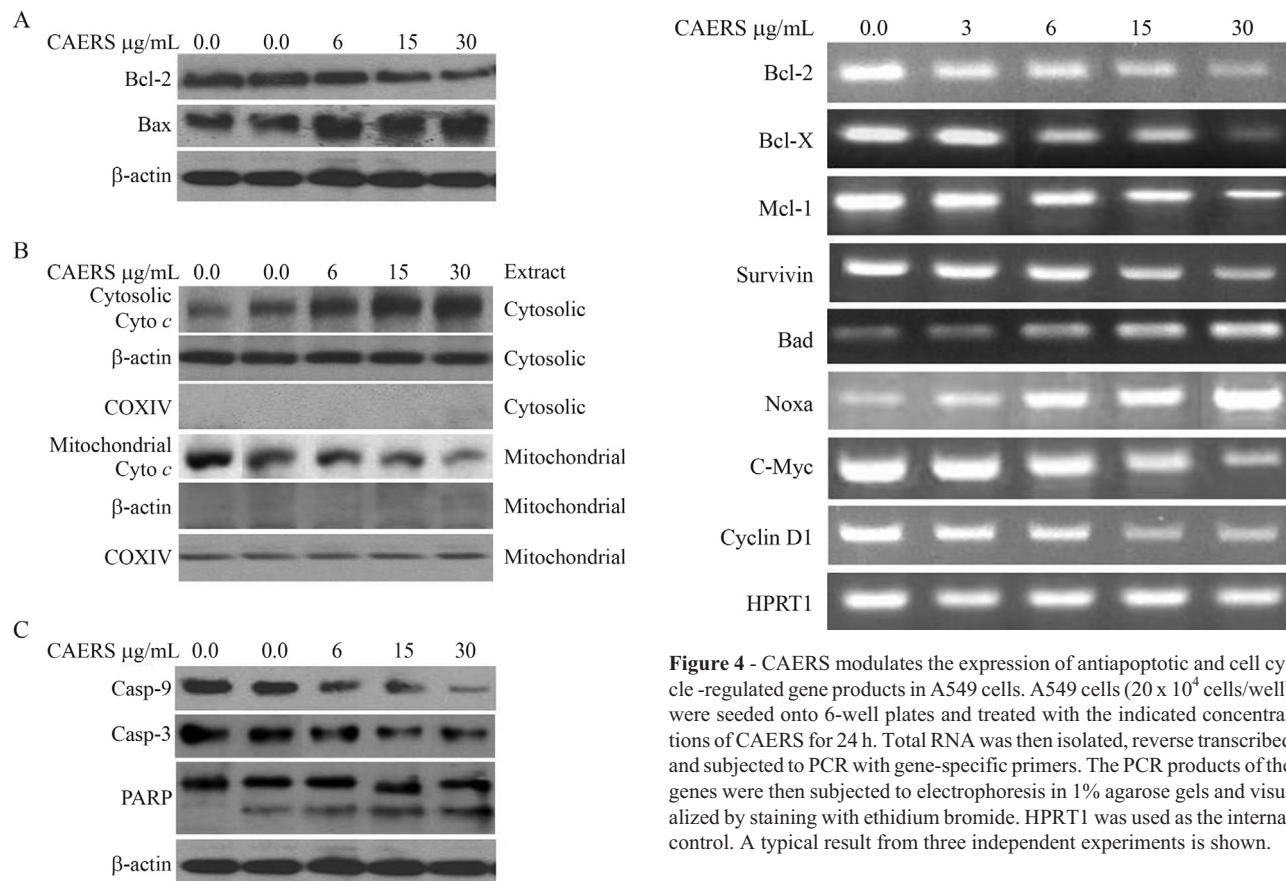


Figure 3 - CAERS modulates expression of apoptosis regulatory proteins and their activation in A549 cells. A549 cells (20×10^4 cells/well) were seeded onto 6-well plates and treated with the indicated concentrations of CAERS for 24 h. Subsequently, 20 µg of cell extract protein isolated from CAERS-treated A549 cells was subjected to SDS-PAGE in 10% polyacrylamide gels, transferred to PVDF membranes and immunoblotted with antibodies against the proteins of interest. Treatment with CAERS increased the Bax/Bcl-2 ratio (A), promoted mitochondrial cyto c release (B) and activated caspases 9 and 3 and PARP cleavage (C). The immunoblots of cyto c (B) were stripped and re-probed with anti-cytochrome oxidase IV (COXIV) to confirm the purity of the cytoplasmic fraction and equal loading of the mitochondrial fraction. In all experiments, the membranes were stripped and re-probed with anti-β-actin antibody as a loading control. The data are representative of three separate experiments.

ulated the expression of this panel of genes in a concentration-dependent manner. Thus, CAERS down-regulated the expression of Bcl-2, Bcl-X_L, Mcl-1, Survivin, c-Myc and cyclin D1, but enhanced that of Bad and Noxa. These data suggest that CAERS induced apoptosis in A549 cells by selectively inhibiting anti-apoptotic gene expression and up-regulating Bad and Noxa expression.

Discussion

Lung cancer is the most frequent cause of cancer-related deaths in men and women worldwide, with NSCLC accounting for 75-80% of lung cancers (Bilello *et al.*, 2002; Jemal *et al.*, 2008). CDDP-based combination treatments

Figure 4 - CAERS modulates the expression of antiapoptotic and cell cycle-regulated gene products in A549 cells. A549 cells (20×10^4 cells/well) were seeded onto 6-well plates and treated with the indicated concentrations of CAERS for 24 h. Total RNA was then isolated, reverse transcribed and subjected to PCR with gene-specific primers. The PCR products of the genes were then subjected to electrophoresis in 1% agarose gels and visualized by staining with ethidium bromide. HPRT1 was used as the internal control. A typical result from three independent experiments is shown.

are the first-line chemotherapy for NSCLC (Johnson, 2000; Wang *et al.*, 2004). However, since current CDDP-based chemotherapy has a narrow therapeutic window between efficacy and unacceptable toxicity (Johnson, 2000; Rama-lingam and Belani, 2004), there is an urgent need to develop low toxicity chemotherapeutics for NSCLC to reduce treatment failure. Recent work has shown that an aqueous extract of *R. stricta* successfully inhibited the proliferation and induced apoptotic cell death in breast cancer cell lines (Baeshen *et al.*, 2012). The present study was done to investigate whether CAERS, an aqueous extract of *R. stricta*, could inhibit A549 cell growth and enhance the cytotoxicity of CDDP; the mechanism of CAERS action was also examined.

The results described here show that CAERS significantly suppressed the growth of human A549 cells in a time- and concentration-dependent manner. Furthermore, cytotoxicity assays indicated that CDDP and CAERS acted synergistically to suppress the growth of A549 cells. In contrast, CAERS had no significant effect on non-malignant human fibroblasts (HF-5 cells), which raises the possibility that CAERS may selectively target lung cancer cells. However, the experiments described here cannot exclude the possibility of tissue-specific differences between human fibroblasts and lung cells. Additional cytotoxicity studies using a normal lung cell line and different lung cancer cell lines, as well as studies *in vivo* in nude mice are nec-

essary to prove that CAERS can inhibit tumor growth without major side effects. Further proof of the growth-suppressing potential of CAERS was provided by the colony formation assay which showed a significant reduction in the number and size of colonies in CAERS-treated cells compared with untreated control cells. Collectively, these data indicate that CAERS could be a promising candidate for restricting the growth of lung cancer cells.

The ability of CAERS to induce cell death in A549 cells was examined in detail in order to elucidate the mechanism by which CAERS markedly enhanced the CDDP-induced inhibition of NSCLC cell growth. The inhibitory activity of CAERS on cell growth was related to the induction of apoptosis since CAERS-treated A549 cells exhibited the typical morphological features of apoptosis (Cruchten and Den Broeck, 2002), such as a loss of cell viability, cell shrinkage, irregularity in cell shape, and cell detachment. In addition, staining with ethidium bromide revealed nuclear condensation, DNA fragmentation and perinuclear apoptotic bodies in CAERS-treated cells. Furthermore, DNA laddering and the comet assay (data not shown) demonstrated that CAERS induced apoptosis in A549 cells and augmented the apoptotic potential of CDDP in A549 cells. Since CDDP can trigger cancer cell death by inducing apoptosis (Sorenson *et al.*, 1990; Wang *et al.*, 2000; Del Bello *et al.*, 2001) it is possible that CAERS enhances the effect of CDDP on A549 cell proliferation partly by augmenting the ability of CDDP to initiate apoptosis.

Most anticancer agents induce DNA damage by interacting with DNA either directly or indirectly; the latter route may involve secondary stress-response signaling pathways that trigger apoptosis by activating the intrinsic (mitochondrial) apoptotic pathway and, in some cases, simultaneously activating the extrinsic (death receptor) pathway (Green, 2000). A variety of stimuli such as stress and drugs induce perturbation of the mitochondrial membrane and the release of mitochondrial proteins, such as cyt *c*, leading to the initiation of apoptotic cascades (Green, 2000). However, the mitochondria-dependent pathway for apoptosis is governed by Bcl-2 family proteins; the proteins Bax and Bcl-2 have opposing roles in initiating mitochondrial apoptotic events and modulating apoptosis (Wong, 2011). Bcl-2 is associated with the outer mitochondrial membrane where it plays a pivotal and overriding protective role by preserving mitochondrial structure and function, thereby preventing the onset of a mitochondrial permeability transition and inhibiting the release of cyt *c* to the cytosol. In contrast, Bax, a dominant-negative inhibitor of Bcl-2, induces a mitochondrial permeability transition and promotes apoptosis (Wong, 2011). Thus, when the level of Bax increases, the mitochondrial membrane becomes permeable to cyt *c*.

Upon its release into cytosol, cyt *c*, together with Apaf-1, activates caspase-9 that then activates caspase-3 (Reed, 2000; Wong, 2011). Active caspase-3 cleaves the

116 kDa PARP protein to an 89 kDa fragment, which is a characteristic marker of the execution of apoptosis (Reed, 2000; Cruchten and Den Broeck, 2002). The findings described here fit the above scenarios perfectly since CAERS significantly enhanced cytosolic cyt *c* that was associated with a concomitant decrease in the level of mitochondrial cyt *c*, suggesting that this treatment resulted in the release of cyt *c* from the mitochondrion into the cytosol. In addition, CAERS enhanced the activation of caspase-9, implying that CAERS mediated A549 cell growth via the caspase-9 apoptotic pathway, in agreement with previous studies showing that the caspase-9-dependent mitochondria-mediated apoptotic pathway is the primary pathway for antitumor agent-induced apoptosis (Khan *et al.*, 2007). Furthermore, western blotting demonstrated down-regulation of Bcl-2 expression and up-regulation of Bax expression.

Based on these observations, it is tempting to speculate that treatment with CAERS resulted in cyt *c* release and the activation of caspase-9 and caspase-3 partly via the disruption of a balance between Bax and Bcl-2. Subsequently, active caspase-3 mediated the cleavage of PARP to account for DNA fragmentation as well as other morphological and biochemical changes during apoptosis (Cruchten and Den Broeck, 2002). CAERS therefore appears to exert its anti-proliferative potentiality on A549 cell growth via the intrinsic apoptosis pathway involving Bcl-2 family proteins and caspase-9 activation. The down-regulation of Bcl-2 and up-regulation of Bax by CAERS corroborates published reports indicating that the ratio of anti-apoptotic Bcl-2 to pro-apoptotic Bax protein at least partly determines the susceptibility of the cell to a death signal (Vander Heiden and Thompson, 1999) and can be used as a predictive marker for therapeutic response to therapy (Mackey *et al.*, 1998). The down-regulation of Bcl-2 by CAERS highlights the potential usefulness of CAERS as an ideal therapeutic agent for treating NSCLC.

RT-PCR showed that CAERS down-regulated the expression of genes known to have a pro-survival role, such as Bcl_xL, Mcl-1 and Survivin (Reed, 2000). For example, Bcl_xL and Mcl-1 suppress the release of cyt *c* from mitochondria and prevent apoptosis (Reed, 2000; Liu *et al.*, 2001) and overexpression of Mcl-1 delayed apoptosis induced by growth factor withdrawal and other cytotoxic agents (Liu *et al.*, 2001). Survivin is selectively expressed in most human neoplasms, including NSCLC, and is associated with a poor prognosis in patients with NSCLC (Zhang *et al.*, 2012); Survivin also confers tumor cell resistance to anticancer agents and ionizing radiation (Pennati *et al.*, 2007). Recent findings suggest that Survivin and Bcl-2 are up-regulated in NSCLC tissues and may act synergistically in the development, invasion and metastasis of NSCLC (Gao *et al.*, 2012). In addition, CAERS down-regulated the mRNA levels of c-Myc and cyclin D1. The c-Myc oncogene promotes cell cycling progression,

plays a vital role in most human cancers (Dang *et al.*, 2006) and cooperates with Mcl-1 in the development of NSCLC (Allen *et al.*, 2011). Similarly, cyclin D1 is a central player in the cell cycle and plays an essential role in the development of NSCLC (Ai *et al.*, 2012). Consequently, the down-regulation of Bcl-2, Bcl_{xL}, Mcl-1, Survivin, c-Myc and cyclin D1 by CAERS imply that this extract could effectively target the survival advantage provided by these effectors. However, it remains unclear whether the down-regulation of mRNA expression by CAERS was due to transcriptional down-regulation, mRNA stabilization or both. On the other hand, CAERS up-regulated the expression of genes involved in counteracting cell survival, such as Bad and Noxa. Down- and up-regulation of Mcl-1 and Noxa expression, respectively, by CAERS is important since studies of molecular targeted therapies have shown that ABT-737, a Bad mimetic, binds with high affinity to BCL-X_L, BCL-2 and BCL-w but not to Mcl-1 (Labi *et al.*, 2008). Hence, therapy with ABT-737 would be ineffective in cells expressing significant amounts of Mcl-1 (van Delft *et al.*, 2006; Huang and Sinicrope, 2008). This would be critical, particularly in tumor cells such as NSCLC that have a high expression of Mcl-1 (Luo *et al.*, 2011) since only Noxa, but not other BH3-only family members, appears to be crucial in fine-tuning cell death decisions by targeting the Mcl-1 for proteasomal degradation (Ploner *et al.*, 2009). Consequently, the down-regulation of Mcl-1 and up-regulation of Noxa by CAERS may tip the balance of events towards apoptosis in A549 cells.

In summary, the results described above have shown that a natural plant-derived antitumor agent (CAERS) inhibits growth and potentiates the anticancer activity of the cytotoxic drug CDDP in human A549 cells. CAERS inhibited A549 cell growth via apoptotic mechanisms. The induction of apoptosis by CAERS was mediated by regulation of the levels and activities of apoptosis regulatory proteins. Together, these findings provide a scientific basis for using a combination of CAERS and CDDP as a potentially effective chemotherapy regimen for treating patients with resistant lung cancer, although further preclinical investigations are warranted. The ability of CAERS to improve the antitumor effects of CDDP in A549 orthotopic xenografts is currently being studied.

Acknowledgments

The author thanks the Deanship of Scientific Research (DSR), King Abdulaziz University, Jeddah, Saudi Arabia for technical and financial support of this research.

References

- Ahmad Y, Fatima K, Le Quesne PPW and Atta-ur-Rahman (1983) Further alkaloidal constituents of the leaves of *Rhazya stricta*. *Phytochemistry* 22:1017-1019.
- Ai T, Wang Z, Zhang M, Zhang L, Wang N, Li W and Song L (2012) Expression and prognostic relevance of STAT3 and cyclin D1 in non-small cell lung cancer. *Int J Biol Markers* 27:132-138.
- Ali BH, Bashir AK, Banna NR and Tanira MO (1995) Central nervous system activity of *Rhazya stricta* Dence in mice. *Clin Exp Pharmacol Physiol* 22:248-253.
- Ali BH, Bashir AK and Tanira MO (1998) The effect of *Rhazya stricta*, a traditional medicinal plant, on the forced swimming test in rats. *Pharmacol Biochem Behav* 59:547-550.
- Ali BH, Al-Qarawi AA, Bashir AK and Tanira MO (2000) Phytochemistry, pharmacology and toxicity of *Rhazya stricta* Decne: A review. *Phytother Res* 14:229-234.
- Allen TD, Zhu CQ, Jones KD, Yanagawa N, Tsao MS and Bishop JM (2011) Interaction between MYC and MCL1 in the genesis and outcome of non-small-cell lung cancer. *Cancer Res* 71:2212-2221.
- Al-Yahya MA, Al-Meshal IA, Mossa JS, Al-Badr AA and Tariq M (1990) Saudi Plants: A Phytochemical and Biochemical Approach. King Saud University Press, Riyadh, pp 123-129.
- Atta-ur-Rahman and Zaman K (1986) 1,2-Dehydroaspidospermidine N-oxide, an alkaloid from *Rhazya stricta*. *Phytochemistry* 25:1779-1780.
- Baeshen NA, Elkady AI, Abuzinadah OA and Mutwakil MH (2012) Potential anticancer activity of medicinal herb, *Rhazya stricta*, against human breast cancer. *Afr J Biotechnol* 11:8960-8972.
- Beadsmore CJ and Scream NJ (2003) Classification, staging and prognosis of lung cancer. *Eur J Radiol* 45:8-17.
- Bilello KS, Murin S and Matthay RA (2002) Epidemiology, etiology, and prevention of lung cancer. *Clin Chest Med* 23:1-25.
- Call JA, Eckhardt SG and Camidge DR (2008) Targeted manipulation of apoptosis in cancer treatment. *Lancet Oncol* 9:1002-1011.
- Cruchten SV and Den Broeck WV (2002) Morphological and biochemical aspects of apoptosis, oncosis and necrosis. *Anat Histol Embryol* 31:214-223.
- Dang CV, O'Donnell KA, Zeller I, Nguyen T, Osthus RC and Li F (2006) The c-Myc target gene network. *Semin Cancer Biol* 16:253-326.
- Danial NN (2009) BAD: Undertaker by night, candyman by day. *Oncogene* 27:S53-S70.
- Debatin KM and Krammer PH (2004) Death receptors in chemotherapy and cancer. *Oncogene* 23:2950-2966.
- Del Bello B, Valentini MA, Zunino F, Comporti M and Maellaro E (2001) Cleavage of Bcl-2 in oxidant- and cisplatin-induced apoptosis of human melanoma cells. *Oncogene* 20:4591-4595.
- Elkady AI (2012) Crude extract of *Nigella sativa* inhibits proliferation and induces apoptosis in human cervical carcinoma HeLa cells. *Afr J Biotechnol* 11:12710-12720.
- El-Kady AI, Sun Y, Li Y-X and Lia DJ (2011) Cyclin D1 inhibits whereas c-Myc enhances the cytotoxicity of cisplatin in mouse pancreatic cancer cells via regulation of several members of the NF-κB and Bcl-2 families. *J Carcinog* 10:24.
- Gao Q, Yang S and Kang MQ (2012) Influence of survivin and Bcl-2 expression on the biological behavior of non-small cell lung cancer. *Mol Med Rep* 5:1409-1414.
- Gargiullo P, Wingo PA, Coates RJ and Thompson TD (2002) Recent trends in mortality rates for four major cancers, by sex and race/ethnicity - United States. *Morb Mortal Wkly Rep* 51:49-53.

- Gilani SA, Kikuchi A, Shinwari ZK, Khattak ZI and Watanabe KN (2007) Phytochemical, pharmacological and ethnobotanical studies of *Rhazya stricta* Decne. *Phytother Res* 21:301-307.
- Green DR (2000) Apoptotic pathways: Paper wraps stone blunts scissors. *Cell* 102:1-4.
- Gridelli C, Rossi A and Maione P (2003) Treatment of non-small cell lung cancer: State of the art and development of new biologic agents. *Oncogene* 22:6629-6638.
- Huang S and Sinicrope FA (2008) BH3 mimetic ABT-737 potentiates TRAIL-mediated apoptotic signaling by unsequestering Bim and Bak in human pancreatic cancer cells. *Cancer Res* 68:2944-2951.
- Jemal A, Tiwari RC, Murray T, Ghafoor A, Samuels A, Ward E, Feuer EJ and Thun MJ (2004) Cancer statistics. *CA Cancer J Clin* 54:8-29.
- Jemal A, Seigal R, Ward E, Hao Y, Xu J, Murray T and Thun M (2008) Cancer statistics. *CA Cancer J Clin* 58:71-96.
- Johnson DH (2000) Evolution of cisplatin-based chemotherapy in non-small cell lung cancer: A historical perspective and the Eastern Cooperative Oncology Group experience. *Chest* 117:S133-S137.
- Khan N, Afaq F and Mukhtar H (2007) Apoptosis by dietary factors: The suicide solution for delaying cancer growth. *Carcinogenesis* 28:233-239.
- Labi V, Grespi F, Baumgartner F and Villunger A (2008) Targeting the Bcl-2-regulated apoptosis pathway by BH3 mimetics: A breakthrough in anticancer therapy? *Cell Death Differ* 15:977-987.
- Liao D, Thakur A, Wu J, Biliran H and Sarkar F (2007) Perspectives on c-Myc, cyclin D1, and their interaction in cancer formation, progression, and response to chemotherapy. *Crit Rev Oncog* 13:93-158.
- Liu H, Perlman H, Pagliari LJ and Pope RM (2001) Constitutively activated Akt-1 is vital for the survival of human monocyte-differentiated macrophages. Role of Mcl-1, independent of nuclear factor (Nf)-kB, Bad, or caspase activation. *J Exp Med* 194:2113-2126.
- Liu JJ, Lin M, Yu JY, Liu B and Bao JK (2011) Targeting apoptotic and autophagic pathways for cancer therapeutics. *Cancer Lett* 300:105-114.
- Luo L, Zhang T, Liu H, Lv T, Yuan D, Yao Y, Lv Y and Song Y (2011) MiR-101 and Mcl-1 in non-small-cell lung cancer: Expression profile and clinical significance. *Med Oncol* 29:1681-1686.
- Mackey TJ, Borkowski A, Amin P, Jacobs SC and Kyprianou N (1998) Bcl-2/Bax ratio as a predictive marker for therapeutic response to radiotherapy in patients with prostate cancer. *Urology* 52:1085-1090.
- Makin G and Dive C (2001) Apoptosis and cancer chemotherapy. *Trends Cell Biol* 11:S22-S26.
- Mukhopadhyay S, Handy GA, Funayama S and Cordell GA (1981) Anticancer indole alkaloids of *Rhazya stricta*. *J Nat Prod* 44:696-700.
- Mukhopadhyay S, El-Sayed A, Handy GA and Cordell GA (1983) *Catharanthus* alkaloids XXXVII. 16-Epi-isotsirikine, a monomeric indole alkaloid with antineoplastic activity from *Catharanthus roseus* and *Rhazya stricta*. *J Nat Prod* 46:409-413.
- Nagata S (2000) Apoptotic DNA fragmentation. *Exp Cell Res* 256:12-18.
- Neuss N (1970) Indole alkaloids. In: Pelletier SW (ed) *Chemistry of the Alkaloids*. Van Nostrand Reinhold, New York, pp 213-266.
- Okada H and Mak TW (2004) Pathways of apoptotic and non-apoptotic death in tumour cells. *Nat Rev Cancer* 4:592-603.
- Pennati M, Folini M and Zaffaroni N (2007) Targeting survivin in cancer therapy: Fulfilled promises and open questions. *Carcinogenesis* 28:1133-1139.
- Ploner C, Kofler R and Villunger A (2009) Noxa: At the tip of the balance between life and death. *Oncogene* 27:S84-S92.
- Ramalingam S and Belani CP (2004) State-of-the-art chemotherapy for advanced non-small cell lung cancer. *Semin Oncol* 31:S68-S74.
- Reed JC (2000) Mechanisms of apoptosis. *Am J Pathol* 157:1415-1426.
- Rom WN, Hay JG, Lee TC, Jiang Y and Tchou-Wong KM (2000) Molecular and genetic aspects of lung cancer. *Am J Respir Crit Care Med* 161:1355-1367.
- Sorenson CM, Barry MA and Eastman A (1990) Analysis of events associated with cell cycle arrest at G2 phase and cell death induced by cisplatin. *J Natl Cancer Inst* 82:749-755.
- Tanira MO, Ali BH, Bashir AK, Dhanasekaran S, Tibacia EM and Elves LM (2000) Mechanism of the hypotensive activity of the alkaloidal fraction of *Rhazya stricta*. *Pharmacol Res* 41:369-378.
- Tice RR, Agurell E, Anderson D, Burlinson B, Hartmann B, Kobayashi H, Miyamae Y, Rojas Y, Ryu J-C and Sasaki YF (2000) Single cell gel/Comet assay: Guidelines for *in vitro* and *in vivo* genetic toxicology testing. *Environ Mol Mutagen* 35:206-221.
- van Delft MF, Wei AH, Mason KD, Vandenberg CJ, Chen L, Czabotar PE, Willis SN, Scott CL, Day CL, Cory S, et al. (2006) The BH3 mimetic ABT-737 targets selective Bcl-2 proteins and efficiently induces apoptosis via Bak/Bax if Mcl-1 is neutralized. *Cancer Cell* 10:389-399.
- Vander Heiden MG and Thompson CB (1999) Bcl-2 proteins: Regulators of apoptosis or of mitochondrial homeostasis? *Nat Cell Biol* 1:E209-E216.
- Wang G, Reed E and Li QQ (2004) Molecular basis of cellular response to cisplatin chemotherapy in non-small cell lung cancer (Review). *Oncol Rep* 12:955-65.
- Wang X, Martindale JL and Holbrook NJ (2000) Requirement for ERK activation in cisplatin-induced apoptosis. *J Biol Chem* 275:39435-39443.
- Wong RSY (2011) Apoptosis in cancer: From pathogenesis to treatment. *Wong J Exp Clin Cancer Res* 30:87.
- Zhang LQ, Wang J, Jiang F, Xu L, Liu FY and Yin R (2012) Prognostic value of survivin in patients with non-small cell lung carcinoma: A systematic review with meta-analysis. *PLoS One* 7:e34100.

Associate Editor: Anamaria Aranha Camargo